



Ollscoil  
Teicneolaíochta  
an Atlantaigh

Atlantic  
Technological  
University

# Automated Detection of COVID-19 using Convolutional Neural Networks and Generative Adversarial Networks

A thesis submitted

by

Ultan Kearns

in partial fulfillment of the requirements for the degree of

Master of Science in Computing in Big Data Analytics and Artificial Intelligence

Supervisor: Dr Paul Greaney

Submitted to Quality and Qualifications Ireland (QQI)

Dearbhú Cáilíochta agus Cáilíochtaí Éireann

March 2023

# Contents

|  |           |
|--|-----------|
| <b>Declaration</b>   | <b>4</b>  |
| <b>Acknowledgements</b>  | <b>5</b>  |
| <b>Acronyms</b>  | <b>6</b>  |
| <b>List of Figures</b>   | <b>7</b>  |
| <b>List of Tables</b>  | <b>11</b> |
| <b>1 Introduction</b>  | <b>1</b>  |
| 1.1 Generative Adversarial Network (GAN) . . . . .                   | 1         |
| 1.2 Artificial Neural Network (ANN) . . . . .                        | 2         |
| 1.3 What is A Convolutional Neural Network? (CNN) . . . . .          | 3         |
| 1.4 Supervised Learning . . . . .                                    | 4         |
| 1.5 Unsupervised Learning . . . . .                                  | 4         |
| 1.6 Tensorflow . . . . .   | 5         |
| 1.7 Keras . . . . .  | 5         |
| 1.8 Background of Problem & Aims of This Paper . . . . .             | 6         |
| 1.9 Datasets . . . . .   | 8         |
| 1.9.1 COVID-19 Chest X-Ray . . . . .                                 | 8         |
| 1.9.2 COVID-19 Radiography Database . . . . .                        | 8         |
| 1.9.3 COVID-19 Pneumonia Normal Chest X-Ray PA Dataset . . . . .     | 8         |
| 1.9.4 Extensive COVID-19 X-Ray and CT Chest Images Dataset . . . . . | 9         |
| 1.9.5 Use of datasets in This Project . . . . .                      | 9         |
| 1.10 Structure of This Thesis . . . . .                              | 9         |
| 1.10.1 Chapter 1 - Introduction . . . . .                            | 9         |
| 1.10.2 Chapter 2 - Literature Review . . . . .                       | 10        |
| 1.10.3 Chapter 3 - Implementation . . . . .                          | 10        |
| 1.10.4 Chapter 4 - Results . . . . .                                 | 10        |

|   |           |
|---|-----------|
| 1.10.5 Chapter 5 - Further Research and Conclusions . . . . .   | 10        |
| <b>2 Literature Review</b>  | <b>11</b> |
| 2.1 Introduction . . . . .  | 11        |
| 2.2 Analysis of Existing Models for Automated COVID-19 Detection . . . . .  | 14        |
| 2.3 Challenges & Limitations of Using Artificial Intelligence in Automated Diagnosis Systems for COVID-19 . . . . . | 21        |
| 2.4 Research into Data Augmentation And Convolutional Neural Networks Architectures . . . . .                       | 21        |
| 2.5 Conclusion . . . . .  | 37        |
| <b>3 Implementation</b>   | <b>38</b> |
| 3.1 Introduction . . . . .  | 38        |
| 3.2 CNN Model Design and Comparison . . . . .   | 39        |
| 3.2.1 Baseline Models . . . . .   | 39        |
| 3.3 Transfer Learning CNN Baseline Models . . . . .   | 48        |
| 3.3.1 Radiography Dataset . . . . .   | 48        |
| 3.3.2 X-Ray COVID-19 Dataset . . . . .  | 51        |
| 3.3.3 Evaluation of TL models for X-Ray COVID-19 dataset . . . . .  | 54        |
| 3.3.4 COVID-19 Chest X-Ray Dataset . . . . .  | 54        |
| 3.3.5 Extensive COVID-19 Dataset CT . . . . .   | 57        |
| 3.3.6 Extensive COVID-19 Dataset X-ray . . . . .  | 60        |
| 3.4 GAN Baseline Design and Comparison . . . . .  | 63        |
| 3.5 GANs for Radiography Dataset . . . . .  | 63        |
| 3.5.1 VAE(Variational Auto Encoder) . . . . .   | 64        |
| 3.5.2 DCGAN(Deep Convolutional GAN Network) . . . . .   | 64        |
| 3.6 GANs for COVID 19 X-ray dataset . . . . .   | 66        |
| 3.6.1 DCGANs . . . . .  | 66        |
| 3.7 GANs for Chest X-ray COVID-19 . . . . .   | 68        |
| 3.8 Extensive COVID-19 X-Ray / CT . . . . .   | 68        |
| 3.8.1 DCGANs . . . . .  | 68        |
| 3.9 GANs in Conjunction . . . . .   | 74        |
| 3.10 Conclusion . . . . .   | 74        |
| <b>4 Results of Research and Conclusions</b>  | <b>75</b> |
| 4.1 Evaluation of Augmented CNN Models . . . . .  | 75        |
| 4.1.1 Radiography CNN Models . . . . .  | 75        |
| 4.1.2 Extensive CNN Models . . . . .  | 79        |
| 4.1.3 X-ray COVID-19 dataset CNN Models . . . . .   | 87        |

|  |           |
|--|-----------|
| 4.2 Evaluation of GAN Models . . . . .                                     | 88        |
| 4.2.1 Radiography GAN Models . . . . .                                     | 88        |
| 4.2.2 Extensive X-Ray GAN Models . . . . .                                 | 91        |
| 4.2.3 Extensive CT GAN Models . . . . .                                    | 92        |
| 4.2.4 X-ray COVID-19 dataset GAN Models . . . . .                          | 92        |
| 4.3 Conclusion . . . . .   | 93        |
| <b>5 Future Work and Research</b>  | <b>94</b> |
| 5.1 Limitations . . . . .  | 94        |
| 5.1.1 Computational Resources Offered by Google Colab Pro . . . . .        | 94        |
| 5.1.2 Run time Limits in Google Colab Pro . . . . .                        | 95        |
| 5.1.3 Lack of Data . . . . .   | 95        |
| 5.1.4 Time . . . . .   | 96        |
| 5.1.5 Financial Limitations . . . . .                                      | 96        |
| 5.2 Future Research . . . . .  | 96        |
| 5.2.1 Suggestions for Future Research . . . . .                            | 96        |
| 5.3 Conclusion of Work . . . . .   | 97        |
| 5.3.1 Issues Faced and How They Should be Mitigated in Future Research . . | 97        |
| 5.3.2 Summary of Results . . . . .   | 97        |
| 5.3.3 Final Words . . . . .  | 97        |

# Declaration

I hereby certify that this material, which I now submit for assessment on the programme of study leading to the award of Master of Science in Computing in Big Data Analytics and Artificial Intelligence, is entirely my own work and has not been taken from the work of others except and to the extent that such work has been cited and acknowledged within the text of my own work. No portion of the work contained in this thesis has been submitted in support of an application for another degree or qualification to this or any other institution. I understand that it is my responsibility to ensure that I have adhered to LYIT's rules and regulations.

I hereby certify that the material on which I have relied on for the purpose of my assessment is not deemed as personal data under the GDPR Regulations. Personal data is any data from living people that can be identified. Any personal data used for the purpose of my assessment has been pseudonymised and the data set and identifiers are not held by LYIT. Alternatively, personal data has been anonymised in line with the Data Protection Commissioners Guidelines on Anonymisation.

I give consent for my work to be held for the purposes of education assistance to future Computing students at LYIT and it will not be shared outside the Department of Computing at LYIT. I understand that my assessment may be shared with any other third party and will be held securely in LYIT in line with the Institute's Records Retention Policy.

Signed: Ultan Kearns

Date: Tuesday 14<sup>th</sup> March, 2023

# Acknowledgements

I would first of all like to thank my supervisor during this project Dr. Paul Greaney, he was a fantastic help throughout the course of writing this thesis and this work could not have been completed without his input and help.

I would also like to thank the lecturers who taught me so much during my postgraduate course, both Doctors Karla Muñoz-Esqueival and Shagufta Henna provided a fantastic introduction into many areas of Artificial Intelligence and the knowledge they imparted has helped me a lot throughout the course of conducting this research.

I would also like to thank Andrew Ng, his deep learning courses provided a great foundation into the realm of deep learning and Artificial Intelligence.

# Acronyms

| Acronym | Stands For  |
|---------|---|
| AI      | Artificial Intelligence                           |
| ANN     | Artificial Neural Network                         |
| CNN     | Convolutional Neural Network                      |
| GAN     | Generative Adversarial Network                    |
| CT      | Computed Topography                               |
| LSTM    | Long short term memory                            |
| AUC     | Area under curve                                  |
| DCNN    | Deep Convolutional Neural Network                 |
| RCNN    | Regions with CNN Features                         |
| VAE     | Varational Auto Encoder                           |
| DCGAN   | Deep Convolutional Generative Adversarial Network |

Table 1: Acronyms used in this thesis

# List of Figures

|      |  |    |
|------|--|----|
| 1.1  | Basic Example of generative adversarial network . . . . .  | 2  |
| 1.2  | Basic Example of Artificial Neural Network . . . . .   | 3  |
| 1.3  | Graph of COVID-19 Statistics by age-range Ireland from October 2021 - December 2021 Courtesy of CSO[16] . . . . .  | 6  |
| 1.4  | Cumulative cases of the COVID-19 virus worldwide courtesy of Our World in Data[17] . . . . .   | 7  |
| 2.1  | Estimated dates of first COVID-19 cases around the World, Image courtesy of Roberts, Rossman and Jarić[29] . . . . .   | 12 |
| 2.2  | Examples of Overfitting, Underfitting and Optimal models, Image courtesy of Abhishek Shrivastava[31] . . . . .   | 13 |
| 2.3  | Examples of CT Qualitative images lung segmentation[32] . . . . .  | 15 |
| 2.4  | Examples of CT qualitative images infection masks[32] . . . . .  | 16 |
| 2.5  | Overview of a Typical LSTM Network[33] . . . . .   | 18 |
| 2.6  | Perfomance of CNN model[33] . . . . .  | 19 |
| 2.7  | Performance of CNN LSTM Model[33] . . . . .  | 20 |
| 2.8  | Example of SMOTE[37] . . . . .   | 22 |
| 2.9  | Results from Experiment One (Data Augmentation Using GANs)[36] . . . . .   | 25 |
| 2.10 | Figure of learning framework for lychee Classification Model[39] . . . . .   | 29 |
| 2.11 | Figure of TransGAN (lychee Surface Defect Detection Based on Deep Convolutional Neural Networks with GAN-Based Data Augmentation)[39] . . . . .  | 30 |
| 2.12 | Figure of SSD-MobileNet V2 Architecture (lychee Surface Defect Detection Based on Deep Convolutional Neural Networks with GAN-Based Data Augmentation)[39] . . . . .   | 31 |
| 2.13 | Figure of Faster RCNN Architecture (lychee Surface Defect Detection Based on Deep Convolutional Neural Networks with GAN-Based Data Augmentation)[39]  | 31 |
| 2.14 | Figure of Faster RCNN Res Block and Inception Module (a) Res block; (b) Inception Module. (lychee Surface Defect Detection Based on Deep Convolutional Neural Networks with GAN-Based Data Augmentation)[39] . . . . . | 32 |

|      |   |    |
|------|---|----|
| 2.15 | Figure of Mean Average Precision of Models. (lychee Surface Defect Detection Based on Deep Convolutional Neural Networks with GAN-Based Data Augmentation)[39]      | 35 |
| 2.16 | Figure of Speed of Models in classifying lychee. (lychee Surface Defect Detection Based on Deep Convolutional Neural Networks with GAN-Based Data Augmentation)[39] | 36 |
| 3.1  | Figure of Swish and ReLU activation functions(Image courtesy of Madhura Ingalkar)[45]   | 40 |
| 3.2  | Figure of Train and Validation Accuracy of X-ray COVID-19 dataset CNN Baseline Model  | 41 |
| 3.3  | Figure of Train and Validation Loss of X-ray COVID-19 dataset CNN Baseline Model  | 41 |
| 3.4  | Figure of Train and Validation Accuracy of Radiography CNN Baseline Model   | 42 |
| 3.5  | Figure of Train and Validation Loss of Radiography CNN Baseline Model   | 43 |
| 3.6  | Figure of Train and Validation Accuracy of COVID-19 chest X-ray CNN Baseline Model  | 44 |
| 3.7  | Figure of Train and Validation Loss of COVID-19 chest X-ray CNN Baseline Model  | 44 |
| 3.8  | Figure of Train and Validation accuracy of Extensive COVID CNN Baseline Model CT  | 46 |
| 3.9  | Figure of Train and Validation Loss of Extensive COVID CNN Baseline Model CT  | 46 |
| 3.10 | Figure of Extensive COVID-19 X-ray CNN Baseline Model Train and Validation Accuracy   | 47 |
| 3.11 | Figure of Extensive COVID-19 X-ray CNN Baseline Model Train and Validation Loss   | 47 |
| 3.12 | Transfer Learning Xception CNN Baseline Train and Validation Accuracy   | 48 |
| 3.13 | Transfer Learning Xception CNN Baseline Train and Validation Loss   | 49 |
| 3.14 | Transfer Learning ResNet50V2 CNN Baseline Train and Validation Accuracy   | 49 |
| 3.15 | Transfer Learning ResNet50V2 CNN Baseline Train and Validation Loss   | 50 |
| 3.16 | Transfer Learning EfficientNetV2S CNN Baseline Train and Validation Accuracy  | 50 |
| 3.17 | Transfer Learning EfficientNetV2S CNN Baseline Train and Validation Loss  | 51 |
| 3.18 | Transfer Learning Xception CNN Baseline Train and Validation Accuracy X-Ray COVID19   | 51 |
| 3.19 | Transfer Learning Xception CNN Baseline Train and Validation Loss X-Ray COVID19   | 52 |
| 3.20 | Transfer Learning ResNet50V2 CNN Baseline Train and Validation Accuracy X-Ray COVID19   | 52 |

---

*LIST OF FIGURES*

---

|   |    |
|---|----|
| 3.21 Transfer Learning ResNet50V2 CNN Baseline Train and Validation Loss X-Ray COVID19 . . . . .                          | 53 |
| 3.22 Transfer Learning EfficientNetV2S CNN Baseline Train and Validation Accuracy X-Ray COVID19 . . . . .                 | 53 |
| 3.23 Transfer Learning EfficientNetV2S CNN Baseline Train and Validation Loss X-Ray COVID19 . . . . .                     | 54 |
| 3.24 Transfer Learning Xception CNN Baseline Train and Validation Accuracy Chest X-Ray . . . . .                          | 55 |
| 3.25 Transfer Learning Xception CNN Baseline Train and Validation Loss X-Ray Chest X-Ray . . . . .                        | 55 |
| 3.26 Transfer Learning ResNet50V2 CNN Baseline Train and Validation Accuracy Chest X-Ray . . . . .                        | 56 |
| 3.27 Transfer Learning ResNet50V2 CNN Baseline Train and Validation Loss X-Ray Chest X-Ray . . . . .                      | 56 |
| 3.28 Transfer Learning EfficientNetV2S CNN Baseline Train and Validation Accuracy Chest X-Ray . . . . .                   | 57 |
| 3.29 Transfer Learning EfficientNetV2S CNN Baseline Train and Validation Loss Chest X-Ray . . . . .                       | 57 |
| 3.30 Transfer Learning Xception CNN Baseline Train and Validation Accuracy Extensive COVID 19 Dataset CT . . . . .        | 58 |
| 3.31 Transfer Learning Xception CNN Baseline Train and Validation Loss Extensive COVID 19 Dataset CT . . . . .            | 58 |
| 3.32 Transfer Learning ResNet50V2 CNN Baseline Train and Validation Accuracy Extensive COVID 19 Dataset CT . . . . .      | 59 |
| 3.33 Transfer Learning ResNet50V2 CNN Baseline Train and Validation Loss Extensive COVID 19 Dataset CT . . . . .          | 59 |
| 3.34 Transfer Learning EfficientNetV2S CNN Baseline Train and Validation Accuracy Extensive COVID 19 Dataset CT . . . . . | 60 |
| 3.35 Transfer Learning EfficientNetV2S CNN Baseline Train and Validation Loss Extensive COVID 19 Dataset CT . . . . .     | 60 |
| 3.36 Transfer Learning Xception CNN Baseline Train and Validation Accuracy Extensive COVID 19 Dataset X-ray . . . . .     | 61 |
| 3.37 Transfer Learning Xception CNN Baseline Train and Validation Loss Extensive COVID 19 Dataset X-ray . . . . .         | 61 |
| 3.38 Transfer Learning ResNet50V2 CNN Baseline Train and Validation Accuracy Extensive COVID 19 Dataset X-ray . . . . .   | 62 |
| 3.39 Transfer Learning ResNet50V2 CNN Baseline Train and Validation Loss Extensive COVID 19 Dataset X-ray . . . . .       | 62 |

|  |    |
|--|----|
| 3.40 Transfer Learning EfficientNetV2S CNN Baseline Train and Validation Accuracy Extensive COVID 19 Dataset X-ray . . . . . | 63 |
| 3.41 Transfer Learning EfficientNetV2S CNN Baseline Train and Validation Loss Extensive COVID 19 Dataset X-ray . . . . .     | 63 |
| 4.1 Radiography Augmented Baseline Model DCGAN Accuracy . . . . .  | 76 |
| 4.2 Radiography Augmented Baseline Model DCGAN Loss . . . . .  | 76 |
| 4.3 Radiography Augmented Xception Model DCGAN Accuracy . . . . .  | 77 |
| 4.4 Radiography Augmented Xception Model DCGAN Loss . . . . .  | 77 |
| 4.5 Radiography Augmented ResNet50V2 Model DCGAN Accuracy . . . . .  | 78 |
| 4.6 Radiography Augmented ResNet50V2 Model DCGAN Loss . . . . .  | 78 |
| 4.7 Radiography Augmented EfficientNetV2S Model DCGAN Accuracy . . . . .   | 79 |
| 4.8 Radiography Augmented EfficientNetV2S Model DCGAN Loss . . . . .   | 79 |
| 4.9 Extensive CT Augmented Baseline Model DCGAN Accuracy . . . . .   | 80 |
| 4.10 Extensive CT Augmented Baseline Model DCGAN Loss . . . . .  | 80 |
| 4.11 Extensive CT Augmented Xception Model DCGAN Accuracy . . . . .  | 81 |
| 4.12 Extensive CT Augmented Xception Model DCGAN Loss . . . . .  | 81 |
| 4.13 Extensive CT Augmented ResNet50V2 Model DCGAN Accuracy . . . . .  | 82 |
| 4.14 Extensive CT Augmented ResNet50V2 Model DCGAN Loss . . . . .  | 82 |
| 4.15 Extensive CT Augmented EfficientNetV2S Model DCGAN Accuracy . . . . .   | 83 |
| 4.16 Extensive CT Augmented EfficientNetV2S Model DCGAN Loss . . . . .   | 83 |
| 4.17 Extensive X-ray Augmented Baseline Model DCGAN Accuracy . . . . .   | 84 |
| 4.18 Extensive X-ray Augmented Baseline Model DCGAN Loss . . . . .   | 84 |
| 4.19 Extensive X-ray Augmented Xception Model DCGAN Accuracy . . . . .   | 85 |
| 4.20 Extensive X-ray Augmented Xception Model DCGAN Loss . . . . .   | 85 |
| 4.21 Extensive X-ray Augmented ResNet50V2 Model DCGAN Accuracy . . . . .   | 86 |
| 4.22 Extensive X-ray Augmented ResNet50V2 Model DCGAN Loss . . . . .   | 86 |
| 4.23 Extensive X-ray Augmented EfficientNetV2S Model DCGAN Accuracy . . . . .  | 87 |
| 4.24 Extensive X-ray Augmented EfficientNetV2S Model DCGAN Loss . . . . .  | 87 |
| 4.25 X-ray COVID-19 Augmented Baseline Model Model DCGAN Accuracy . . . . .  | 88 |
| 4.26 X-ray COVID-19 Augmented Baseline Model Model DCGAN Loss . . . . .  | 88 |

# List of Tables

|      |  |    |
|------|--|----|
| 1    | Acronyms used in this thesis . . . . .   | 6  |
| 2.1  | Results of Standard CNN Network - A combined deep CNN-LSTM network for the detection of COVID-19 using X-ray images . . . . .  | 19 |
| 2.2  | Results of CNN - A combined deep CNN-LSTM network for the detection of COVID-19 using X-ray images . . . . .   | 20 |
| 2.3  | GAN Architectures used for experiments in[36]) . . . . .   | 24 |
| 2.4  | Results of Cancer data set using different GAN Architectures (Data Augmentation using GANs)[36] . . . . .  | 25 |
| 2.5  | Results and label distribution of Diabetes data set using different GAN Architectures (Data Augmentation using GANs)[36] . . . . .   | 26 |
| 2.6  | Classification results on imbalanced test set (Data Augmentation using GANs)[36]   | 26 |
| 2.7  | Classification results on balanced test set (Data Augmentation using GANs)[36]   | 27 |
| 2.8  | Comparison of distribution of data augmented vs original(lychee Surface Defect Detection Based on Deep Convolutional Neural Networks with GAN-Based Data Augmentation)[39] . . . . . | 29 |
| 2.9  | Results of models before Augmentation(lychee Surface Defect Detection Based on Deep Convolutional Neural Networks with GAN-Based Data Augmentation)[39] . . . . .                    | 33 |
| 2.10 | Improvement of model accuracy after Augmentation(lychee Surface Defect Detection Based on Deep Convolutional Neural Networks with GAN-Based Data Augmentation)[39] . . . . .         | 33 |
| 2.11 | Mean average precision before Augmentation(lychee Surface Defect Detection Based on Deep Convolutional Neural Networks with GAN-Based Data Augmentation)[39] . . . . .               | 34 |
| 2.12 | Mean average precision after Augmentation(lychee Surface Defect Detection Based on Deep Convolutional Neural Networks with GAN-Based Data Augmentation)[39] . . . . .                | 34 |

|   |    |
|---|----|
| 2.13 Comparison of accuracy of base models vs models with data augmentation(lychee Surface Defect Detection Based on Deep Convolutional Neural Networks with GAN-Based Data Augmentation)[39] . . . . . | 36 |
| 3.1 X-ray COVID-19 dataset CNN baseline model architecture . . . . .  | 39 |
| 3.2 X-ray COVID-19 dataset CNN baseline model hyperparameters . . . . .   | 40 |
| 3.3 X-ray COVID-19 dataset CNN baseline model results . . . . .   | 40 |
| 3.4 Radiography CNN baseline model architecture . . . . .   | 42 |
| 3.5 Radiography CNN baseline model hyperparameters . . . . .  | 42 |
| 3.6 Radiography CNN baseline results . . . . .  | 42 |
| 3.7 COVID-19 chest X-ray CNN baseline model architecture for COVID-19 Chest X-ray Dataset . . . . .   | 43 |
| 3.8 COVID-19 chest X-ray CNN baseline model hyperparameters for COVID-19 Chest X-ray Dataset . . . . .  | 44 |
| 3.9 COVID-19 chest X-ray CNN baseline model results for COVID-19 Chest X-ray Dataset . . . . .  | 44 |
| 3.10 Extensive COVID-19 CT Dataset CNN baseline model architecture . . . . .  | 45 |
| 3.11 Extensive CT CNN baseline model hyperparameters . . . . .  | 45 |
| 3.12 Extensive CT CNN baseline model results . . . . .  | 45 |
| 3.13 Extensive COVID-19 X-Ray CNN baseline model architecture . . . . .   | 46 |
| 3.14 Extensive COVID-19 X-Ray CNN baseline model hyperparameters . . . . .  | 47 |
| 3.15 Extensive COVID-19 X-Ray CNN baseline model results . . . . .  | 47 |
| 3.16 DCGAN for Producing Synthetic COVID-19 Mask Data From Radiography Dataset . . . . .  | 65 |
| 3.17 DCGAN for Producing Synthetic COVID-19 X-Ray Data From Radiography Dataset . . . . .   | 66 |
| 3.18 DCGAN for Producing Synthetic Normal Class Data for X-ray COVID19 dataset  | 68 |
| 3.19 DCGAN for Producing Synthetic X-ray COVID Class Data for Extensive COVID 19 Dataset . . . . .  | 69 |
| 3.20 DCGAN for Producing Synthetic CT COVID Class Data for Extensive COVID 19 Dataset . . . . .   | 72 |
| 3.21 DCGAN for Producing Synthetic CT Non COVID Class Data for Extensive COVID 19 Dataset . . . . .   | 73 |

## **Abstract**

This paper aims to analyze the applications of generative adversarial networks or GANs in overcoming issues of data-shortages in relation to developing convolutional neural networks to automate the diagnosis of COVID-19 in patients. There have been many COVID-19 data-sets compiled but some suffer from lack of data-quality and data shortages[1][2]. In this paper I aim to create and train multiple convolutional neural networks or CNNs to analyze X-Rays of patients lungs to automate the detection of COVID-19. The CNN will be trained with a number of images generated from different GAN architectures to determine which will prove most efficient in automating the detection of COVID-19. I also aim to use the GANs in conjunction with one and other to try out different combinations to see if feeding images generated by one GAN to other GANs will produce more accurate results when training the model. In the results section of this Thesis I will compare and contrast the results of the various architectures and determine which proved most effective in it's diagnostic potential.

# Chapter 1

## Introduction

### 1.1 Generative Adversarial Network (GAN)

A generative adversarial network or GAN for short first appeared in a 2014 paper by Ian Goodfellow et al[3]. In this paper Goodfellow et al propose a new way to generate data via an adversarial process. The GAN essentially works as follows: two models are trained, a generative model  $G$  which will generate the content from the data and another model  $D$  which will be the discriminator, judging if data created by the model came from the dataset rather than  $G$ . The goal of this training is to ensure data generated from  $G$  is realistic enough to fool the discriminator  $D$  into believing that the generated content came from the training set. It is in this way that we can create realistic "fake" data from the generative model.

There are a number of GAN architectures which are useful in different scenarios, such as CycleGans[4] which are useful for translating images from a source domain  $X \rightarrow Y$  in which  $Y$  is the target domain, StyleGan, which was created by NVIDIA which allows more control over the generative process[5] and PixelRNN, which can recreate images when given a fraction of the original and can generate new images based on probability[6].

This dissertation examines a number of different generative adversarial network architectures and will use them in conjunction with each other, by feeding content generated by one architecture into another to develop a more diverse training set for the final model.

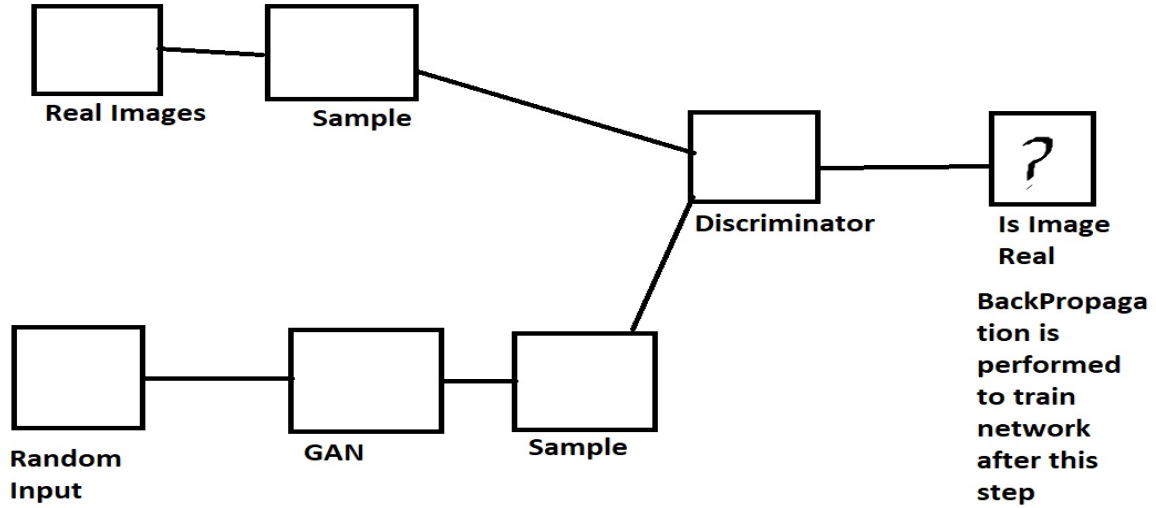


Figure 1.1: Basic Example of generative adversarial network

As we can see from the image above1.1, we start the process by taking a sample of real images from the training data, then passing it to the discriminator. We also take a sample from the GAN created images and pass that to the discriminator which will then determine if the images are real or fake. After the discriminator determines if the image is real or fake then backpropagation is performed to train the model so that it can differentiate better between samples that came from the training set and those which came from  $G$ .

## 1.2 Artificial Neural Network (ANN)

An artificial neural network, or ANN for short, is a network of neurons or nodes which are used for training a model to perform a certain task. They are made up of an input layer,  $N$  hidden layers, and finally an output layer. Each layer has its own activation function and will adjust its weights and biases to determine the final output of the model.[7] These networks are heavily inspired by biological processes which occur in the brain. Artificial neural networks are a general-purpose model used to solve a number of common problems.

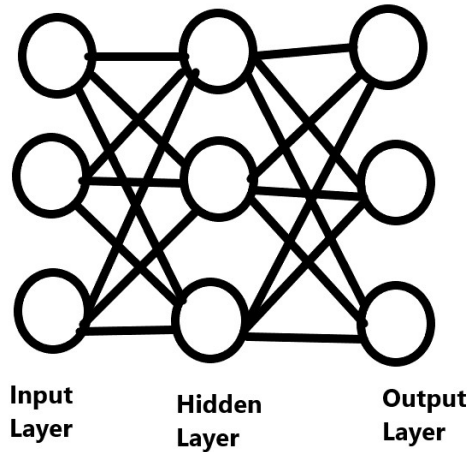


Figure 1.2: Basic Example of Artificial Neural Network

A basic example of an artificial neural network is shown in Figure 1.2. As shown in the figure, the network has an input layer, a hidden layer, and an output layer. Generally when creating these networks we determine the number of neurons in both the input and the output layers based on the different classifications we are trying to predict. The above network could be used to predict if an image is of a cat, a dog, or a fish for example. There can multiple hidden layers in an ANN and the number of neurons in each layer can be adjusted. In reality, artificial neural networks will typically be far bigger than the example given above in terms of neurons and hidden layers but for illustrative purposes, the above diagram will suffice. Each neuron will also have its own weight, bias, and an activation function which will determine whether a neuron fires or not. Common activation functions include ReLU (Rectified Linear Units), sigmoid function and tanh.

### 1.3 What is A Convolutional Neural Network? (CNN)

A convolutional neural network, or CNN for short, is a type of neural network which is primarily used for tasks involving image and pattern recognition [7]. The structure is similar to an ANN in which we have an input layer,  $N$  hidden layers, and finally an output layer. As with the Artificial Neural Network each of these layers will have an activation function and its own weights and biases to determine the final output for a given input. The model will take an image as input, the image is made up of vectors (RGB) or a similar format and from that image the model will determine certain patterns. For example, the output might be a classification of whether or not COVID-19 is present. This application will be discussed in more detail later in the dissertation.

There are a few ways in which CNNs differ from ANNs, in that they are comprised of three types of layers which are the convolutional layers, pooling layers, and fully connected layers[7].

The convolutional layer is responsible for extracting features from an image and generating a  $2D$  activation map, the pooling layer will reduce the parameters of a given input by means of downsampling, and finally the fully connected layers will then determine and classify the output for a given input. The convolutional layer's parameters utilize learnable kernels(a kernel acts as a filter used to extract features from images), and this layer also produces a  $2D$  activation map which will be used to determine if a neuron fires or not for a given input. We can adjust hyper parameters in the convolutional layer to greatly reduce the complexity of the model through optimization, which can be achieved by adjusting the following hyper parameters: depth, stride and zero padding.

Depth is related to the output volume produced by the convolutional layers in the model which can be manually set by adjusting the number of neurons in each layer. Reducing the depth of the model can greatly decrease the training time but at the expense of performance. Stride is related to the spatial dimensionality of the input which will determine the receptive field (every neuron is connected only to a small region of the input - this region is referred to as the receptive field[7]), if the stride is set to a low integer we will produce extremely large activations, and if it is set too high the network won't produce enough activations.

Finally, zero-padding will pad the border of the images ingested by the model with 0s, reducing their dimensionality. Padding is useful for increasing the accuracy of the model as it can possibly eliminate areas of the image which are not useful for the model and can also improve training time times in some use cases.[8]

Through the adjustment of the hyperparameters mentioned above, and through the utilization of different activation functions, the accuracy of the convolutional neural network can be improved through a process of trial and error.

## **1.4 Supervised Learning**

Supervised learning is a type of learning involving the use of labeled data to train the model[9]. The data is typically labeled manually by a data scientist, which can be a long and laborious process depending on a number of factors (size of the data, number of classes, etc.), but offers many benefits when it comes to training models. Supervised learning performs extremely well at tasks involving classification (classifying data into a given category), and regression (understanding the relationships between independent and dependent variables).

## **1.5 Unsupervised Learning**

Unsupervised learning is a type of machine learning which involves using unlabelled data to train machine learning models[9]. This type of machine learning requires no human intervention since the data is unlabelled and the model will detect relationships between data

based on the raw data fed in to the model. This type of machine learning is used for tasks such as: clustering (grouping data together based on shared characteristics or features), association (finding relationships between features), and dimensionality reduction (reducing the number of features in a given dataset without compromising the integrity of said data). The key differences between supervised and unsupervised learning are: labeled versus unlabeled datasets, and finding relationships in data (unsupervised) or trying to predict and classify data (supervised).

In this dissertation we examine the use of both labeled and unlabelled datasets to train and test the model.

## 1.6 Tensorflow

Tensorflow is an open-source library used for machine-learning and artificial intelligence research worldwide[10]. Tensorflow provides numerous modules and classes which form the foundation for building both the generative adversarial network and the convolutional neural network. There have been numerous case studies proving the efficacy of Tensorflow in solving many AI / ML problems and the library is used by research teams in organisations such as Google, Airbnb, ARM, Coca-Cola, Intel, and many more[11].

Given the reputation and widespread use of Tensorflow, and the vast amount of documentation around the framework, it seems an ideal library for the implementation of GANs and CNNs for this study.

## 1.7 Keras

Keras is a deep-learning framework for Python which provides a number of helpful functions and methods for creating and training the CNN[12]. Keras is built on top of Tensorflow and simplifies data loading, pre-processing and the overall building of the model. Keras is commonly used by data-scientists and researchers due to the powerful methods it offers and the time it saves. The additional classes and modules Keras provides on top of Tensorflow will help to reduce the time taken to build and develop of building both the convolutional neural network and the generative adversarial network.

Like Tensorflow, Keras has been used by a number of companies and is well recognised in the Artificial Intelligence community. Its uses include computer vision, natural language processing, generative deep-learning and reinforcement learning amongst others[13].

## 1.8 Background of Problem & Aims of This Paper

COVID-19 is a highly transmissible virus which has caused a worldwide pandemic and has claimed many lives. There have been 616,951,418 cases worldwide and 6,530,281 deaths as of the 4th of October 2022[14]. During the pandemic, Ireland alone had a total of over 1.6 million confirmed cases and nearly 8,000 deaths[15]. This has led many researchers to pursue the goal of automating the detection of COVID-19 to partially relieve the immense pressure put on medical staff throughout the pandemic.

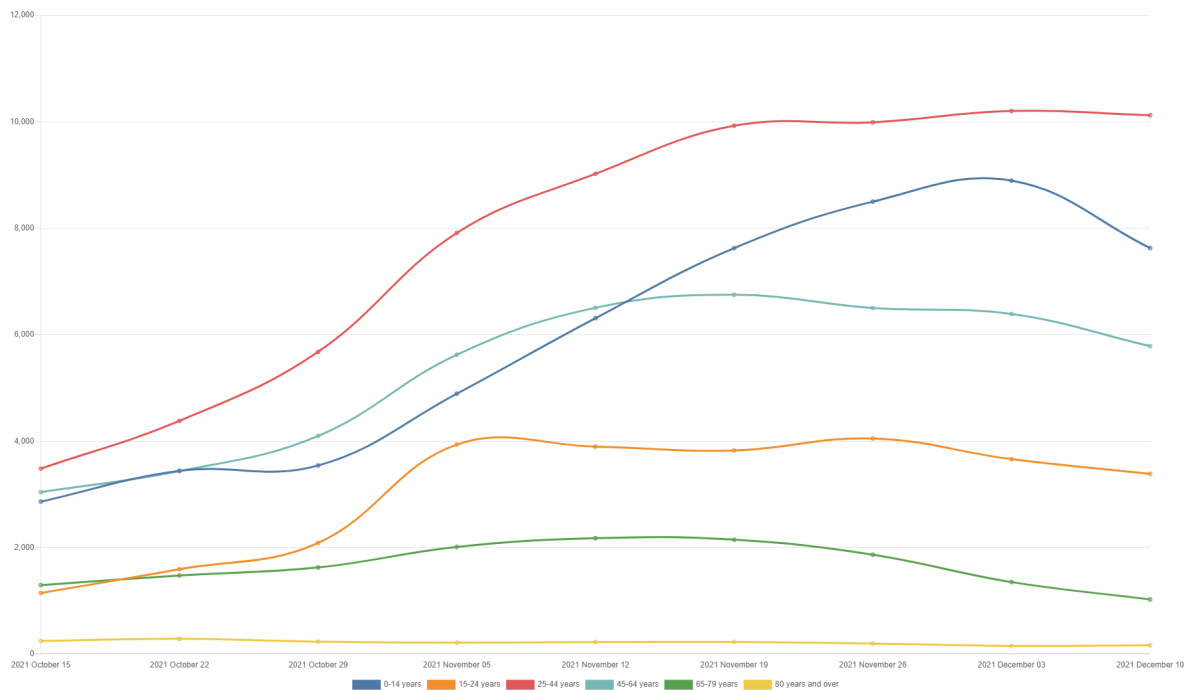
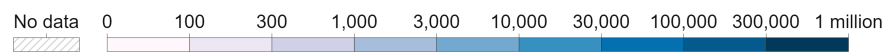


Figure 1.3: Graph of COVID-19 Statistics by age-range Ireland from October 2021 - December 2021 Courtesy of CSO[16]

Cumulative confirmed COVID-19 cases per million people, Oct 9, 2022  
Due to limited testing, the number of confirmed cases is lower than the true number of infections.

Our World  
in Data



Source: Johns Hopkins University CSSE COVID-19 Data

CC BY

Figure 1.4: Cumulative cases of the COVID-19 virus worldwide courtesy of Our World in Data[17]

The main objective of this research is to develop a robust model which can accurately analyze X-Rays of patients and determine from said X-rays if the patient is afflicted with COVID-19. This will be achieved by utilizing a number of different GAN architectures which will create realistic "fake data" which will then be used to train a number of models. From this training we plan to compare and contrast the results when generating data with different architectures to determine the best configuration for data generation to train the CNN model. There has been some success in utilizing convolutional neural networks to automate the detection of the virus[18][19]. Through the use of data augmentation utilizing a variety of GAN architectures, such convolutional models will be improved upon and made more accurate. We plan on utilizing existing data sets which are listed in the next section when training the Generative Adversarial Models, through trial and error we plan on determining the best architecture of GANs to use for training the model for this use-case.

## 1.9 Datasets

Before beginning the training of the model it is important to explore and understand each of the datasets. There are a total of three datasets which will be used in the course of this research, we will explain more about these datasets below.

### 1.9.1 COVID-19 Chest X-Ray

The COVID-19 Chest X-ray data set is a data set which is comprised of labeled X-Ray Images taken from a number of patients. This dataset contains 357 X-ray images of COVID positive patients, and Chest X-Rays of those afflicted with another disease (MERS, SARS, and ARDS). This dataset also includes a metadata file listing the diagnosis of the patient along with a number of other features.[20] In total this dataset contains 11 classes, the images do not have a consistent resolution which may cause issues as resizing each image may lead to a loss in image quality. The loss in quality will cause problems when evaluating the model's accuracy.

### 1.9.2 COVID-19 Radiography Database

The COVID-19 Radiography Database is made up of 3,616 images of chest X-Rays taken from COVID positive patients, 10,192 Images of lung X-Rays taken from healthy patients, and 1,345 X-ray images of viral pneumonia positive patients. All images in this dataset are PNG (Portable Network Graphic) images and are at a resolution of height 299 pixels and width 299 pixels eliminating the need for preprocessing of the images, the dataset also includes metadata for each of the images in this dataset showing a number of features with the diagnosis of the patient as well. The data in this dataset was gathered by a team of researchers from Qatar University, Doha, Qatar, and the University of Dhaka, Bangladesh along with their collaborators from Pakistan and Malaysia.[21]

### 1.9.3 COVID-19 Pneumonia Normal Chest X-Ray PA Dataset

The COVID-19 Pneumonia Normal Chest X-Ray PA dataset is comprised of a train set containing 74 Normal X-Ray Images taken from healthy Patients and afflicted with Pneumonia and a test set containing a Normal set containing 20 chest X-Rays taken from healthy patients and a Pneumonia set containing 20 images. The images in this dataset are unlabelled and no metadata is offered, however, the images are segregated into separate files listing the diagnosis.[22]

#### **1.9.4 Extensive COVID-19 X-Ray and CT Chest Images Dataset**

This dataset was added fairly late in the project due to data limitations in both the COVID-19 Chest X-Ray and the COVID-19 Pneumonia Normal Chest X-Ray PA Dataset. This dataset is comprised of 17099 X-ray and CT images which were generated with various augmentation techniques. Some of the images in this dataset come from the previously mentioned datasets namely the COVID-19 Pneumonia Normal Chest X-Ray PA Dataset and the COVID-19 Chest X-Ray. Given the large number of images in this dataset it may prove useful when training GANs to reproduce images as some of the other datasets have proven to lack the data needed to reasonably train a GAN to reproduce the X-Rays.

The dataset is broken up into two folders containing X-Rays and CT Scans respectively. Both folders contain images which are categorized into two further subfolders one containing COVID Positive X-Ray and CT-Scans and the other containing COVID negative X-Ray and CT scans[23].

#### **1.9.5 Use of datasets in This Project**

we plan to use each of these datasets to train and test the model and use data augmentation to increase the train and test sets by utilizing Generalized Adversarial Networks. When using these datasets in conjunction it is my hope that the GAN will have enough data to be effective when generating new sample images to train the final model.

### **1.10 Structure of This Thesis**

This thesis is broken into 5 chapters in total, this section will include the headings of the chapters and a brief summary of each chapter below:

#### **1.10.1 Chapter 1 - Introduction**

This chapter will offer the reader of this thesis a brief introduction to a number of core concepts which will be necessary to understand before diving deeper into this thesis. It is important that the reader has a basic understanding of generative adversarial networks, convolutional neural networks, artificial neural networks, supervised & unsupervised learning, and the overall question that this research proposes before discussing the implementation or discussing pertinent literature in this field.

In this section we will frame the research question, explain what a generative adversarial network is, its function, and how it works, We will also explain artificial neural networks and convolutional neural networks, and we will discuss the basic methodologies relating to the implementation of this project. We will also discuss the libraries used to implement the

practical artifact, datasets used to train the model and give the reader of this thesis a clear understanding of the key aims of this research.

#### **1.10.2 Chapter 2 - Literature Review**

In this section we will review pertinent literature related to the problem domain and discuss the ideas and concepts presented in these papers. We will also review the results from the research conducted in these papers and use them as a metric to gauge the performance of my own model. The papers will also be compared and contrasted and we will discuss the findings and how useful these papers were when conducting my own research. It is very important to understand the problem domain before beginning the implementation of this project to ensure that we are not "reinventing the wheel". This section will also provide the reader of this thesis with the most up-to-date progress made within the problem domain.

#### **1.10.3 Chapter 3 - Implementation**

In this section we will discuss the architecture of the convolutional model, the various architectures of generative adversarial networks implemented, how the models were trained and the overall design of the code implemented, and the rationale behind certain design choices. we will also show the results from training the models and discuss how through trial and error we were able to improve the various models and will include code samples so that the models can be reviewed by the reader or re-implemented by them.

#### **1.10.4 Chapter 4 - Results**

In this section, we will review the results achieved from training the best models and suggest how they may possibly be improved. we will be showing lots of graphs/tables in this section to gauge each model's test/dev set errors and we will also be comparing and contrasting the effects of the different GAN architectures implemented as well as discussing the results of the convolutional model.

#### **1.10.5 Chapter 5 - Further Research and Conclusions**

In this section, we will discuss further research that may need to be done by any researchers who would like to build upon this research. we will also review where the models could be improved and what we'd do differently if we were to conduct this research again. we will also discuss common issues we faced during the implementation of this project and how we overcame them. This section will be a summary of all the research conducted, the code, and my experience overall throughout the writing of this thesis.

This will be the final section of the paper and will tie the entire thesis together.

# **Chapter 2**

## **Literature Review**

### **2.1 Introduction**

The first reported cases of COVID-19 occurred in Wuhan, China on December 12th, 2019[24], when a number of patients began to exhibit "symptoms of an atypical pneumonia-like illness that does not respond well to standard treatments". It was not until December 31, 2019, that the World Health Organization(WHO) Country Office in China was informed of several more cases of this strange virus described as "pneumonia of unknown etiology", the symptoms of this new virus were shortness of breath and fever. All the initial cases observed seem to have been connected to a market called Huanan Seafood Wholesale Market. On January 1st of 2020, the Huanan Seafood Wholesale Market was shut down amid concerns over the spread of this new virus. On January 3rd the Government of China alerted the World Health Organization that they had identified over 40 new cases of this pneumonia-like disease, and on the 5th of January, Chinese public health officials shared the genetic sequence of the new virus with the world through a database that could be accessed by the public. Following the release of this information the CDC (Centers for Disease Control and Prevention), which is a US Government funded healthcare research agency, began an investigation into the origins of this new virus. The origins of COVID-19 are not clear and are still being researched. The most likely explanation offered by scientists is that it originated in the Huanan Seafood Wholesale Market from animals sold there - a likely culprit is the Raccoon Dog which is used for fur and food in China[25], but other theories suggest that a lab leak at a biological weapons facility[26] may be responsible for the creation of the virus. Some researchers are currently suggesting that blood samples taken from animals sold at the Hunan Market and samples from the people who sold them may lead to definitive evidence of the disease's origins[25]. Although the origins of COVID-19 still remain up for debate it is clear that when studying the virus, its high transmission rate and the speed at which it can spread made it one of the deadliest viruses in human history.[27][28]

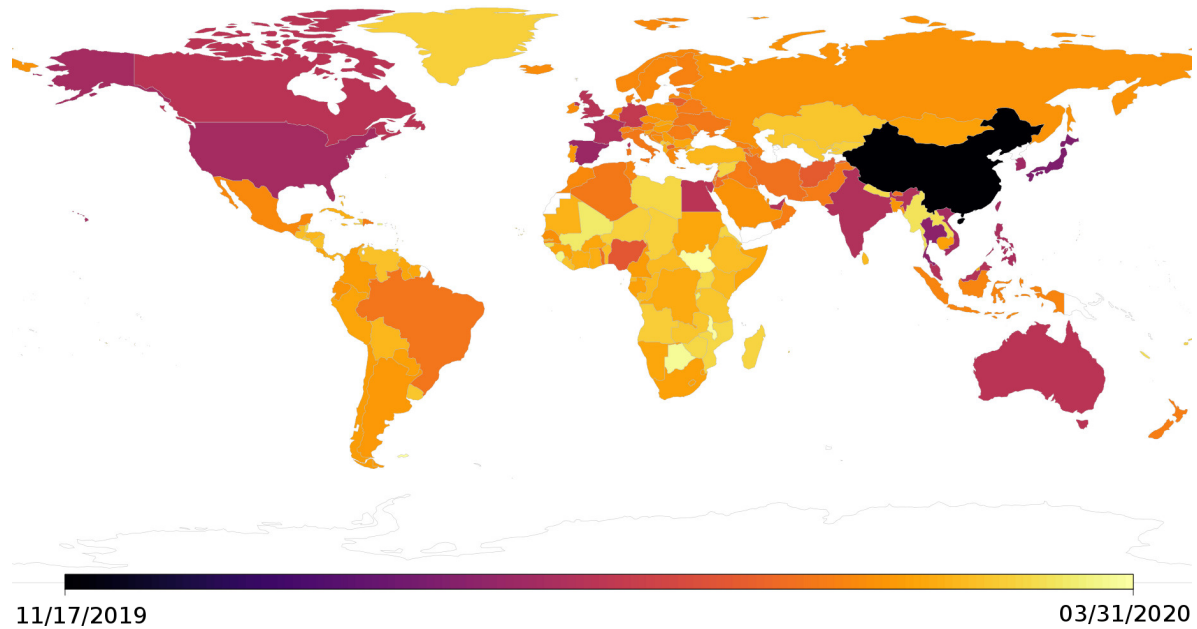


Figure 2.1: Estimated dates of first COVID-19 cases around the World, Image courtesy of Roberts, Rossman and Jarić[29]

Due to this rapid spread of the virus, many governments were unprepared for dealing with such an outbreak. The artificial intelligence community had published many papers and conducted much research into designing automated tools which could relieve medical professionals of the extreme stress they were under. Unfortunately, most of the models trained were of no use to medical professionals and some were even deemed harmful[30]. There were many limitations when it came to training automated diagnostic tools for COVID-19, such as incorrect assumptions about the data, lack of data quality, and lack of data in general. Due to the lack of quality data and the urgent need for diagnostic tools, many of the models were trained using poor-quality data or incorrect data. Such poor models would have had drastic effects if patients who were COVID positive were diagnosed as negative by the model, and models suffering from high false negative rates would have drastic consequences for the patients afflicted with COVID.

The models trained on what have been termed as "Frankenstein Datasets" suffered immensely, as some of the data came from the same source, meaning the same data from the training set could have been present in the test set. This would severely impact the performance of the model, as it would have to overfit the data from which it was trained. These models which were overfitted on the data would seem to have high accuracy but ultimately would perform poorly on real-world data.

|                                    | <b>Underfitting</b>  | <b>Just right</b>   | <b>Overfitting</b>  |
|------------------------------------|--|---|---|
| <b>Symptoms</b>                    | <ul style="list-style-type: none"> <li>• High training error</li> <li>• Training error close to test error</li> <li>• High bias</li> </ul> | <ul style="list-style-type: none"> <li>• Training error slightly lower than test error</li> </ul> | <ul style="list-style-type: none"> <li>• Very low training error</li> <li>• Training error much lower than test error</li> <li>• High variance</li> </ul> |
| <b>Regression illustration</b>     |  |   |   |
| <b>Classification illustration</b> |  |   |   |
| <b>Deep learning illustration</b>  |  |   |   |
| <b>Possible remedies</b>           | <ul style="list-style-type: none"> <li>• Complexify model</li> <li>• Add more features</li> <li>• Train longer</li> </ul>                  |   | <ul style="list-style-type: none"> <li>• Perform regularization</li> <li>• Get more data</li> </ul>   |

Figure 2.2: Examples of Overfitting, Underfitting and Optimal models, Image courtesy of Abhishek Shrivastava[31]

Figure 2.2 above shows how a model's performance can be analyzed. Underfitting yields a high training error and high bias meaning that the model will perform poorly on the training, test, and dev sets. Overfitting leads to a very low training error which will be lower than the test, and dev set error and wouldn't be fit for purpose when analyzing real-world data. The optimal model has a training error that is slightly lower or in and around the same accuracy as the test and dev sets.

The lack of medical experience also played a role in the poor performance of these models as many of the AI researchers training these models would be unfamiliar with flaws in the data. The bias of the radiologist labeling the X-rays of patients also played a role as the radiologist could have inaccurately diagnosed the patient as COVID positive or negative. Private Artificial Intelligence companies also played a role in poor model development as published models from researchers tied to the company also showed that these models had a

high risk of bias.[30]

As the pandemic progressed more and more data was made available to researchers which was able to mitigate some of the problems stated above, leading to more accurate and robust models which we will explore in the later sections.

## **2.2 Analysis of Existing Models for Automated COVID-19 Detection**

In a paper by Mahmoudi, Benamour et al [32] researchers investigated a deep-learning approach to creating a diagnostic tool for COVID-19. The research involved utilizing data taken from computed topography scans. These scans segmented the infected regions of a patient's lungs to determine if said patient was afflicted with the COVID-19 virus. The researchers also used a technique called contrast limited adaptive histogram equalization which is a pre-processing method that removes noise and intensity to create a homogeneous dataset. The researchers also removed black slices from the images so that only the region of interest was highlighted, further enhancing the performance of the model. U-Net architecture, which is based on convolutional neural network encoders and decoders, was used in the creation of this model to allow for more timely and accurate image segmentation to generate the lung and infection segmentation models. Four-fold cross-validation (where the dataset is sliced into four equal parts(depending on the size for odd datasets there may be set with the remainder of values if not equally divisible by four), then the model is trained on one or multiple sections, and tested with another section. The final model is taken from the model with the best performance) and was then used to analyze the performance of the model along with a three-layered CNN architecture which was comprised of additional fully-connected layers followed by a softmax output layer which was used for classification of the images.

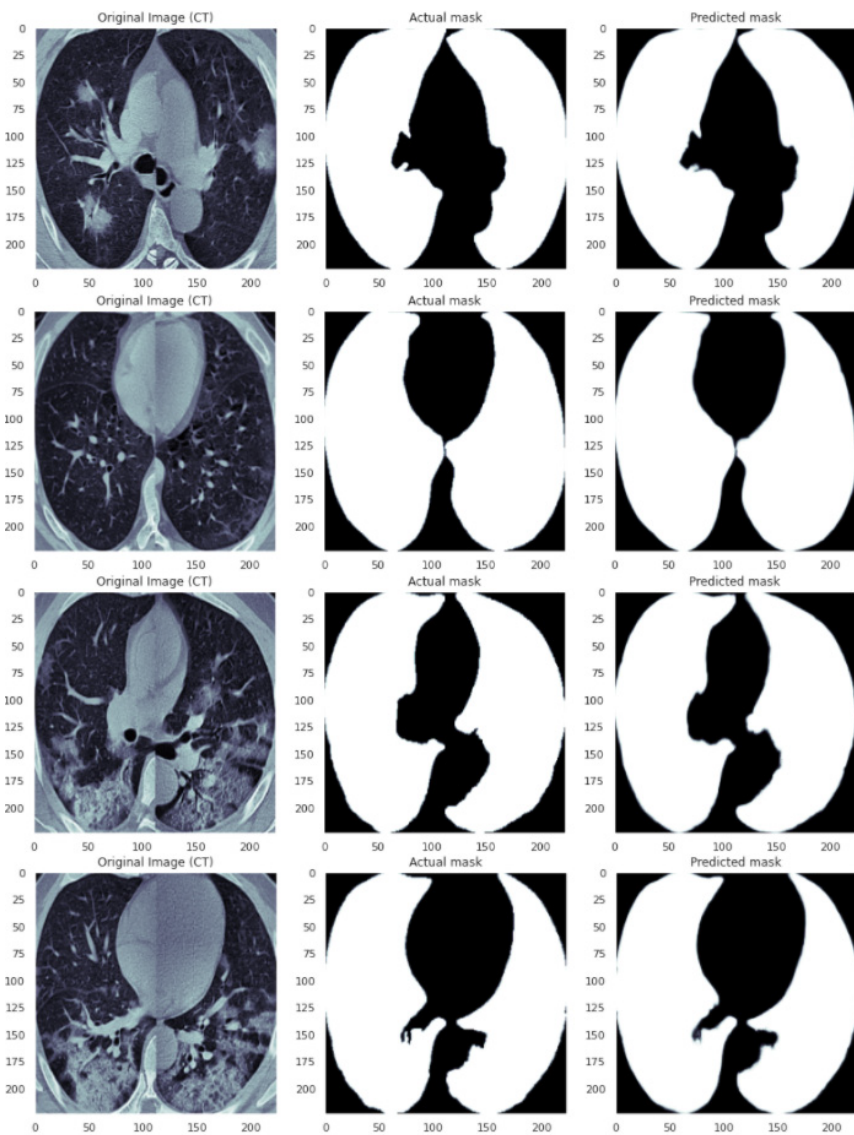


Figure 2.3: Examples of CT Qualitative images lung segmentation[32]

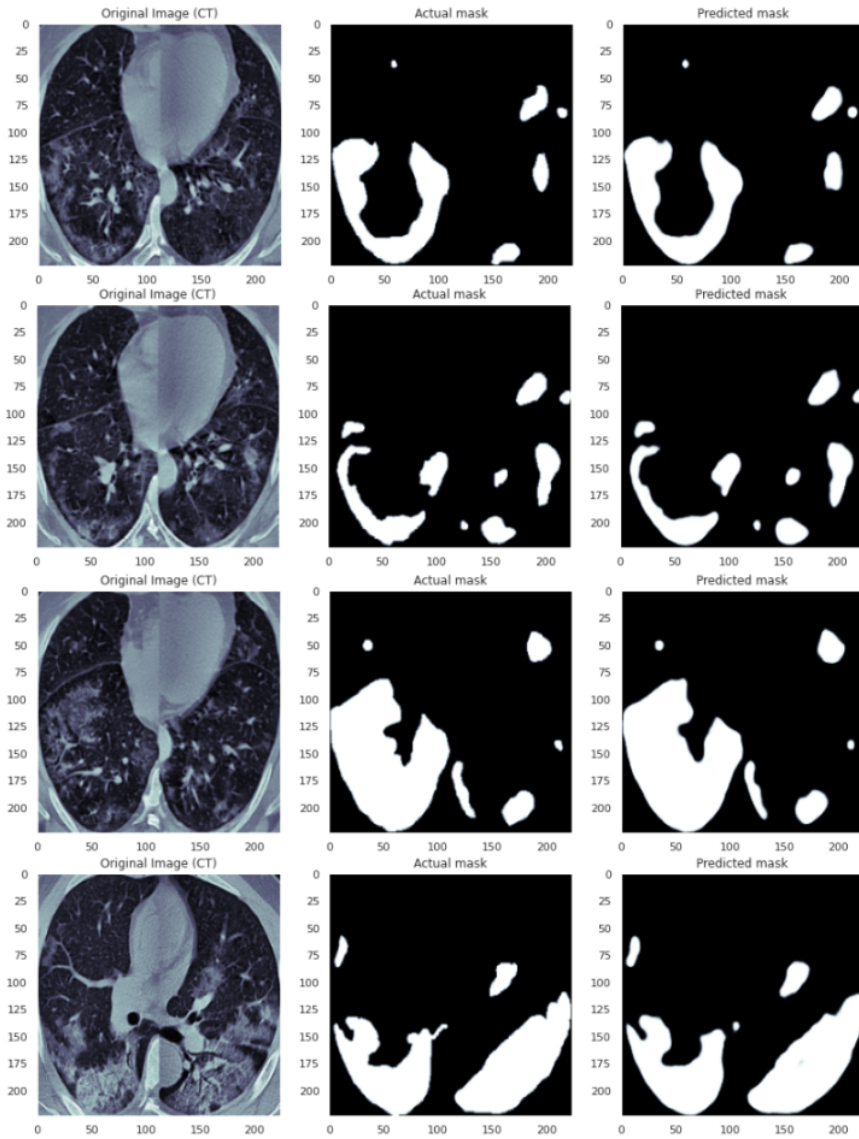


Figure 2.4: Examples of CT qualitative images infection masks[32]

Figure 2.3 shows the result of the lung segmentation results between the ground truth and the researchers' proposed four slice model, which is compromised of four slices taken from different CT scans. The first column shows the original CT scan, the second column shows ground truth, and finally, the third column shows predicted lung masks.

Figure 2.4 we can observe the qualitative comparison between the researchers' infection segmentation results which is made up of four slices from different CT scans and the ground truth. The first column shows the original CT scan, the second column shows the ground truth, and finally, the third column shows predicted infection masks

Utilizing a 70% - 30% training set and validation set split, the researchers demonstrated that the proposed system achieved a dice score (a value ranging from 0 - 1, used to gauge perfor-

mance by comparing the results of the output of the model to that of the ground truth, where 1 is a perfect overlap and 0 is no overlap) of 98% and 91% for lung and infection segmentation tasks. Additionally, the system accurately diagnosed patients afflicted with COVID-19 98% of the time. The development of this model suffered from a lack of data, as only 20 CT scans were used to train and test the model. The limited data set used suggests the researcher's model may have possibly been overfitting the training data. The researchers mention as much in the conclusion section of this paper. They discuss how the main limitation of the study is the use of a small but sufficient amount of training data. The restrictions on data collection coupled with the high cost of labelling the data meant that the researchers were only able to utilize the 20 CT scans for both training and testing the model. From the conclusion section of this paper, it is clear that there is a high potential for bias in the data set used by the researchers. The possibly mislabelled images links back to the "Frankenstein Datasets" which I mentioned in the introduction section of this literature review.

In another paper by Islam, Islam, and Asraf[33] we see a new method being used by researchers to develop an automated diagnostic tool. The researchers used a combination of a convolutional neural network with LSTM (long short-term memory), they used the convolutional neural network for deep feature extraction and LSTM for detection of COVID-19 using an extracted feature. They also used a dataset containing 4575 X-ray images which included 1525 images of COVID-19 X-rays. The experimental results of the system are as follows: 99.4% accuracy, AUC (area under curve) accuracy of 99.9%, specificity of 99.2%, sensitivity of 99.3% , and finally an F1 score of 98.9%. The researchers suggest that this system could be further improved in the abstract if more data were available to the researchers. As we can see this study also appears to suffer from a lack of data as per the previous paper discussed. The lack of data is clearly visible but by utilizing an LSTM network the researchers further improved upon the diagnostic model discussed in the previous paper by Mahmoudi et al. The dataset used was also greater in size than the dataset used in the prior paper, this would lead to a more robust model with a greater ability to generalize.

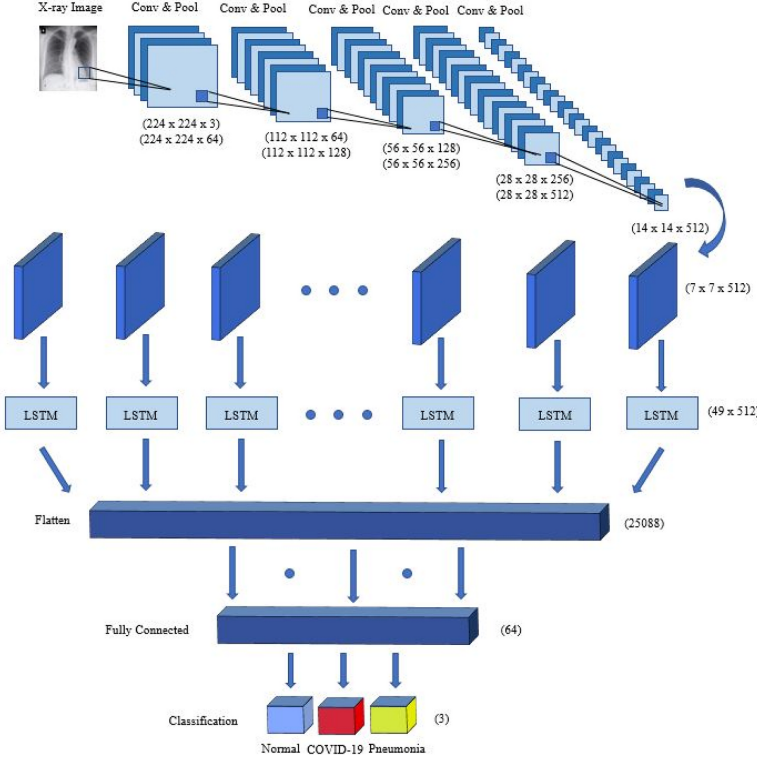


Figure 2.5: Overview of a Typical LSTM Network[33]

The model benefited from the use of LSTM, as an LSTM network has an internal memory that is utilized to learn from experience with long-term states. LSTM is based on recurrent neural networks, and improves upon them by using memory blocks instead of conventional RNN units, this helps to solve the vanishing and exploding gradient problem[34]. In addition to the memory blocks, there is also a cell state which saves long-term states, the cell states being the main difference between recurrent neural networks and LSTM. The network is capable of remembering and connecting previous information to present data[35]. The LSTM Network is comprised of three gates the input gate which is termed the "forget gate", an update gate, and finally an output gate. These gates essentially determine which data is worth remembering and which data can be forgotten.

The results achieved by the various models are shown in figure 2.6 and figure 2.7

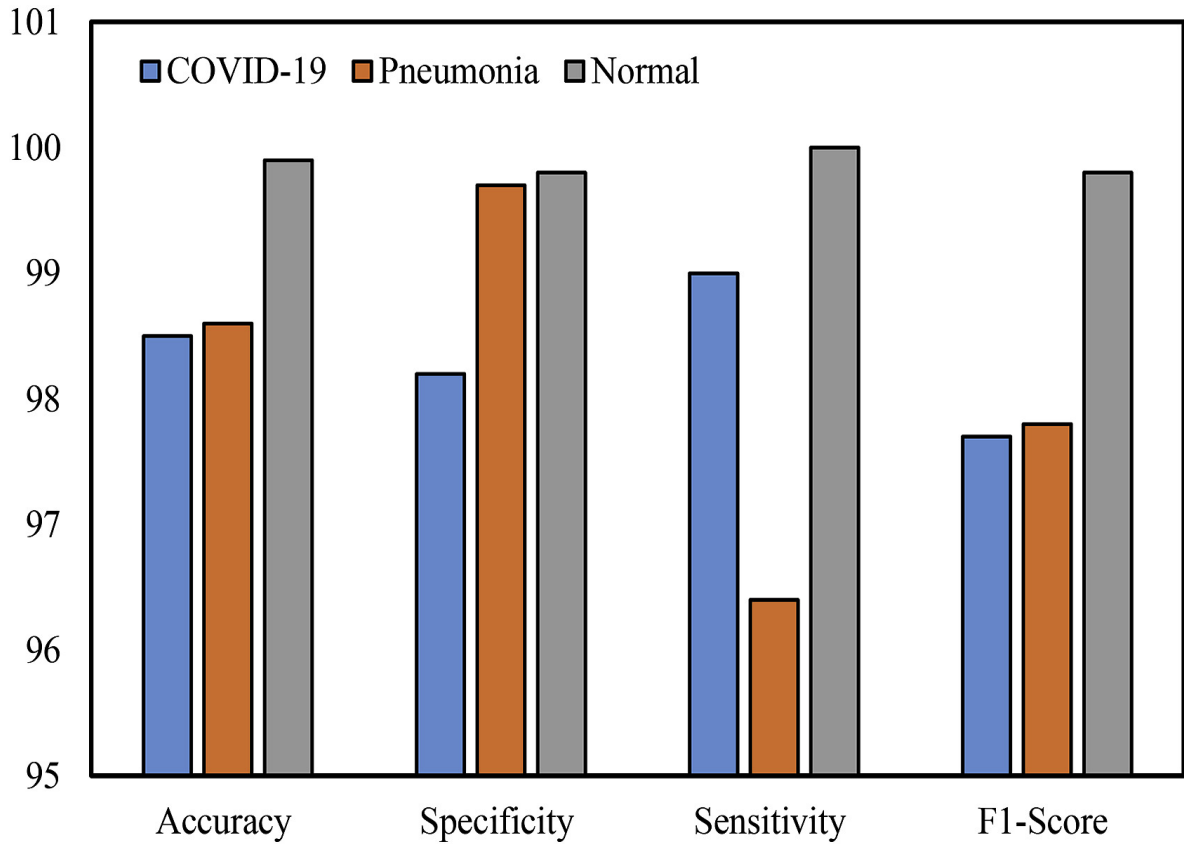


Figure 2.6: Perfomance of CNN model[33]

Figure 2.6 shows the performance of a standard CNN model the accuracy ratings are as follows:

| Class     | Accuracy | Specificity | Sensitivity | F1-Score |
|-----------|----------|-------------|-------------|----------|
| COVID-19  | 98.5     | 98.2        | 99.0        | 97.7     |
| Pneumonia | 98.6     | 99.7        | 96.4        | 97.8     |
| Normal    | 99.9     | 99.8        | 100.0       | 99.8     |

Table 2.1: Results of Standard CNN Network - A combined deep CNN-LSTM network for the detection of COVID-19 using X-ray images

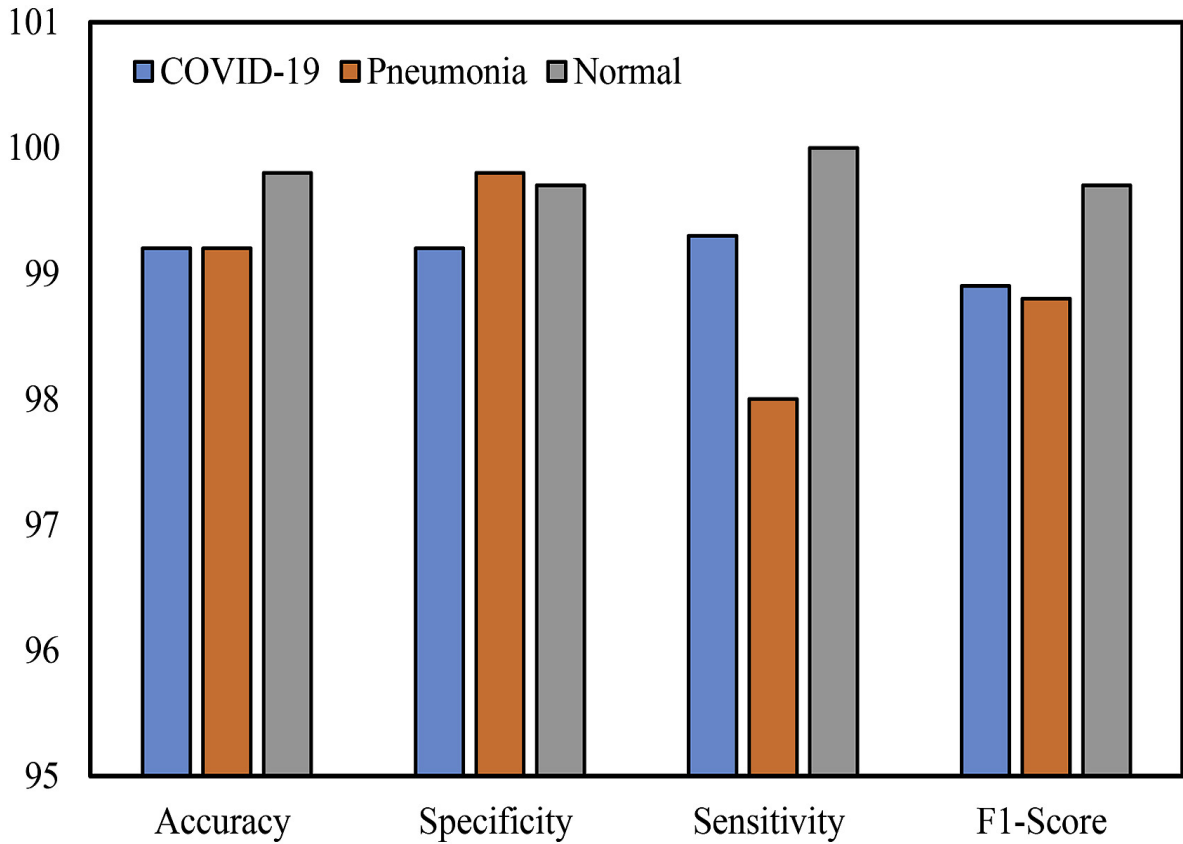


Figure 2.7: Performance of CNN LSTM Model[33]

| Class     | Accuracy | Specificity | Sensitivity | F1-Score |
|-----------|----------|-------------|-------------|----------|
| COVID-19  | 99.2     | 99.2        | 99.3        | 98.9     |
| Pneumonia | 99.2     | 99.8        | 98.0        | 98.8     |
| Normal    | 99.8     | 99.7        | 100.0       | 99.7     |

Table 2.2: Results of CNN - A combined deep CNN-LSTM network for the detection of COVID-19 using X-ray images

From figure 2.7 it is clear that the model utilizing LSTM outperformed the basic CNN model on almost all fronts (with the exception of classification of normal patients which experienced a small decrease in accuracy), yielding a higher accuracy, specificity, sensitivity and F1 score for identifying COVID-19, and Pneumonia from X-rays.

Despite the results achieved by the model, the final model suffers from lack of data which the researchers address in the conclusion section of this paper. The other shortcoming of this model is that it focuses on posterior-anterior view of X-Rays meaning that it cannot diagnose X-Rays which are in other formats. The authors of the paper also address that X-Rays, where the patient is afflicted with multiple diseases, cannot be efficiently classified by the model and the model's accuracy was not compared with that of radiologists. Data augmentation may

prove useful for such a model using a combination of CNN and LSTM.

### **2.3 Challenges & Limitations of Using Artificial Intelligence in Automated Diagnosis Systems for COVID-19**

In a paper by Huang, Yang and others, researchers offer an analysis of the challenges of developing Artificial Intelligence to aid in the diagnosis of COVID-19. As mentioned previously in this thesis the challenges include: lack of data, lack of data quality and the use of poorly merged data sets termed as Frankenstein data sets when training models. There are, however, more challenges that are faced when developing diagnostics tools, as discussed in the previously cited paper[33] it is very difficult to find people who are COVID-19 positive and asymptomatic due to them not getting treatment as no symptoms are apparent. The labelling of data is also an issue as the X-rays of patients may only show moderate signs of COVID-19 which yields a risk of mislabelled data by clinicians. There is also a risk of false positives and false negatives when developing a diagnostic tool. False positives would cause a patient to unnecessarily be quarantined and false negatives could cause a patient to inadvertently spread COVID-19 to others. Some patients who have already been infected with the virus may show no signs on CT images which also yield high false negative rates making it difficult to distinguish COVID positive patients from COVID negative patients.

To mitigate these challenges the researchers suggest that when developing an Artificially Intelligent diagnostic system the developer should combine chest imaging, exposure history and laboratory tests when training and testing the model. Such data, however, is hard to come by as there are multiple laws concerning data-collection and ethical questions regarding the patient's right to privacy.

### **2.4 Research into Data Augmentation And Convolutional Neural Networks Architectures**

Data augmentation allows artificial intelligence researchers to artificially inflate the size of the amount of data, this is done by utilizing existing data and detecting patterns in the data. From the original data, new data is produced using various methods such as rotating images, applying filters, altering various aspects of the image (such as padding, cropping, and zooming), etc. There are numerous techniques and methodologies for using data augmentation but for the purpose of this thesis we will be using Generative Adversarial Networks to create new data<sup>1.1</sup> for the purpose of improving upon existing automated diagnostic models for COVID-19. There are multiple different types of GAN architecture that have been covered in the introduction section of this thesis. The key advantages of using data augmentation

are as follows: larger training set to train models on, reduces overfitting and helps to prevent underfitting of the model, reduces costs / time of collecting new data, and increases the ability of the trained model to generalize. There are however some challenges when it comes to using data augmentation such as: inability to reduce bias of new data(if there is bias in the existing data the new data will also contain bias), hard to generate discrete data such as text, and the data generated will need to be evaluated.

In a paper by Tanaka and Aranha[36] the researchers outline two algorithms to oversample the minority class within the data with the aim of balancing the data set. These two methodologies are called SMOTE (Synthetic Minority Over-sampling Technique)[37] and ADASYN (Adaptive Synthetic Sampling Approach for Imbalanced Learning)[38].

SMOTE works by creating artificial samples based on the position of the data, it selects a random point in the least represented class of data and identifies data of the same class using the  $k$ -nearest neighbour algorithm which is a form of unsupervised learning. For each pair a new point is generated in the vector between the two pieces of data, the new point is then positioned at a random percentage away from the original point.[36]

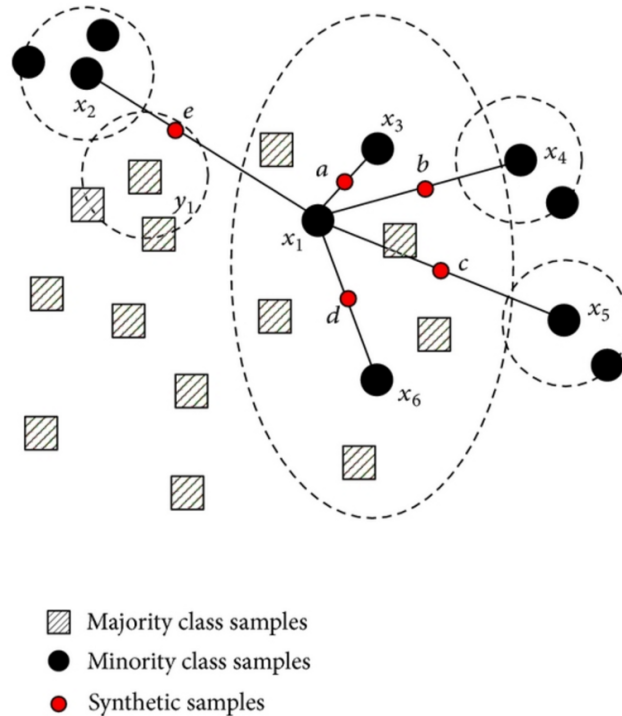


Figure 2.8: Example of SMOTE[37]

As we can see from figure2.8 the algorithm functions by detecting points between minority class samples, the points being determined by the  $k$ -nearest neighbour algorithm. This ensures that the newly generated data will be similar to the already existing data of the minority

class. This may prove useful when developing the Generative Adversarial Network to create synthetic COVID-19 X-Rays.

ADASYN works in a similar way to SMOTE and was originally based on SMOTE. Both function in much the same way but the key difference lies in ADASYN adding a random small bias value to the points, breaking linear correlation to their parents. The bias that ADASYN adds helps to increase the amount of variance within the synthetic data. In this research paper the authors decided to evaluate the utility of GANs to generate synthetic numerical data in two domains, one domain is concerned with training a classifier using purely synthetic data and the other domain to balance a data set by oversampling the minority class using synthetic data. The first domain's performance was measured by comparing the classifier's performance on the original dataset with the classifier's performance on the synthetic data set which will be created by variations in the GAN architecture. The researchers gauged the performance of the second domain by comparing the performance of the classifier on imbalanced data oversampled with a standard GAN, SMOTE, and ADASYN as well as the original data set which is not oversampled. SMOTE and ADASYN produce desirable results but the drawback is that they do not generalize well with sparse data and outliers according to the researchers.

In both experimental domains, the researchers used the following GAN architecture to generate the synthetic data

- Leaky ReLU as activation function with a negative slope of 0.2
- batch size of 5
- learning rate of  $2 \times 10^{-4}$
- use of dropout in the GAN generator with a probability of 0.3
- Binary cross-entropy as loss function
- Adam as the optimizer
- No convolution layers
- If the generator has more than one layer, they are ordered in ascending size
- In the discriminator, layers are ordered in descending size if there is more than 1 layer

[36] They also used the following architectures to generate the data:

| Data Set Name | Architecture of GAN   |
|---------------|---|
| Original Data | The first 70% of the original database                              |
| 256/512/1024  | Generated by a GAN with 3 hidden layers with size 256, 512 and 1024 |
| 256/512       | Generated by a GAN with 2 hidden layers with size 256 and 512       |
| 256           | Generated by a GAN with 1 hidden layer with size 256                |
| 128/256/512   | Generated by a GAN with 3 hidden layers with size 128, 256 and 512  |
| 128/256       | Generated by a GAN with 2 hidden layers with size 128 and 256       |
| 128           | Generated by a GAN with 1 hidden layer with size 128                |

Table 2.3: GAN Architectures used for experiments in[36])

choices in the above architecture are standard within the literature in this area. The performance of the GAN was then tested on 3 data sets which are listed below.

- Pima Indians Diabetes data Database
- Breast Cancer Wisconsin Data Set (Diagnostic)
- Credit Card Fraud Detection

Using these data sets the researchers conducted a number of experiments to judge the performance of data augmentation when testing the classifier. Experiment 1 involved training the classifier using the synthetic data generated by the GAN. The GAN was trained on the original data set for 1500 epochs. After training, the GAN was then used to generate synthetic data containing the same amount of data as the original data set. The classification label used by the GAN is a continuous value between 0 and 1, the value is then made discrete (either 0 or 1) by rounding it off to the closest integer. The synthetic data was then used to train a classification tree and the tree was then tested using the test subset of the original data set. The GAN was trained using labeled class data also, this means that the synthetic data can have any class and the GAN itself determines how data should be classified. The tests for experiment one were conducted on the diabetes and cancer data sets, these data sets were not very unbalanced in terms of classes. The findings of this experiment are visible in figure 2.9 where the researchers compared classes in the newly generated synthetic data with data in the original data set.

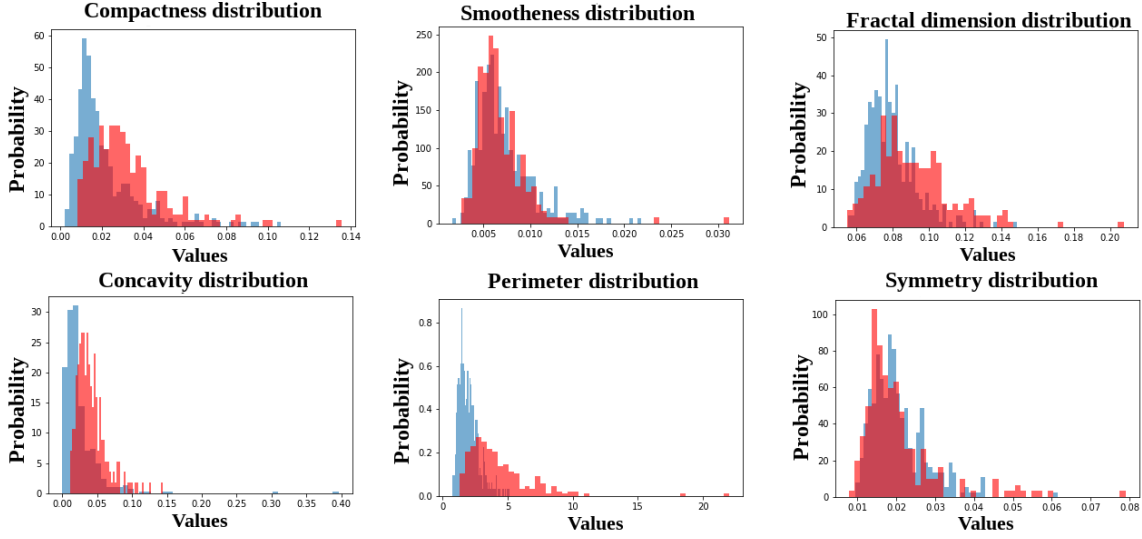


Figure 2.9: Results from Experiment One (Data Augmentation Using GANs)[36]

The blue region in the image2.9 represents the distribution of features in the original data set where as the red represents the distribution of features in the newly created synthetic data. Figure 2.9 shows that the synthetic data has a much more varied distribution. From using the synthetic data the researchers were able to obtain the following results shown in table2.4

| Database          | Label Proportion | Test Accuracy |
|-------------------|------------------|---------------|
| Original Data Set | 56.53/43.47      | 0.888         |
| 256/512/1024      | 52.26/47.74      | 0.818         |
| 256/512           | 56.28/43.72      | 0.941         |
| 256               | 56.78/43.22      | 0.906         |
| 128/256/512       | 54.02/45.98      | 0.953         |
| 128/256           | 58.04/41.96      | 0.935         |
| 128               | 54.27/45.73      | 0.912         |

Table 2.4: Results of Cancer data set using different GAN Architectures (Data Augmentation using GANs)[36]

These results indicate that classifiers trained with the synthetic data generated by the various GAN architectures had superior results than the classifier trained with the original data set. The only exception to this was the GAN with an architecture of 256/512/1024 which showed a small reduction in test accuracy.

| Database          | Label Proportion | Test Accuracy |
|-------------------|------------------|---------------|
| Original Data Set | 64.8/35.2        | 0.748         |
| 256/512/1024      | 71.69/28.31      | 0.7           |
| 256/512           | 67.23/32.77      | 0.548         |
| 256               | 67.6/32.4        | 0.748         |
| 128/256/512       | 60.15/39.85      | 0.661         |
| 128/256           | 65.18/34.82      | 0.739         |
| 128               | 54.27/45.73      | 0.697         |

Table 2.5: Results and label distribution of Diabetes data set using different GAN Architectures (Data Augmentation using GANs)[36]

The results of classifiers trained on the GAN architectures did not perform as well as those trained on the original data set when using the Diabetes data set. As we can see from the table above the classifiers trained using synthetic data struggled to match the performance of classifiers trained with the original data set. The GAN with the architecture of 1 hidden layer consisting of 256 units did manage to match the performance of the classifier trained on the original data set, the rationale for using the synthetic data would therefore be to increase the generalization of the model.

In the second experiment conducted by the researchers, they tested the oversampling of the minority class in the data set by using both SMOTE and ADASYN. The study proceeded as follows: The training set was separated based on the target class. The GANs were then trained only on minority-class data. The GAN was then used to add new synthetic data to the data set thus increasing the instances of the minority class. The researchers increased the instances of the minority class until the data set was balanced. The newly balanced data set was then used to train a classifier. The classifier was then tested on two data sets the original set and the balanced version which was created by undersampling the majority class. The results obtained from this experiment are shown in table 2.6

| Database  | Accuracy | Precision | Recall |
|-----------|----------|-----------|--------|
| Original  | 0.999    | 0.896     | 0.556  |
| SMOTE     | 0.958    | 0.026     | 0.861  |
| ADASYN    | 0.958    | 0.026     | 0.861  |
| 128       | 0.798    | 0.051     | 0.806  |
| 256       | 0.986    | 0.077     | 0.789  |
| 128 / 256 | 0.974    | 0.045     | 0.82   |
| 256 / 512 | 0.964    | 0.033     | 0.808  |

Table 2.6: Classification results on imbalanced test set (Data Augmentation using GANs)[36]

| Database  | Accuracy | Precision | Recall |
|-----------|----------|-----------|--------|
| Original  | 0.782    | 1.0       | 0.565  |
| SMOTE     | 0.912    | 0.959     | 0.861  |
| ADASYN    | 0.921    | 0.979     | 0.861  |
| 128       | 0.807    | 0.89      | 0.806  |
| 256       | 0.894    | 0.998     | 0.789  |
| 128 / 256 | 0.902    | 0.981     | 0.82   |
| 256 / 512 | 0.888    | 0.962     | 0.808  |

Table 2.7: Classification results on balanced test set (Data Augmentation using GANs)[36]

It's clear from the tables above the use of SMOTE and ADASYN underperformed in accuracy on the imbalanced test set but had higher recall when compared with the original. In the second table, when tested on the balanced test set, SMOTE and ADASYN outperformed the original in terms of accuracy and recall. This is due to the original data set being imbalanced, the tree trained on this data set predicts almost all samples as negative. The GAN using a hidden layer of 128 performed very poorly in both instances when compared with other GAN architectures and this is called out by the researchers in the paper. Oversampling the minority seemed to increase the recall score of the classifier but at the expense of precision. The results shown above will prove useful in guiding the development of the architecture used in the GANs to generate synthetic COVID data, and to over sample the minority of the classes within the various datasets I plan on using to train the classifier, this will be discussed further in later chapters.

Through this research, the researchers found that when dealing with very unbalanced test sets, the GAN outperformed both SMOTE and ADASYN when it came to accuracy and precision but had a lower overall recall score. Depending on the context of the problem domain accuracy and precision may be preferred over recall or recall may be preferred over accuracy and precision.

When developing the GANs for generating synthetic data to train COVID-19 classifier, there are questions that will need to be answered when deciding to use SMOTE and ADASYN over a traditional GAN architecture. A higher accuracy and precision would be useful in diagnosing COVID-19 in all patients while reducing the risk of unnecessary quarantining due to false positives. However, a higher recall would yield a higher overall identification of COVID positive patients but at the expense of precision, this would help to reduce the transmission of the virus but at the expense of causing unnecessary quarantines of patients.

There are a few limitations the researchers of this paper addressed in this study. The research was conducted using only three data sets it is unclear if the results found in the paper will be similar when utilizing other data sets. There are also many other considerations to take into account when using GANs, such as mislabelled data, the size of the dataset, amongst other

factors which may influence the creation of the synthetic data.

In another paper, by Wang and Xiao[39] a convolutional neural network was used in order to detect defects in harvested lychee fruit. The data set used was then augmented with synthetic data generated with a GAN. To train the classifier and the GAN, researchers created a data set of 3743 samples which were divided into 3 categories: mature, defects, and rot. The data set created by the researchers suffered from an imbalance much like the data set in the paper previously discussed[36]. To address the imbalance within the data set the researchers used a transformer-based GAN to augment the data and create a more diverse and balanced data set which was used to train the classifier to classify the lychee fruit. The researchers created three deep convolutional neural network models which included SSD-MobileNet V2, Faster RCNN-ResNet50, and Faster RCNN-Inception-ResNet V2. The models were trained with different settings to evaluate and contrast their performance. The researchers found from the evaluations of the models that the data augmentation did in fact increase the performance of the classifiers.

There is much need for automation within this particular domain as human fatigue can affect the classification of lychee fruit and incorrect classification of lychee is costly to businesses both in monetary terms and in terms of reputation. This problem domain within artificial intelligence has been extensively studied, commonly used methods for detecting defects within fruit are: region growing method, minimum outer rectangle method, threshold segmentation, edge detection,  $k$ -mean clustering, and contour finding[39]. Recent progress made in the field of deep learning has demonstrated superior results in a wide range of computer vision tasks among other tasks. Through the use of a DCNN the authors of this paper [39] hope to show superior performance in comparison to traditional machine learning methods currently in use. The researchers decided to use black leaf lychee samples purchased in two batches from Jiang-bei fruit wholesale market in Huzhou city which is located in Guangdong, China when comprising the data set. The first batch contained 2042 mature lychees, which contained 1216 sample which had cracks but had no signs of rot. To gather rot samples for the data set the researchers placed 625 cracked lychee samples in a dry environment at room temperature so they rotted naturally. 495 samples were exposed to sunlight until dry and rotted. The second batch contained 865 lychees that were used as a test sample. The two batches were then placed in foam boxes with ice packs for freshness and shipped back to the researcher's lab to maintain the fruit's freshness. Data diversity was accomplished by gathering lychee images at six locations in Huizhou College at various times, the images were also taken from different angles. A total of 5014 images were collected for the data set by the researchers.

When training the neural network the researchers used data augmentation to reduce the risk of overfitting the model and to improve generalisation. The training set was augmented with synthetic data generated by the GAN below is a table of the distribution of categories from the original data set which the researchers were using to train the model.

| Category | Original | Original Percentage | Training | Test | Generated | Augmented Training set |
|----------|----------|---------------------|----------|------|-----------|------------------------|
| Mature   | 1648     | 44.03%              | 1298     | 350  | 102       | 1400                   |
| Defects  | 964      | 25.75%              | 700      | 164  | 600       | 1400                   |
| Rot      | 1331     | 30.22%              | 896      | 235  | 504       | 1400                   |
| Total    | 3743     | 100.00%             | 2994     | 749  | 1206      | 4200                   |

Table 2.8: Comparison of distribution of data augmented vs original(lychee Surface Defect Detection Based on Deep Convolutional Neural Networks with GAN-Based Data Augmentation)[39]

As shown in the table above the augmented data offers a much more balanced dataset with all classes of lychee being represented in equal proportion. Classifiers trained on the original dataset may have possibly created a model which would create a high bias for the most represented class of lychee in the dataset.

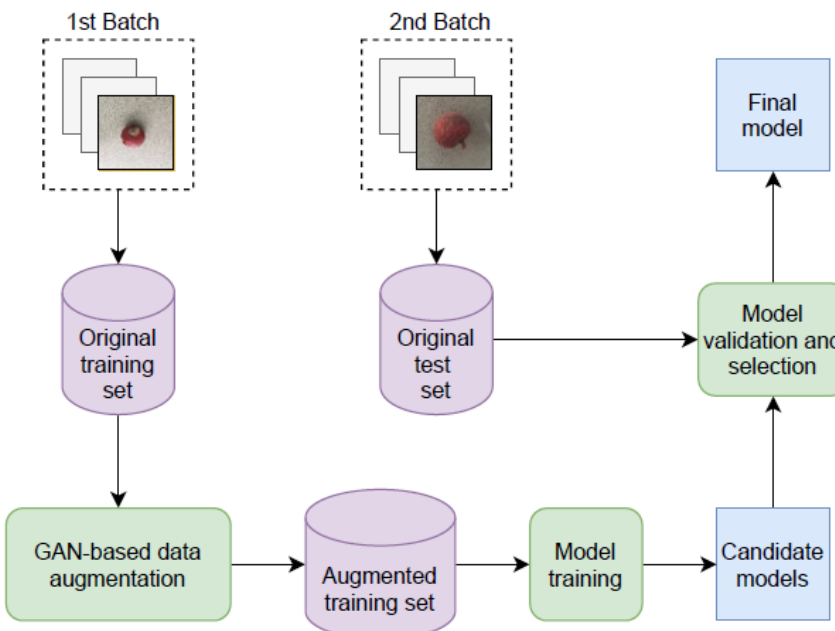


Figure 2.10: Figure of learning framework for lychee Classification Model[39]

Figure 2.10 shows the overall configuration of the learning framework for the lychee surface defect detection model. The original training set was used to train the GAN and from the newly augmented training set the DCNN models were trained to detect defects. The DCNN models were then validated on a test set to compare each model's performance.

In this paper, the researchers decided to use a variation of GAN known as TransGAN. This version of a GAN is based on purely transformers without the use of convolutions. This version of a GAN consists of a transformer encoder which is made up of a multi-head self-

attention module stacked by a feed-forward multilayer perceptron. This version of a GAN has traditionally been used for natural language processing but has also found applications in computer vision. In this version of a GAN both the generator  $G$  and discriminator,  $D$  are created using transformer encoder blocks. TransGAN has a multi-stage mechanism that will progressively upscale and downscale the image resolution to prevent excessive memory consumption. There is also a grid self-attention module which is developed for the first partition, this is used to reduce the computational load. TransGAN has shown superior results in generative modeling and hence was adopted by the researchers.[39][40]

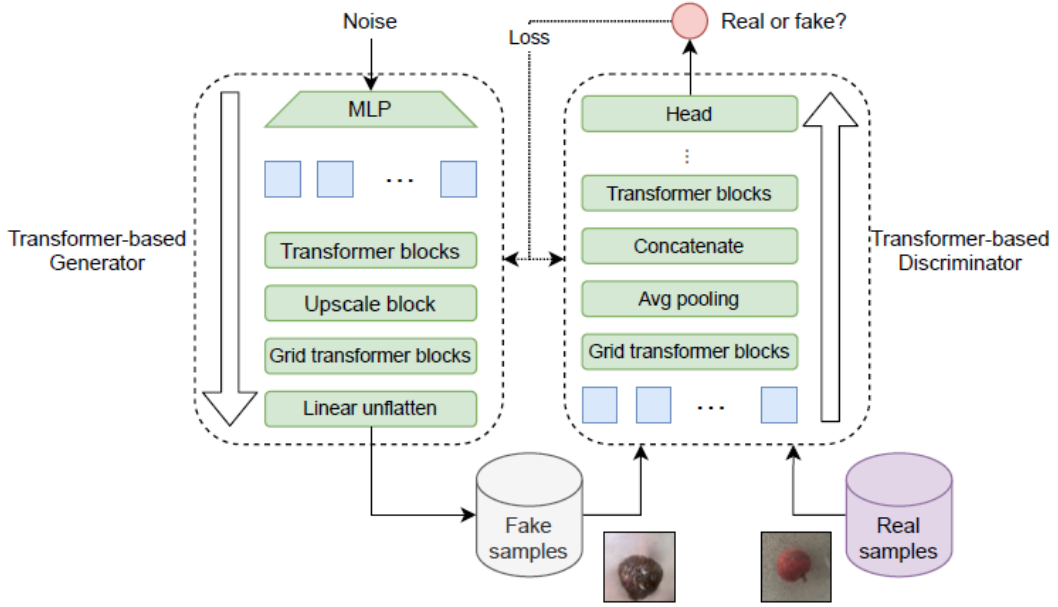


Figure 2.11: Figure of TransGAN (lychee Surface Defect Detection Based on Deep Convolutional Neural Networks with GAN-Based Data Augmentation)[39]

There are a variety of DCNNs used in this paper, we will show diagrams used by the researchers and explain each before further investigating the results of this paper as it's important to understand how each DCNN functions and compare each model's advantages and disadvantages.

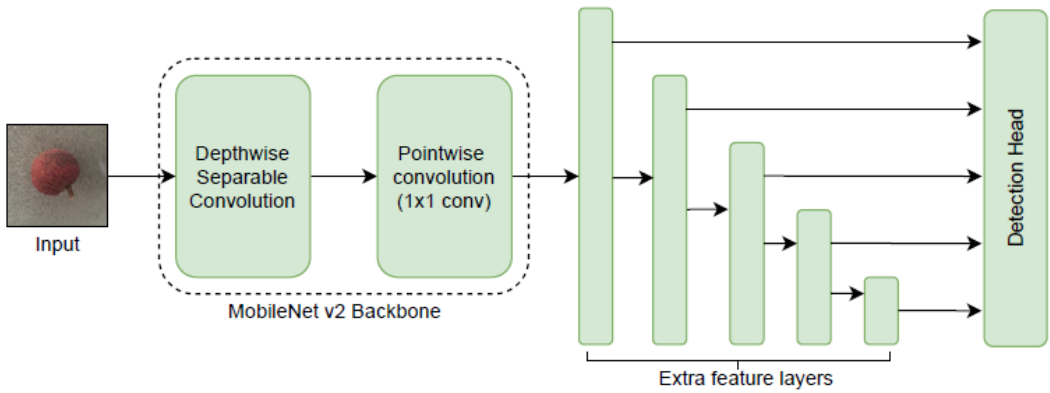


Figure 2.12: Figure of SSD-MobileNet V2 Architecture (lychee Surface Defect Detection Based on Deep Convolutional Neural Networks with GAN-Based Data Augmentation)[39]

Figure 2.12 shows an example of an SSD-MobileNet V2 DCNN as shown the input goes through a depthwise separable convolution and a pointwise convolution. The goal of SSD is to perform object localization and classification in a single forward pass of the network. SSD uses multi-scale feature mapping which allows the neural network to simulate the process of the human eye when detecting and classifying objects. MobileNet is a lightweight deep neural network which has proven to be efficient at performing a number of tasks. The model consists of two hyper-parameters, a width multiplier, and a resolution multiplier. These hyperparameters can be tuned to yield a higher latency or a higher accuracy for speed. Batch Normalization and a ReLU activation function are added after each convolutional layer. The original version of the MobileNet (V1) consisted of an input layer, 13 convolutional layers, an average pooling layer and a fully connected layer[39]. In MobileNetV2 two new features were added, a linear bottleneck between layers and a shortcut connection between bottlenecks which allowed for more efficient training.

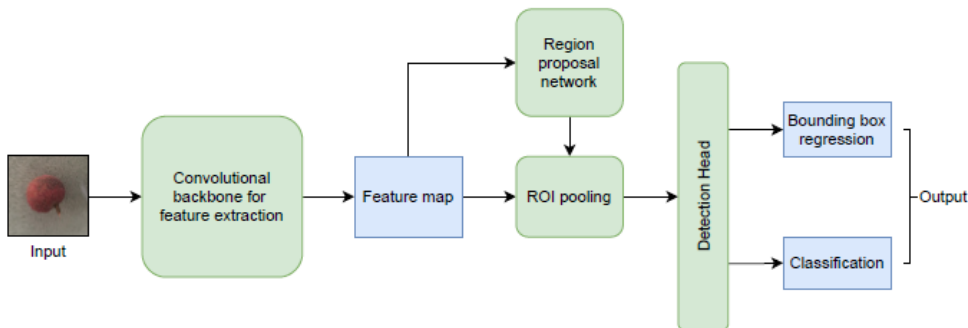


Figure 2.13: Figure of Faster RCNN Architecture (lychee Surface Defect Detection Based on Deep Convolutional Neural Networks with GAN-Based Data Augmentation)[39]

Figure 2.13 shows the architecture of an RCNN-ResNet50 DCNN, this model was originally proposed by Girshick et al in a 2014 paper [41]. This proposed DCNN model performs a selective search and extracts 2000 regions from a given image, the regions extracted are called region proposals. Candidate region proposals are warped into a square and then passed into a CNN that generates a 4096 dimensional feature vector, this feature vector is then passed to a support vector machine for classification. This model is not suited for real time detection as the researchers found it took approximately 47 seconds to classify a single image, if using this architecture in the COVID-19 diagnostics CNN model there might possibly be a trade-off in terms of time and accuracy. Due to the long time taken to classify an image, the researchers proposed a new architecture aptly termed "Faster RCNN" which would eliminate the selective search and instead input the entire image into the CNN to produce the convolutional feature map. This architecture does not have to process 2000 proposals every time it classifies an image, which reduces the amount of time taken by the model to classify the image.

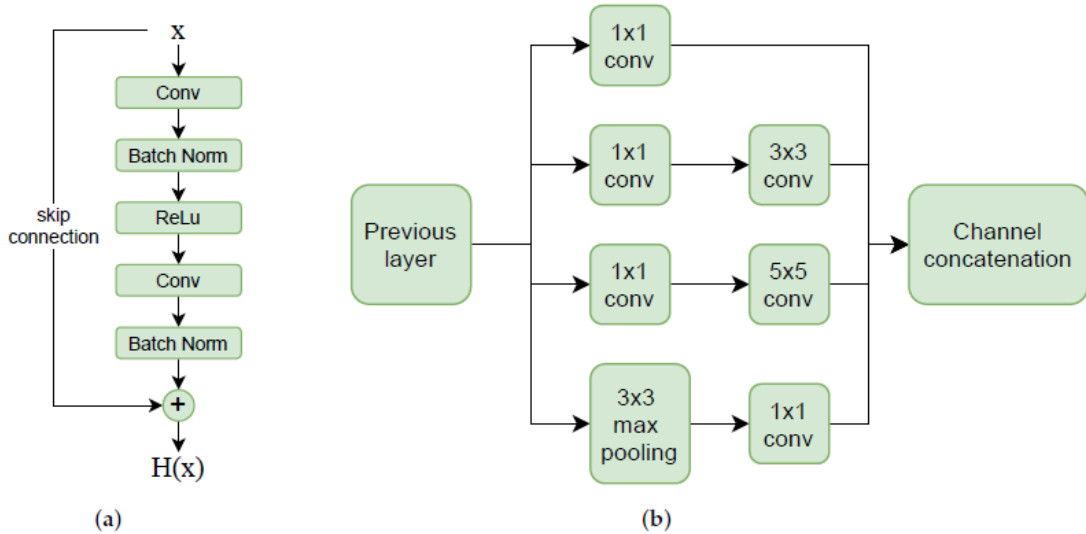


Figure 2.14: Figure of Faster RCNN Res Block and Inception Module (a) Res block; (b) Inception Module. (lychee Surface Defect Detection Based on Deep Convolutional Neural Networks with GAN-Based Data Augmentation)[39]

The final model proposed by the researchers aims at including an inception model to offer superior local topology for the neural network. The module (b) which is shown in figure 2.14 performs multiple convolutional operations on the image input to the model in parallel and combines all the results into a deep feature map. The model uses different filters to perform convolution operations on the input and obtains different information about the image. Processing all the operations in parallel and combining the feature maps allows for a much better image representation.

The researchers used the following configuration to train the TransGAN to generate synthetic data

- Learning rate of  $1 \times 10^{-4}$
- Adam as an optimizer
- batch size of 64 for both the generator and discriminator models
- The training ran for 220 epochs

The DCNNs were then trained on both the original and augmented training sets, training 6 different models in total. Each trained model took an image as input and output a box for each detected lychee with a predicted category along with a confidence score. The hyperparameter settings for each model were as follows:

- Weight decay of  $5 \times 10^{-4}$
- Momentum of  $8 \times 10^{-1}$
- Verification Period of 5000
- Batch Size of 32
- Learning Rate of  $5 \times 10^{-3}$
- And ran for a total of 1500 epochs

The results before augmentation for the models are shown in the table below 2.9

| Name of Model                   | Accuracy |
|---------------------------------|----------|
| SSD-MobileNet V2                | 89.95%   |
| Faster RCNN-ResNet50 V2         | 91.57%   |
| Faster RCNN-Inception-ResNet V2 | 91.25%   |

Table 2.9: Results of models before Augmentation(lychee Surface Defect Detection Based on Deep Convolutional Neural Networks with GAN-Based Data Augmentation)[39]

The researchers found that training on the GAN-augmented data that the performance increased by the following amounts for each of the models.

| Name of Model                   | Performance Gain |
|---------------------------------|------------------|
| SSD-MobileNet V2                | 2.86%            |
| Faster RCNN-ResNet50 V2         | 1%               |
| Faster RCNN-Inception-ResNet V2 | 0.58%            |

Table 2.10: Improvement of model accuracy after Augmentation(lychee Surface Defect Detection Based on Deep Convolutional Neural Networks with GAN-Based Data Augmentation)[39]

As we can see from the above table 2.10 SSD-MobileNet V2 had the most gains in terms of performance. Due to the large imbalance between classes in the dataset the performance gap is quite large. The mean average precision performance gaps between classes before augmentation is shown in the table below 2.11

| Name of Model                   | Mean Average Precision |
|---------------------------------|------------------------|
| SSD-MobileNet V2                | 9.45%                  |
| Faster RCNN-ResNet50 V2         | 6.12%                  |
| Faster RCNN-Inception-ResNet V2 | 7.77%                  |

Table 2.11: Mean average precision before Augmentation(lychee Surface Defect Detection Based on Deep Convolutional Neural Networks with GAN-Based Data Augmentation)[39]

After the augmentation process, the researchers found that the mean average precision performance gaps between classes were reduced for each of the three models to the values shown in table 2.12

| Name of Model                   | Mean Average Precision Performance |
|---------------------------------|------------------------------------|
| SSD-MobileNet V2                | 1.78%                              |
| Faster RCNN-ResNet50 V2         | 4.45%                              |
| Faster RCNN-Inception-ResNet V2 | 2.35%                              |

Table 2.12: Mean average precision after Augmentation(lychee Surface Defect Detection Based on Deep Convolutional Neural Networks with GAN-Based Data Augmentation)[39]

As we can see from the above values the augmentation process yielded better quality models that can better differentiate between the three classes of fruit (rotten, defective, and mature). The model which has shown the most improvement in terms of mean average precision was Faster RCNN-ResNet50, however the researchers found that Faster RCNN-Inception-ResNet V2 was the most accurate in detecting rotten samples.

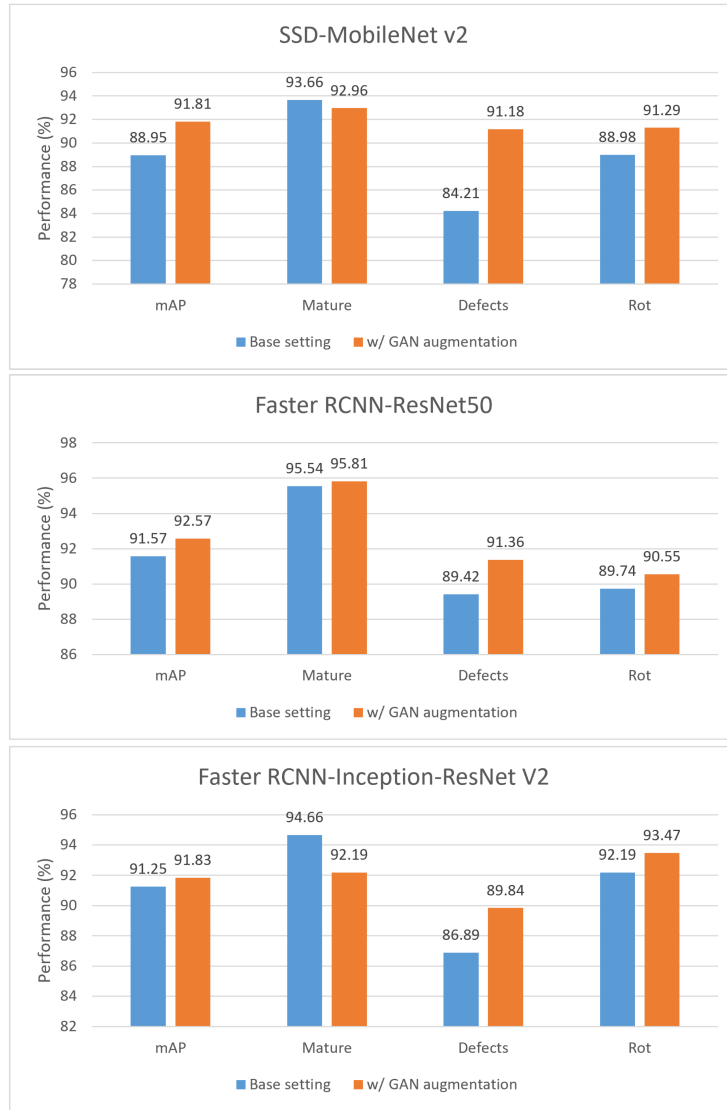


Figure 2.15: Figure of Mean Average Precision of Models. (lychee Surface Defect Detection Based on Deep Convolutional Neural Networks with GAN-Based Data Augmentation)[39]

Given that detecting defects in lychee is a time-sensitive job the researchers compared each of the three models in terms of detection speed. This is also a significant factor when developing the diagnostic models for detecting COVID-19 as the sooner the virus can be detected the sooner it can be treated effectively.

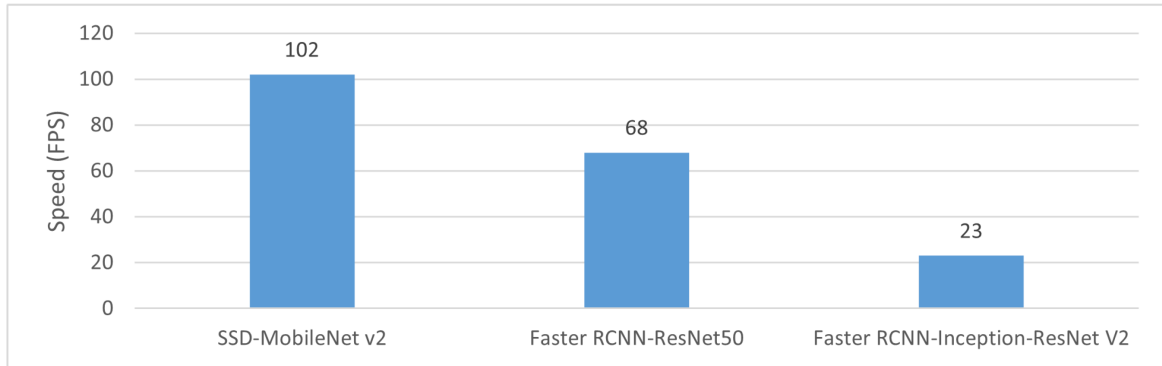


Figure 2.16: Figure of Speed of Models in classifying lychee. (lychee Surface Defect Detection Based on Deep Convolutional Neural Networks with GAN-Based Data Augmentation)[39]

As we can see above SSD-MobileNet V2 classifies the lychee faster than the other two models although all 3 models met the researcher's requirement for lychee defect detection. These results are of particular interest and may prove useful when designing the automated diagnosis tool for COVID-19. SSD-MobileNet V2 could perhaps diagnose the patients faster than the medical professionals analyzing the patient, thus freeing up time for medical professionals to assist other patients.

I will list the accuracy of each of the models with and without data augmentation below to compare and contrast the classification performance.

| Model                           | Setting          | Acc    | Rec    | Spe    | F1     |
|---------------------------------|------------------|--------|--------|--------|--------|
| SSD-MobileNet V2                | Base setting     | 89.81% | 90.08% | 89.89% | 89.46% |
|                                 | GAN Augmentation | 91.96% | 92.06% | 91.99% | 91.92% |
| Faster RCNN-ResNet50.50         | Base Setting     | 91.82% | 92.23% | 91.95% | 91.72% |
|                                 | GAN Augmentation | 92.76% | 92.96% | 92.80% | 92.55% |
| Faster RCNN-Inception-ResNet V2 | Base Setting     | 91.96% | 92.07% | 91.98% | 91.54% |
|                                 | GAN Augmentation | 92.36% | 91.74% | 92.22% | 91.86% |

Table 2.13: Comparison of accuracy of base models vs models with data augmentation(lychee Surface Defect Detection Based on Deep Convolutional Neural Networks with GAN-Based Data Augmentation)[39]

As shown in the above table 2.13 all of the models had better accuracy, recall(with the exception of Faster RCNN Inception model), specificity and F1 score with the data augmented data set. This shows that the classifiers were more accurate when classifying the fruit when they were trained on a more balanced data set.

## 2.5 Conclusion

From analyzing existing models for the automated detection of COVID-19 it appears that data quality and data shortage are key areas where improvements could be made to improve the overall accuracy and usability of the existing models. From the analysis of the current paradigms in convolutional neural networks and data augmentation of this thesis it is clearly shown that data augmentation has proven very useful in a wide range of applications which range from detecting defects in lychee to identifying credit card fraud. Given the positive results shown in the given problem domains, it seems a reasonable conjecture that the use of data augmentation would also prove useful for COVID-19 detection. In the next sections of this thesis, I will discuss the implementation methods used when creating both the convolutional models and the data augmentation models, the results of the models implemented, and further research which could be conducted into this area. It will be interesting to see if the findings of the papers explored above are transferable to this new problem domain.

# Chapter 3

## Implementation

### 3.1 Introduction

Initially, when starting the development of this model, we looked at various tools and options to implement the model in code. We settled on using Jupyter Notebooks along with a number of libraries to help make the development of this model easier and faster. The useful thing about Jupyter Notebooks is that they can be opened in a browser and all the code can be run from a single page. We will detail the development of this model both in this thesis and include notes in the notebook itself to explain my rationale behind implementing the model in a certain way. During the initial phase of implementation, I used both the Keras documentation [12] and Tensorflow documentation [10] as references to ensure that the model's development was following standard practices and to ensure that the model was optimized to allow training in a timely manner.

Due to the limited support for AMD graphics cards(currently I use a 6700XT which does not have RoCM support[42]) in a variety of popular AI frameworks/libraries at the time of my writing this thesis, we decided it was best to use Google Colab Pro when training both the CNNs and the GANs this may offer some limitations in terms of memory and computational power. Google Colab Pro, however, does offer a lot of advantages when it comes to quickly setting up an environment in which to train these models, it is for this reason that I have chosen to use it for training the models.

For the purpose of reproducible results, we included the following lines of code `np.random.seed(9)` and set the random seed of Keras to 10 so that other researchers can reproduce the results and build upon this study. All the datasets are loaded and split using a seed of 1337 also so that the train/test split is the exact same every time.

## 3.2 CNN Model Design and Comparison

In this section I will compare and contrast each CNN's architecture and design when evaluating on both the original datasets and augmented datasets. The goal of this section is to determine which architecture works best when creating the automated diagnostic system and whether or not the augmented dataset is increasing the model's generalization ability and the model's accuracy. Initially when training the models I thought about using early-stopping to improve the accuracy and reduce the loss of these models, I decided against this due to the harm it may cause the model's generalization ability. All the models listed below use the entire data available when they are being trained.

### 3.2.1 Baseline Models

When starting the implementation phase, we decided to use the following resource to develop baseline CNN models[43]. We plan on modifying this resource to achieve a relatively high training/validation accuracy when training on the original dataset. We plan on using these models to get a metric with which we can compare models generated on the original dataset to the models which are generated on the synthetic dataset. It is in this way we can accurately compare the effects of the synthetic dataset on the accuracy of the implemented models.

After this initial comparison is done with the models trained on the original dataset versus the models trained on the synthetic dataset. We then plan on focusing on which architectures would work best when developing the CNN and how the models trained on the synthetic dataset can be improved.

To start I decided to use the following settings when developing a CNN to be used when training on the x-ray COVID-19 dataset. This dataset is made up of images that are labeled either 1 or 0 with 1 being COVID-positive and 0 being COVID-negative. I have included the architecture of the layers of the model in the table below3.1

| Layer Number | Layer Type             | Layer Size | Kernel Size | Strides | Padding | Activation |
|--------------|------------------------|------------|-------------|---------|---------|------------|
| 1            | Conv2D Layer           | 16         | (3,3)       | 2       | Same    | Swish      |
| 2            | SeparableConv2D Layer  | 32         | (3,3)       | None    | Same    | Swish      |
| 3            | SeparableConv2D Layer  | 64         | (3,3)       | None    | Same    | Swish      |
| 4            | MaxPooling2D           | 2          | 2           | None    | Same    | None       |
| 5            | Residual               | 64         | (3,3)       | 2       | Same    | Swish      |
| 6            | SeparableConv2D        | 128        | (3,3)       | None    | Same    | Swish      |
| 7            | GlobalAveragePooling2D | 1          | None        | None    | None    | Sigmoid    |

Table 3.1: X-ray COVID-19 dataset CNN baseline model architecture

For the padding the keyword "same" means that the input is padded with 0s evenly, both up and down and left and right of the image. The input was also scaled to normalize the data

using the following line of code ”`1.0 / 255)(inputs)`” After each layer batch normalization was performed excluding the residual, max pooling, and global average pooling 2D layers. The use of the activation function “swish” was chosen due to studies showing it’s performance matched or outperformed ReLU for certain tasks[44]. Swish differs slightly in comparison to ReLU in that there isn’t a sharp rise as the weight approaches 0.

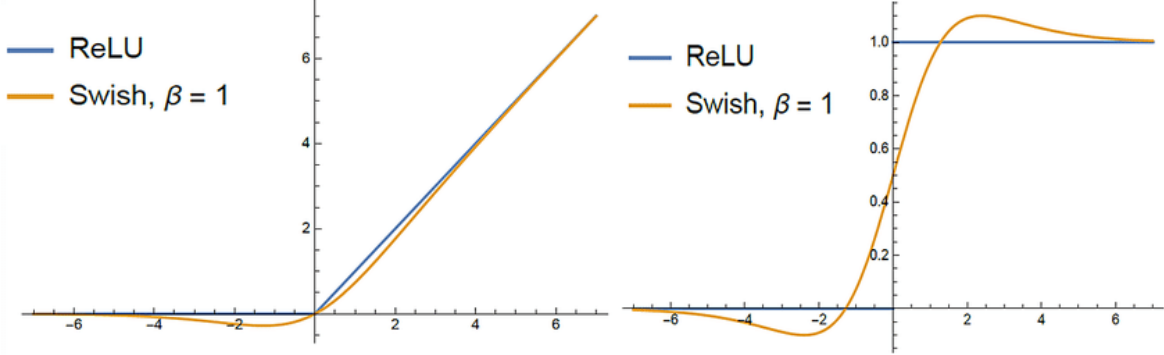


Figure 3.1: Figure of Swish and ReLU activation functions(Image courtesy of Madhura Ingallalikar)[45]

The model uses a dropout of 0, given the small size of the dataset I didn’t want to drop neurons from the network. The model was trained using a 70/30 training-validation split as I found this worked the best when training and testing the model. I also used the following settings when using `model.compile()`

| Optimizer                             | Loss Function       | Metric   | Batch Size | Steps Per Epoch | Number of Epochs |
|---------------------------------------|---------------------|----------|------------|-----------------|------------------|
| Adam with a learning rate of $1e - 3$ | Binary CrossEntropy | Accuracy | 16         | 9               | 10               |

Table 3.2: X-ray COVID-19 dataset CNN baseline model hyperparameters

The model was trained for a total of 37 epochs with 1 step per epoch (again due to the limitations in the size of the dataset) and achieved the following results.

| Training Loss | Training Accuracy | Validation Loss | Validation Accuracy |
|---------------|-------------------|-----------------|---------------------|
| 0.4352        | 0.8106            | 0.6788          | 0.8393              |

Table 3.3: X-ray COVID-19 dataset CNN baseline model results

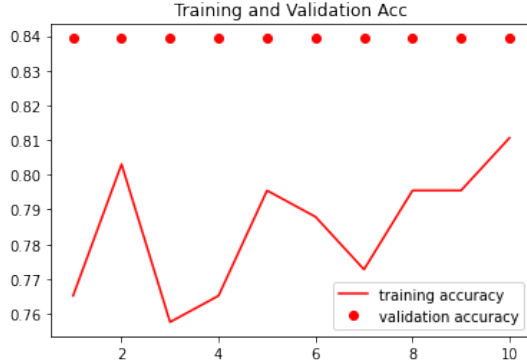


Figure 3.2: Figure of Train and Validation Accuracy of X-ray COVID-19 dataset CNN Baseline Model

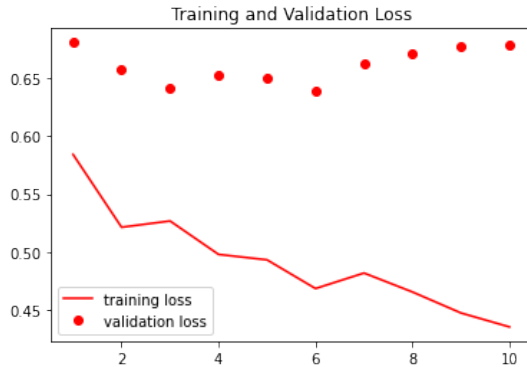


Figure 3.3: Figure of Train and Validation Loss of X-ray COVID-19 dataset CNN Baseline Model

As is shown from the results above3.3 the model appears to have a static validation accuracy and a relatively static validation loss. The model also appears to be underfitting when it comes to the training data. This is possibly due to the relatively small size of the dataset which is comprised of 188 images.

After finishing the CNN implementation for the X-ray COVID-19 dataset we then moved on to designing the model with the radiography dataset. This dataset is much larger than the original dataset, the radiography dataset contains a total of 30,306 image files broken into three classes. In comparison, the X-ray COVID-19 dataset only contains 188 images belonging to two classes. When designing this Convolutional network more thought had to be given to the split and which activation function to use for output, given that there are multiple classes. When designing the CNN we decided to implement a much larger neural network given the amount of data available. We tried using the initial network which was used for the X-ray COVID-19 dataset but the results were poor, increasing the size of the network led to better results. When training the model I also found that a train/test split of 75:25 worked best

using 75% of the data to train and 25% to test.

| Layer Number | Layer Type             | Layer Size | Kernel Size | Strides | Padding | Activation |
|--------------|------------------------|------------|-------------|---------|---------|------------|
| 1            | Conv2D Layer           | 64         | (3,3)       | 2       | Same    | ReLU       |
| 2            | SeparableConv2D Layer  | 128        | (3,3)       | 2       | Same    | ReLU       |
| 3            | SeparableConv2D Layer  | 256        | (3,3)       | 2       | Same    | ReLU       |
| 4            | SeparableConv2D Layer  | 512        | (3,3)       | 2       | Same    | ReLU       |
| 5            | MaxPooling2D           | 3          | 2           | None    | Same    | None       |
| 6            | Residual               | 512        | (3,3)       | 2       | Same    | ReLU       |
| 7            | SeparableConv2D        | 1024       | (3,3)       | None    | Same    | ReLU       |
| 8            | GlobalAveragePooling2D | 3          | None        | None    | None    | Softmax    |

Table 3.4: Radiography CNN baseline model architecture

| Optimizer                             | Loss Function                   | Metric   | Batch Size | Steps Per Epoch | Number of Epochs |
|---------------------------------------|---------------------------------|----------|------------|-----------------|------------------|
| Adam with a learning rate of $1e - 3$ | sparse categorical crossentropy | Accuracy | 8          | 2842            | 20               |

Table 3.5: Radiography CNN baseline model hyperparameters

In this model we achieved a higher accuracy when using ReLU as opposed to swift the final results of the model are as follows:

| Training Loss | Training Accuracy | Validation Loss | Validation Accuracy |
|---------------|-------------------|-----------------|---------------------|
| 0.2721        | 0.8882            | 0.2749          | 0.8893              |

Table 3.6: Radiography CNN baseline results

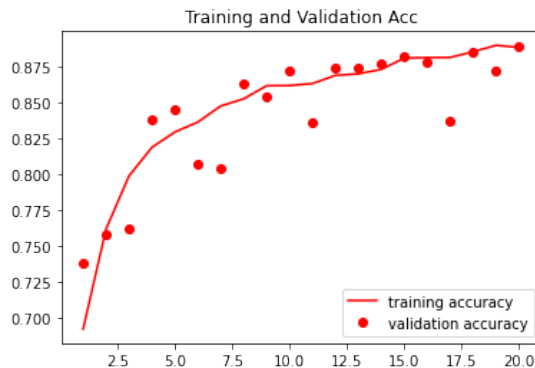


Figure 3.4: Figure of Train and Validation Accuracy of Radiography CNN Baseline Model



Figure 3.5: Figure of Train and Validation Loss of Radiography CNN Baseline Model

As shown in the table 3.6 above we can see that the model has better results when compared with the first baseline model. One of the reasons for this is that we are dealing with a much larger dataset so the model has more images that it can learn features from, this yields a much higher accuracy when compared with the first baseline model which was trained on a much more limited dataset.

The third baseline CNN model was trained using the COVID-19 chest X-ray dataset. This dataset didn't have a standardised resolution for images so the images had to be resized which could possibly lead to lack of data quality and consistency when resized. When training the model there was a high degree of validation loss which is to be expected given the dataset size. The model was trained with a train / test split of 90% for the training set and 10% for the test set. The architecture of this model is as follows:

| Layer Number | Layer Type             | Layer Size | Kernel Size | Strides | Padding | Activation |
|--------------|------------------------|------------|-------------|---------|---------|------------|
| 1            | Conv2D Layer           | 32         | (3,3)       | 2       | Same    | Swish      |
| 2            | SeparableConv2D Layer  | 64         | (3,3)       | 2       | Same    | Swish      |
| 3            | SeparableConv2D Layer  | 128        | (3,3)       | 2       | Same    | Swish      |
| 4            | SeparableConv2D Layer  | 256        | (3,3)       | 2       | Same    | Swish      |
| 5            | SeparableConv2D Layer  | 512        | (3,3)       | 2       | Same    | Swish      |
| 6            | MaxPooling2D           | 3          | 2           | None    | Same    | None       |
| 7            | Residual               | 512        | (3,3)       | 2       | Same    | Swish      |
| 8            | SeparableConv2D        | 128        | (3,3)       | None    | Same    | Swish      |
| 9            | GlobalAveragePooling2D | 11         | None        | None    | None    | Softmax    |

Table 3.7: COVID-19 chest X-ray CNN baseline model architecture for COVID-19 Chest X-ray Dataset

| Optimizer                             | Loss Function            | Metric   | Batch Size | Steps Per Epoch | Number of Epochs |
|---------------------------------------|--------------------------|----------|------------|-----------------|------------------|
| Adam with a learning rate of $1e - 3$ | categorical crossentropy | Accuracy | 4          | 79              | 10               |

Table 3.8: COVID-19 chest X-ray CNN baseline model hyperparameters for COVID-19 Chest X-ray Dataset

Due to the small size of the dataset the batch size was set to a low number. The steps per epoch and number of epochs were also relatively low when compared with the other datasets due to the limited amount of data present. The model's performance is shown in the table below:

| Training Loss | Training Accuracy | Validation Loss | Validation Accuracy |
|---------------|-------------------|-----------------|---------------------|
| 0.8372        | 0.7975            | 7.2848          | 0.6571              |

Table 3.9: COVID-19 chest X-ray CNN baseline model results for COVID-19 Chest X-ray Dataset

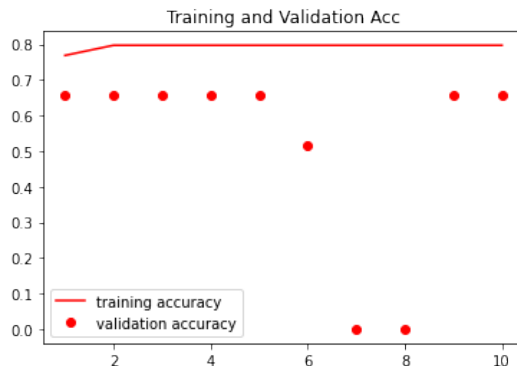


Figure 3.6: Figure of Train and Validation Accuracy of COVID-19 chest X-ray CNN Baseline Model

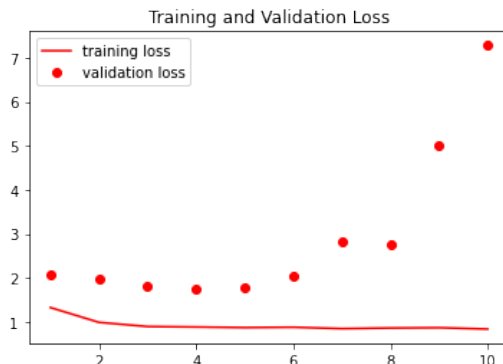


Figure 3.7: Figure of Train and Validation Loss of COVID-19 chest X-ray CNN Baseline Model

As shown in the table above 3.9 the model has a high degree of loss and the accuracy isn't very good on either the training or the validation set. This is to be expected as the dataset is quite small and contains a large number of classes. The model suffers from insufficient data and has performed poorly due to data imbalance as well as lack of standardised image resolutions.

The fourth and fifth baseline models were trained using the Extensive COVID Dataset. This dataset is comprised of two different categories of images, one category of images being X-ray images and the other being CT scans. Two different CNNs were trained, one was trained using the X-ray images and the other using the CT images. The first baseline model for the Extensive COVID Dataset was trained on the CT images and the second baseline model was trained using the X-ray images.

The first model was created with a train / validation split of 80% for the training set and 20% for the validation set. When creating the baseline model I tried a number of different architectures but found the following worked the best:

| Layer Number | Layer Type            | Layer Size | Kernel Size | Strides | Padding | Activation |
|--------------|-----------------------|------------|-------------|---------|---------|------------|
| 1            | Conv2D Layer          | 32         | (3,3)       | 2       | Same    | ReLU       |
| 2            | SeparableConv2D Layer | 64         | (3,3)       | 2       | Same    | ReLU       |
| 3            | SeparableConv2D       | 128        | None        | None    | Same    | ReLU       |
| 4            | SeparableConv2D       | 256        | (3,3)       | None    | Same    | ReLU       |
| 5            | SeparableConv2D       | 512        | (3,3)       | None    | Same    | ReLU       |
| 6            | residual              | 512        | (3,3)       | 2       | Same    | ReLU       |
| 7            | SeparableConv2D       | 1024       | (3,3)       | None    | None    | ReLU       |
| 8            | activation layer      | 1          | None        | None    | None    | Sigmoid    |

Table 3.10: Extensive COVID-19 CT Dataset CNN baseline model architecture

| Optimizer   | Loss Function       | Metric   | Batch Size | Steps Per Epoch | Number of Epochs |
|---|---------------------|----------|------------|-----------------|------------------|
| RMSprop with a learning rate of $10^{-3}$ and a momentum of $10^{-3}$ | binary crossentropy | Accuracy | 16         | 403             | 10               |

Table 3.11: Extensive CT CNN baseline model hyperparameters

| Training Loss | Training Accuracy | Validation Loss | Validation Accuracy |
|---------------|-------------------|-----------------|---------------------|
| 0.2212        | 0.9018            | 0.5822          | 0.8012              |

Table 3.12: Extensive CT CNN baseline model results

The training / validation accuracy and loss for this model are visible in the images included below

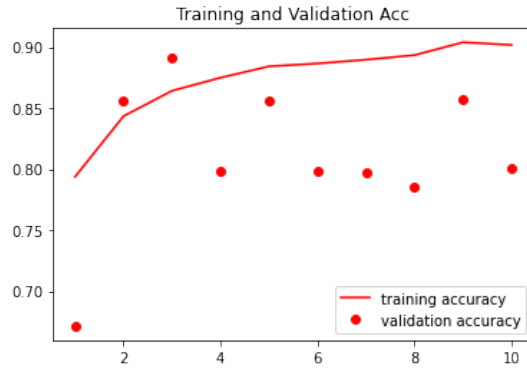


Figure 3.8: Figure of Train and Validation accuracy of Extensive COVID CNN Baseline Model CT

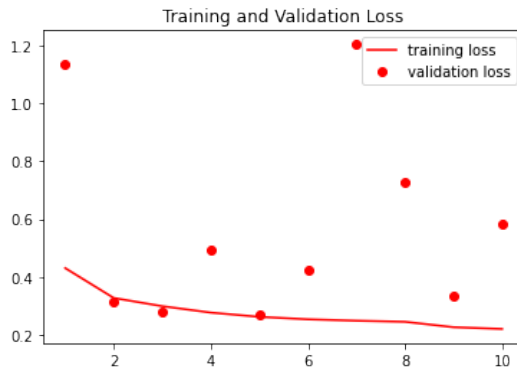


Figure 3.9: Figure of Train and Validation Loss of Extensive COVID CNN Baseline Model CT

The X-Ray model was created with a train / validation split of 80% for the training set and 20% for the validation set. When creating the baseline model I tried a number of different architectures but found the following worked the best:

| Layer Number | Layer Type            | Layer Size | Kernel Size | Strides | Padding | Activation |
|--------------|-----------------------|------------|-------------|---------|---------|------------|
| 1            | Conv2D Layer          | 32         | (3,3)       | 2       | Same    | ReLU       |
| 2            | SeparableConv2D Layer | 64         | (3,3)       | 2       | Same    | ReLU       |
| 3            | SeparableConv2D       | 128        | None        | None    | Same    | ReLU       |
| 4            | SeparableConv2D       | 256        | (3,3)       | None    | Same    | ReLU       |
| 5            | SeparableConv2D       | 512        | (3,3)       | None    | Same    | ReLU       |
| 6            | residual              | 512        | (3,3)       | 2       | Same    | ReLU       |
| 7            | SeparableConv2D       | 1024       | (3,3)       | None    | None    | ReLU       |
| 8            | activation layer      | 1          | None        | None    | None    | Sigmoid    |

Table 3.13: Extensive COVID-19 X-Ray CNN baseline model architecture

| Optimizer   | Loss Function       | Metric   | Batch Size | Steps Per Epoch | Number of Epochs |
|---|---------------------|----------|------------|-----------------|------------------|
| RMSprop with a learning rate of $10^{-3}$ and a momentum of $10^{-3}$ | binary crossentropy | Accuracy | 16         | 477             | 10               |

Table 3.14: Extensive COVID-19 X-Ray CNN baseline model hyperparameters

| Training Loss | Training Accuracy | Validation Loss | Validation Accuracy |
|---------------|-------------------|-----------------|---------------------|
| 0.1948        | 0.9280            | 0.5361          | 0.7420              |

Table 3.15: Extensive COVID-19 X-Ray CNN baseline model results

The training / validation accuracy and loss for this model are visible in the images included below

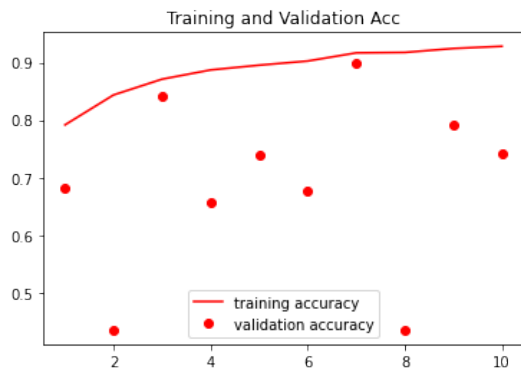


Figure 3.10: Figure of Extensive COVID-19 X-ray CNN Baseline Model Train and Validation Accuracy



Figure 3.11: Figure of Extensive COVID-19 X-ray CNN Baseline Model Train and Validation Loss

### 3.3 Transfer Learning CNN Baseline Models

Here I will compare the transfer learning baseline models, Keras offers a large number of pretrained models[46]. For the sake of time I have chosen the following three pretrained models to compare and contrast their effectiveness when automating COVID-19 Diagnosis, these models are: Xception, ResNet50V2, and EfficientNetV2S. When choosing the pretrained models I had to carefully consider both their performance and size for use in this project. Some models had parameters in excess of 100 million parameters which would have caused Colab Pro to crash due to computational resource limitations. Thus the models chosen had a reasonable number of parameters to avoid crashes when training the CNNs, the model with the highest number of parameters was ResNet50V2 which has 25.6M trainable parameters and the other two models have approximately 20 - 25 million parameters.

The weights used with all the transfer models come from models trained using the ImageNet dataset[47]. The ImageNet dataset is comprised of 14,197,122 images and contains 1,000 classes.

#### 3.3.1 Radiography Dataset

##### Xception

This model contains 21,386,795 parameters including a layer of 256 ReLU units and an additional layer of 3 softmax units which were appended to the model. The model ran for a total of 10 epochs with 2842 steps per epoch. The model also used sparse categorical cross entropy for the loss function and for the optimizer used Adam with a learning rate of  $1e-3$ . The model achieved a final result of 0.9328 training accuracy with 0.1679 loss and had a validation accuracy of 0.9145 with a validation loss of 0.2138. This is a relatively small but significant improvement in comparison to the original baseline models. The figures below show the training / validation accuracy 3.12 and training / validation loss 3.13.

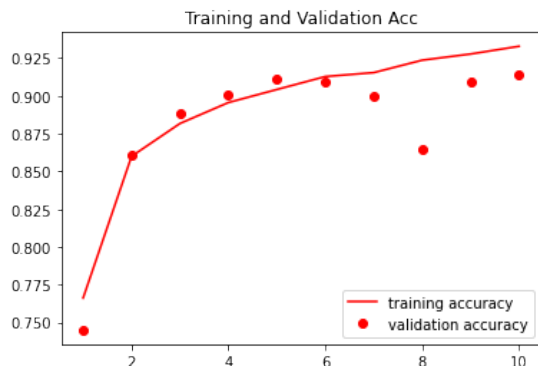


Figure 3.12: Transfer Learning Xception CNN Baseline Train and Validation Accuracy

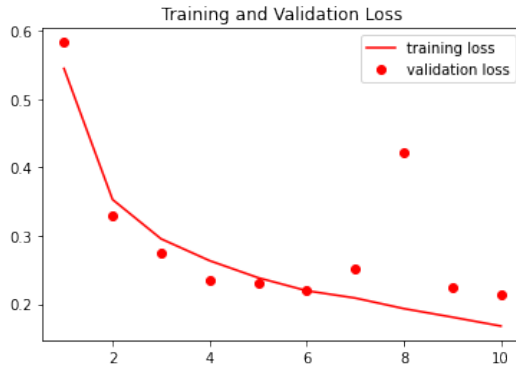


Figure 3.13: Transfer Learning Xception CNN Baseline Train and Validation Loss

### ResNet50V2

This model had a total of 24,090,115 parameters including a layer of 256 ReLU units and an additional layer of 3 softmax units which were appended to the model. This model had the same number of epochs and steps per epoch as exception(10 epochs with 2842 steps) and also used the same optimizer with the same learning rate(Adam with  $1e - 3$  as the learning rate). The model performed slightly worse than Xception and finished with a training accuracy of 0.9031 and a training loss of 0.2395 and had a validation accuracy of 0.8898 with a validation loss of 0.2840. The images below show the training / validation accuracy 3.14 and training / validation loss 3.15.

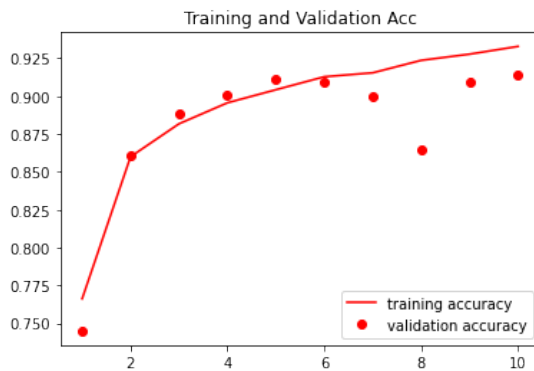


Figure 3.14: Transfer Learning ResNet50V2 CNN Baseline Train and Validation Accuracy

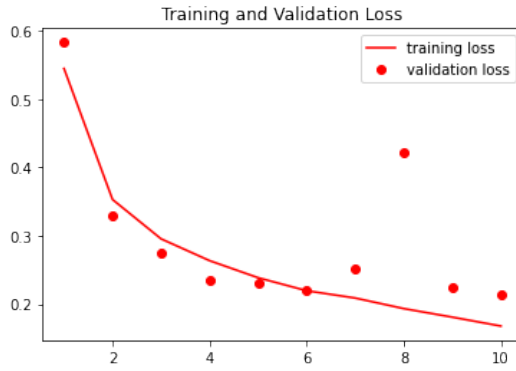


Figure 3.15: Transfer Learning ResNet50V2 CNN Baseline Train and Validation Loss

As shown in the figures above Xception outperforms this model when it comes to both the training accuracy and validation accuracy as well as the loss.

### EfficientNetV2S

EfficientNetVS2 is a model with a total of 20,660,067 parameters including a layer of 256 ReLU units and an additional layer of 3 softmax units which were appended to the model. Like the previous models this model was trained for a total of 10 epochs with 2842 steps within each epoch. It uses Adam as an optimizer with a learning rate of  $1e-3$ . The model performed worse than Xception but better than ResNet50V2 on both the training and validation sets and had a similar performance as Xception but managed to have a slightly lower validation accuracy and slightly higher losses for both the training and validation sets. The model has a training accuracy of 0.9247 and a training loss of 0.1896 and a validation accuracy of 0.9120 and a validation loss of 0.2348. The images below show the training / validation accuracy 3.16 and training / validation loss 3.17.

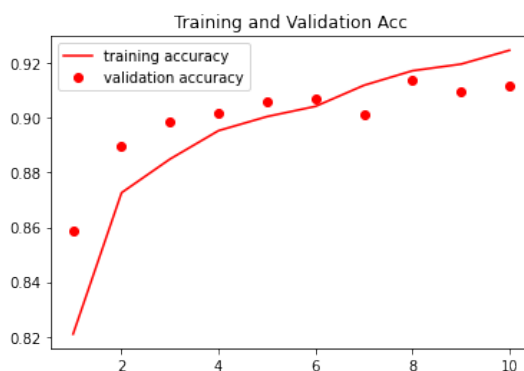


Figure 3.16: Transfer Learning EfficientNetV2S CNN Baseline Train and Validation Accuracy



Figure 3.17: Transfer Learning EfficientNetV2S CNN Baseline Train and Validation Loss

### 3.3.2 X-Ray COVID-19 Dataset

#### Xception

This model has a total of 22,960,681 parameters including a layer of 1024 ReLU units and a layer of 1 Sigmoid unit which were appended to the model. The model uses binary crossentropy as a loss function and uses Adam as an optimizer with a learning rate of  $1e - 3$ . The model ran for a total of 10 epochs with 9 step per epoch. The model achieved a training accuracy of 0.9470 with a training loss of 0.1696 and a validation accuracy of 0.5714 with a validation loss of 2.2749. The images below show both the training / validation accuracy 3.18 and the training / validation loss 3.19.

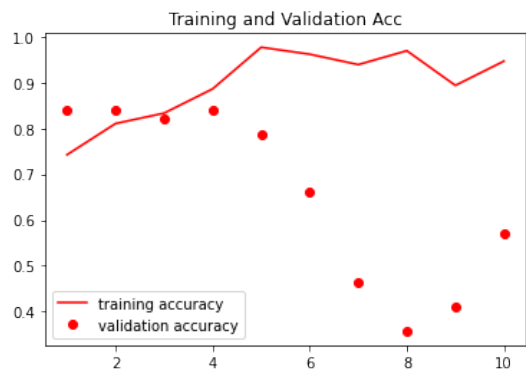


Figure 3.18: Transfer Learning Xception CNN Baseline Train and Validation Accuracy X-Ray COVID19

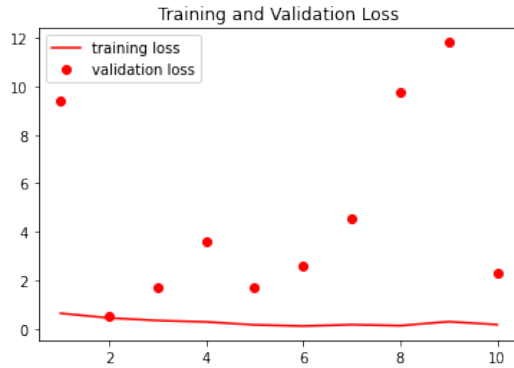


Figure 3.19: Transfer Learning Xception CNN Baseline Train and Validation Loss X-Ray COVID19

### ResNet50V2

This model has a total of 25,664,001 with an additional layer of 1024 ReLU units and another layer of 1 sigmoid unit which was appended to the model. The model uses binary crossentropy as a loss function and Adam with a learning rate of  $1e - 3$  as an optimizer. The model ran for a total of 10 epochs with 9 steps per epoch and achieved a training accuracy of 0.8561 and a training loss of 0.3202 along with a validation accuracy of 0.4464 and a validation loss of 5.8362. The images below show both the training / validation accuracy<sup>3.20</sup> and the training / validation loss<sup>3.21</sup>

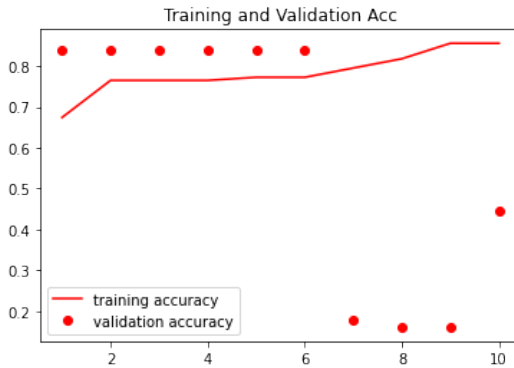


Figure 3.20: Transfer Learning ResNet50V2 CNN Baseline Train and Validation Accuracy X-Ray COVID19

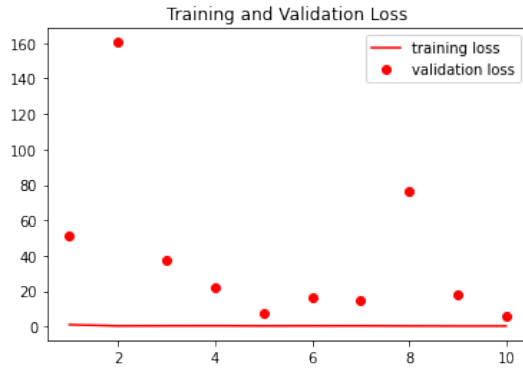


Figure 3.21: Transfer Learning ResNet50V2 CNN Baseline Train and Validation Loss X-Ray COVID19

### EfficientNetV2S

This model has a total of 21,644,129 parameters with an additional layer of 1024 ReLU units and another layer of 1 sigmoid unit. The model uses binary crossentropy as a loss function and Adam as an optimizer with a learning rate of  $1e - 3$ . The model runs for a total of 10 epochs with 9 step per epoch. The model achieved a training accuracy of 0.9015 with a training loss of 0.2079 and a validation accuracy of 0.8036 and a validation loss of 0.7739. The images below show both the training / validation accuracy 3.22 and the training / validation loss 3.23

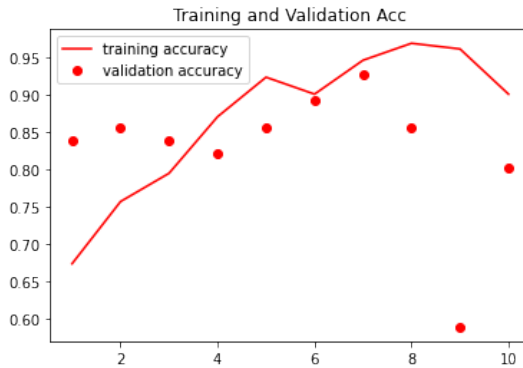


Figure 3.22: Transfer Learning EfficientNetV2S CNN Baseline Train and Validation Accuracy X-Ray COVID19

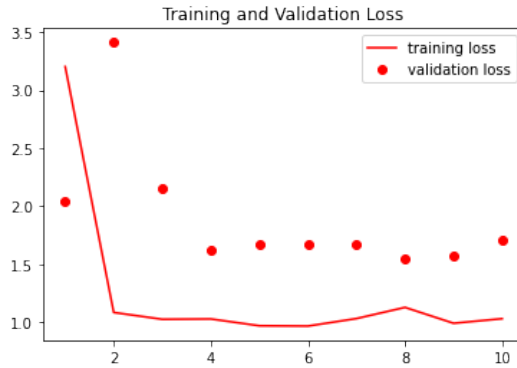


Figure 3.23: Transfer Learning EfficientNetV2S CNN Baseline Train and Validation Loss X-Ray COVID19

### 3.3.3 Evaluation of TL models for X-Ray COVID-19 dataset

This dataset has a lack of data as it only comprises of 188 images. It is not surprising to see that the models are greatly overfitting the dataset. Due to its limited size this dataset may not be suitable for training a GAN in later sections.

### 3.3.4 COVID-19 Chest X-Ray Dataset

#### Xception

This model has a total of 22,970,931 parameters including an additional layer of 1024 ReLU units and another layer of 11 softmax units which were appended to the model. The model uses categorical crossentropy as a loss function along with Adam with a learning rate of  $1 \times 10^{-3}$  as an optimizer. The model runs for a total of 10 epochs with 79 step per epoch and achieved a training accuracy of 0.7975 and a training loss of 0.6109 along with a validation accuracy of 0.6571 and a validation loss of 1.6387. The images below show both the training / validation accuracy 3.24 and the training / validation loss 3.25

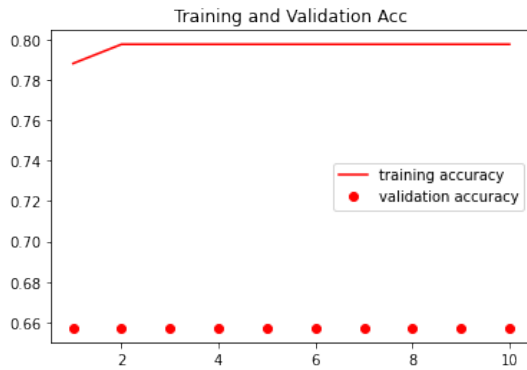


Figure 3.24: Transfer Learning Xception CNN Baseline Train and Validation Accuracy Chest X-Ray



Figure 3.25: Transfer Learning Xception CNN Baseline Train and Validation Loss X-Ray Chest X-Ray

## ResNet50V2

This model has a total of 25,674,251 parameters including an additional layer of 1024 ReLU units and another layer of 11 softmax units which were appended to the model. The model uses categorical crossentropy as a loss function along with Adam with a learning rate of  $1 \times 10^{-3}$  as an optimizer. The model runs for a total of 10 epochs with 79 step per epoch and achieved a training accuracy of 0.7975 and a training loss of 0.9676 along with a validation accuracy of 0.6571 and a validation loss of 1.5587. The images below show both the training / validation accuracy 3.26 and the training / validation loss 3.27

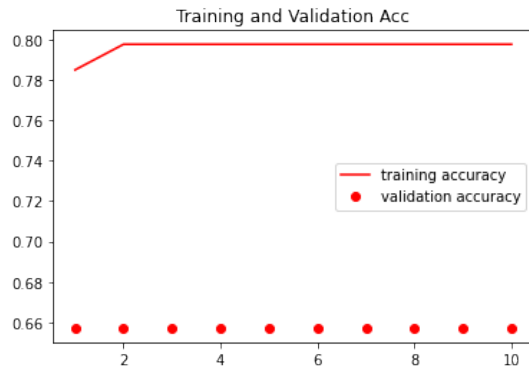


Figure 3.26: Transfer Learning ResNet50V2 CNN Baseline Train and Validation Accuracy Chest X-Ray

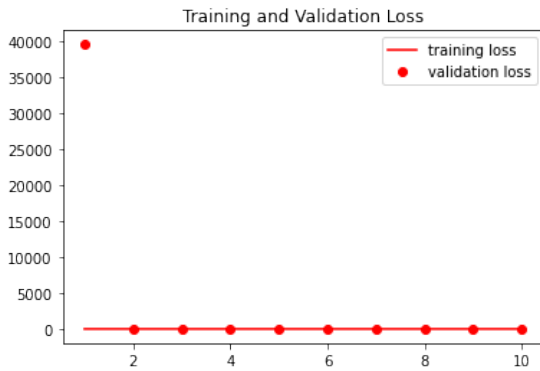


Figure 3.27: Transfer Learning ResNet50V2 CNN Baseline Train and Validation Loss X-Ray Chest X-Ray

### EfficientNetV2S

This model has a total of 21,654,379 parameters including an additional layer of 1024 ReLU units and another layer of 11 softmax units which were appended to the model. The model uses categorical crossentropy as a loss function along with Adam with a learning rate of  $1 \times 10^{-2}$  as an optimizer. The model runs for a total of 10 epochs with 79 step per epoch and achieved a training accuracy of 0.7975 and a training loss of 1.0280 along with a validation accuracy of 0.6571 and a validation loss of 1.7049. The images below show both the training / validation accuracy 3.28 and the training / validation loss 3.29

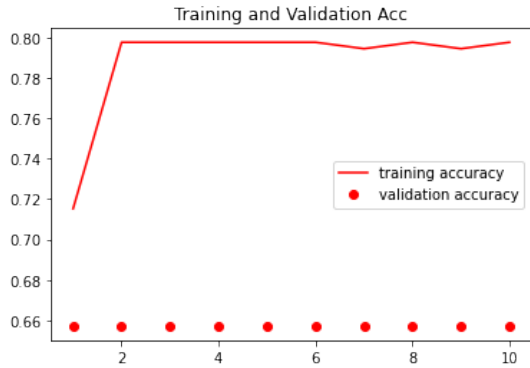


Figure 3.28: Transfer Learning EfficientNetV2S CNN Baseline Train and Validation Accuracy Chest X-Ray

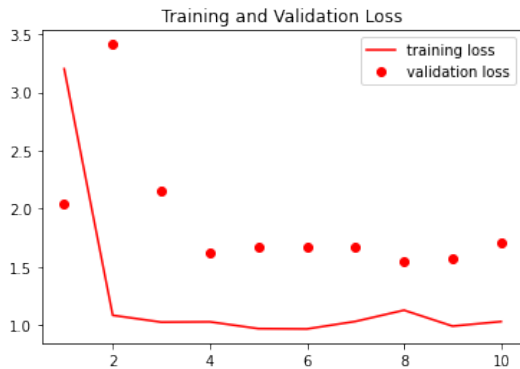


Figure 3.29: Transfer Learning EfficientNetV2S CNN Baseline Train and Validation Loss Chest X-Ray

### 3.3.5 Extensive COVID-19 Dataset CT

#### Xception

This model is comprised of 21,386,281 parameters in total including an additional layer of 256 neurons using ReLU activation and an output layer of 1 neuron using a sigmoid activation function. The model was trained for a total of 10 epochs with a total of 403 steps per epoch and uses RMSprop as an optimizer with a learning rate of  $10^{-3}$  and a momentum of  $10^{-3}$ . The model achieved a training accuracy of 0.9913 and a training loss of 0.0278 along with a validation accuracy of 0.9317 and a validation loss of 0.2731 . Both the training / validation accuracy and training / validation loss are visible in the plots below.

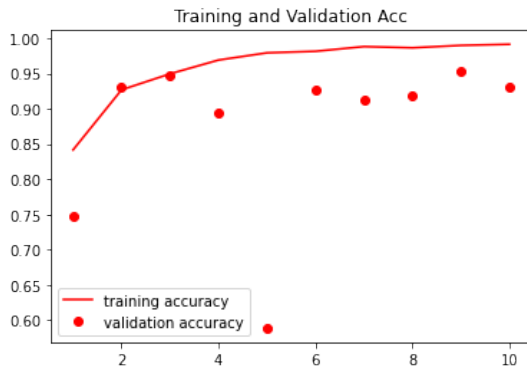


Figure 3.30: Transfer Learning Xception CNN Baseline Train and Validation Accuracy Extensive COVID 19 Dataset CT

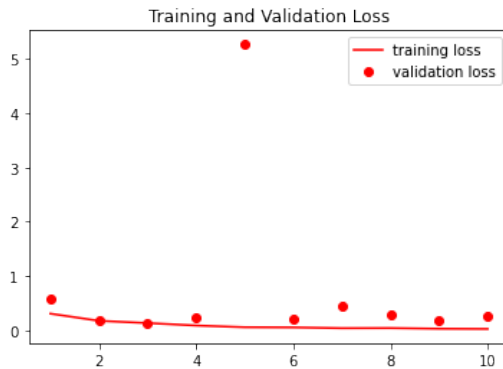


Figure 3.31: Transfer Learning Xception CNN Baseline Train and Validation Loss Extensive COVID 19 Dataset CT

## ResNet50V2

This model is comprised of 24,089,601 parameters in total including an additional layer of 256 neurons using ReLU activation and an output layer of 1 neuron using a sigmoid activation function. The model was trained for a total of 10 epochs with 403 steps per epoch and uses RMSprop as an optimizer with a learning rate of  $10^{-3}$  and a momentum of  $10^{-3}$ . The model achieved a training accuracy of 0.9362 and a training loss of 0.1631 along with a validation accuracy of 0.8379 and a validation loss of 0.4626. Both the training / validation accuracy and training / validation loss are visible in the plots below.

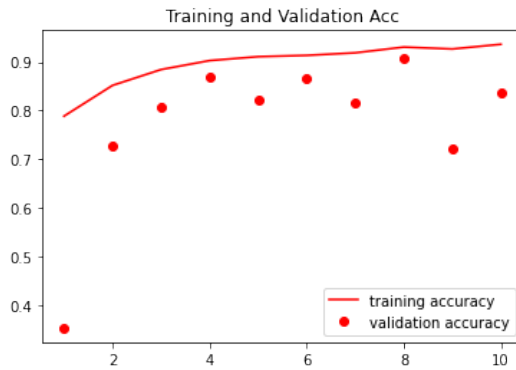


Figure 3.32: Transfer Learning ResNet50V2 CNN Baseline Train and Validation Accuracy Extensive COVID 19 Dataset CT

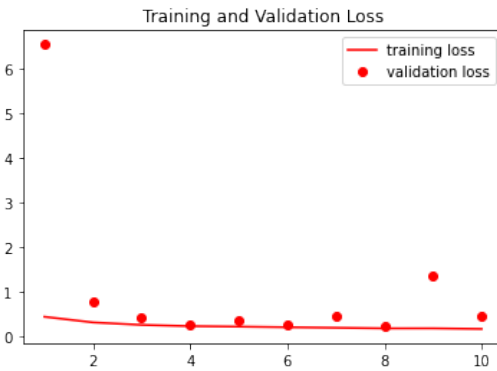


Figure 3.33: Transfer Learning ResNet50V2 CNN Baseline Train and Validation Loss Extensive COVID 19 Dataset CT

### EfficientNetV2S

This model is comprised of 20,659,553 parameters in total including an additional layer of 256 neurons using ReLU activation and an output layer of 1 neuron using a sigmoid activation function. The model was trained for a total of 10 epochs with 403 steps per epoch and uses RMSprop as an optimizer with a learning rate of  $10^{-3}$  and a momentum of  $10^{-5}$ . The model achieved a training accuracy of 0.9898 and a training loss of 0.0350 along with a validation accuracy of 0.9689 and a validation loss of 0.1257. Both the training / validation accuracy and training / validation loss are visible in the plots below.

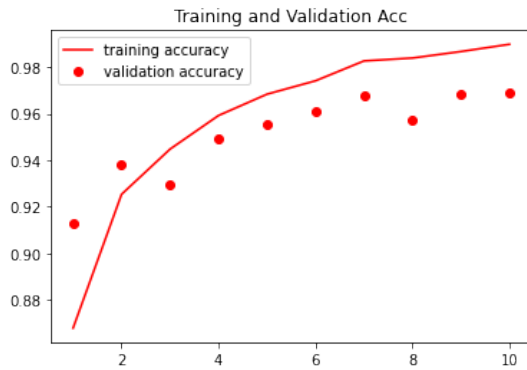


Figure 3.34: Transfer Learning EfficientNetV2S CNN Baseline Train and Validation Accuracy Extensive COVID 19 Dataset CT



Figure 3.35: Transfer Learning EfficientNetV2S CNN Baseline Train and Validation Loss Extensive COVID 19 Dataset CT

### 3.3.6 Extensive COVID-19 Dataset X-ray

#### Xception

This model is comprised of 21,386,281 parameters in total including an additional layer of 256 neurons using ReLU activation and an output layer of 1 neuron using a sigmoid activation function. The model was trained for a total of 10 epochs with a total of 477 steps per epoch and uses RMSprop as an optimizer with a learning rate of  $10^{-3}$  and a momentum of  $10^{-3}$ . The model achieved a training accuracy of 0.9847 and a training loss of 0.0412 along with a validation accuracy of 0.9418 and a validation loss of 0.3183 . Both the training / validation accuracy and training / validation loss are visible in the plots below.

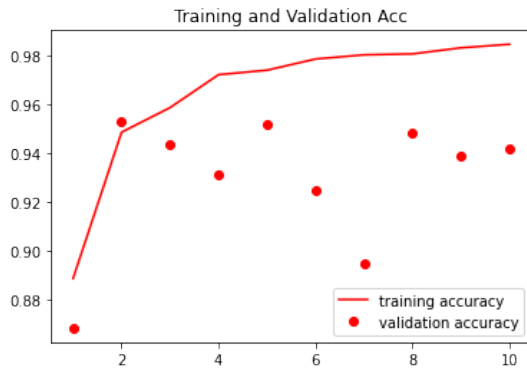


Figure 3.36: Transfer Learning Xception CNN Baseline Train and Validation Accuracy Extensive COVID 19 Dataset X-ray

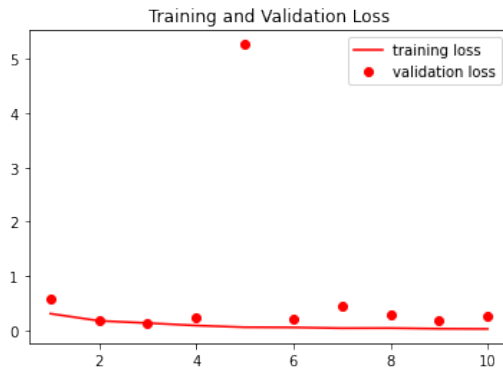


Figure 3.37: Transfer Learning Xception CNN Baseline Train and Validation Loss Extensive COVID 19 Dataset X-ray

## ResNet50V2

This model is comprised of 24,089,601 parameters in total including an additional layer of 256 neurons using ReLU activation and an output layer of 1 neuron using a sigmoid activation function. The model was trained for a total of 10 epochs with 477 steps per epoch and uses RMSprop as an optimizer with a learning rate of  $10^{-3}$  and a momentum of  $10^{-3}$ . The model achieved a training accuracy of 0.9368 and a training loss of 0.1786 along with a validation accuracy of 0.6890 and a validation loss of 0.9138. Both the training / validation accuracy and training / validation loss are visible in the plots below.

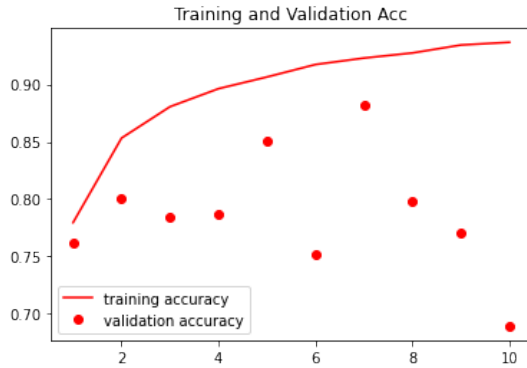


Figure 3.38: Transfer Learning ResNet50V2 CNN Baseline Train and Validation Accuracy Extensive COVID 19 Dataset X-ray

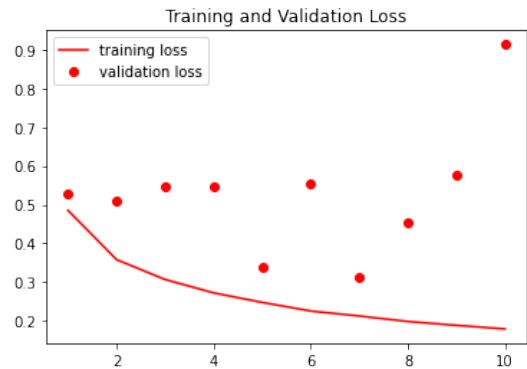


Figure 3.39: Transfer Learning ResNet50V2 CNN Baseline Train and Validation Loss Extensive COVID 19 Dataset X-ray

## EfficientNetV2S

This model is comprised of 20,659,553 parameters in total including an additional layer of 256 neurons using ReLU activation and an output layer of 1 neuron using a sigmoid activation function. The model was trained for a total of 10 epochs with 477 steps per epoch and uses RMSprop as an optimizer with a learning rate of  $10^{-3}$  and a momentum of  $10^{-5}$ . The model achieved a training accuracy of 0.9827 and a training loss of 0.0452 along with a validation accuracy of 0.9560 and a validation loss of 0.2095. Both the training / validation accuracy and training / validation loss are visible in the plots below.

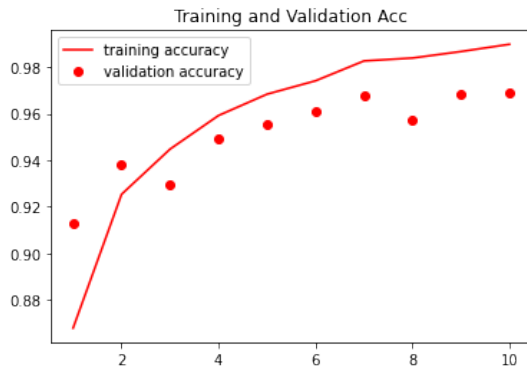


Figure 3.40: Transfer Learning EfficientNetV2S CNN Baseline Train and Validation Accuracy Extensive COVID 19 Dataset X-ray

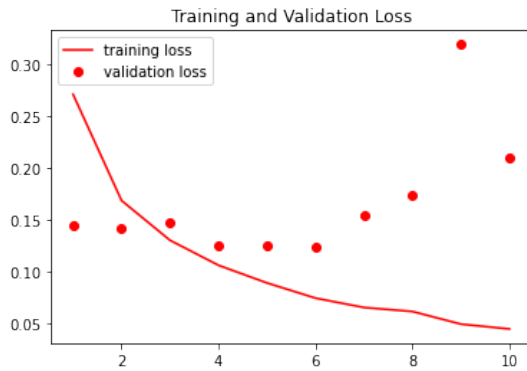


Figure 3.41: Transfer Learning EfficientNetV2S CNN Baseline Train and Validation Loss Extensive COVID 19 Dataset X-ray

### 3.4 GAN Baseline Design and Comparison

In this section I will detail the designs of the GANs and their architectures when augmenting classes in each database. I will also compare the different results and effects each GAN architecture had when producing synthetic data.

### 3.5 GANs for Radiography Dataset

Due to a large imbalance between classes in the dataset I decided to explore the use of GANs to create synthetic data for both the COVID positive images which comprise 7,232 images in this dataset and the Pneumonia positive images which comprise 2,690 images. The normal class(healthy patients) is very over-represented in the data as it is comprised of 20,384 images, due to this imbalance the CNNs trained from this dataset will be heavily biased towards identifying the normal patients. For this reason I have chose to use a number of Generative

Adversarial Architectures to synthetically augment the classes lacking in data to balance the dataset and increase the generalization and robustness of the CNN models.

### 3.5.1 VAE(Variational Auto Encoder)

#### COVID-19 Class Augmentation

#### Pneumonia Class Augmentation

### 3.5.2 DCGAN(Deep Convolutional GAN Network)

#### COVID-19 Mask Class Augmentation

When designing the DCGAN I experimented with a number of architectures, some of these architectures led to the GAN only producing black squares which was a sign of mode collapse. Mode collapse occurs when the discriminator gets stuck at a local minimum and the generator learns to only produce the same type of image over and over again to fool the discriminator. I found switching from an ADAM optimizer to RMSPROP and experimenting with the learning rate and momentum led to far better results. The model produced some promising results, the following architecture was used to create the generator and discriminator:

```
1  discriminator = keras.Sequential(  
2      [  
3          keras.Input(shape=(128, 128, 3)),  
4          layers.Conv2D(64, kernel_size=4, strides=2, padding="same"),  
5          layers.LeakyReLU(alpha=0.5),  
6          layers.Conv2D(128, kernel_size=4, strides=2, padding="same"),  
7          layers.LeakyReLU(alpha=0.5),  
8          layers.Conv2D(128, kernel_size=4, strides=2, padding="same"),  
9          layers.LeakyReLU(alpha=0.5),  
10         layers.Flatten(),  
11         layers.Dropout(0.2),  
12         layers.Dense(1, activation="sigmoid"),  
13     ],  
14     name="discriminator",  
15 )  
16 discriminator.summary()  
17  
18 # Create the generator.  
19 generator = keras.Sequential(  
20     [  
21         keras.Input(shape=(latent_dim,)),
```

```

22     layers.Dense(8 * 8 * 128),
23     layers.Reshape((8, 8, 128)),
24     layers.Conv2DTranspose(256, kernel_size=4, strides=2,
25       ↳ padding="same"),
26     layers.LeakyReLU(alpha=0.2),
27     layers.Conv2DTranspose(512, kernel_size=4, strides=2,
28       ↳ padding="same"),
29     layers.LeakyReLU(alpha=0.2),
30     layers.Conv2DTranspose(1024, kernel_size=4, strides=2,
31       ↳ padding="same"),
32     layers.LeakyReLU(alpha=0.2),
33     layers.Conv2DTranspose(64, kernel_size=4, strides=2, padding="same"),
34     layers.LeakyReLU(alpha=0.2),
35     layers.Conv2D(3, kernel_size=5, padding="same",
36       ↳ activation="sigmoid"),
37   ],
38   name="generator",
39 )
40 generator.summary()

```

The design of this GAN was based off of a Keras tutorial and the code was refactored for the purposes of this project[48]. The following hyper parameters were used when training the DCGAN model to generate synthetic COVID-19 mask images:

| Latent Dimension | Generator Optimizer | Discriminator Optimizer | Generator Learning Rate | Discriminator Learning Rate | Generator Momentum | Discriminator Momentum | Steps per Epoch | Batch Size | Number of Epochs |
|------------------|---------------------|-------------------------|-------------------------|-----------------------------|--------------------|------------------------|-----------------|------------|------------------|
| 256              | RMSPROP             | RMSPROP                 | $1 \times 10^{-5}$      | $1 \times 10^{-5}$          | 0                  | 0                      | 452             | 8          | 100              |

Table 3.16: DCGAN for Producing Synthetic COVID-19 Mask Data From Radiography Dataset

With this model architecture I was able to achieve a final loss of 0.5476 for the discriminator and 1.0187 for the generator.

### COVID-19 X-Ray Class Augmentation

Given the success achieved with the mask DCGAN I decided to reuse the architecture. The results at first were blurry and had little resemblance to the actual data. I decided to experiment with a number of different hyper parameters and found the parameters in the table below worked best:

| Latent Dimension | Generator Optimizer | Discriminator Optimizer | Generator Learning Rate | Discriminator Learning Rate | Generator Momentum | Discriminator Momentum | Steps per Epoch | Batch Size | Number of Epochs |
|------------------|---------------------|-------------------------|-------------------------|-----------------------------|--------------------|------------------------|-----------------|------------|------------------|
| 128              | RMSPROP             | RMSPROP                 | $1 \times 10^{-4}$      | $1 \times 10^{-4}$          | 0                  | 0                      | 452             | 8          | 100              |

Table 3.17: DCGAN for Producing Synthetic COVID-19 X-Ray Data From Radiography Dataset

With this model architecture I was able to achieve a final loss of 0.6859% for the discriminator and 0.8015% for the generator.

### Pneumonia Mask Class Augmentation

The design of this DCGAN was based off the above COVID-19 DCGAN for generating masks and shares the same architecture the only difference being this model ran with 169 steps per epoch. The design yielded relatively similar results, although the losses for the pneumonia mask DCGAN was lower. The model finished training with a loss of 0.9474 and a loss of 0.5936 for the discriminator.

### Pneumonia X-ray Class Augmentation

The X-ray DCGAN for the pneumonia class is a copy of the above COVID-19 DCGAN the only difference being the Pneumonia X-Ray DCGAN uses a latent space of 256 and ran with 169 steps per epoch. The model achieved a final loss of 0.6901 for the discriminator and a loss of 0.7534 for the generator.

## 3.6 GANs for COVID 19 X-ray dataset

### 3.6.1 DCGANs

There were some setbacks when training GANs on this dataset in particular due to the very limited amount of data it contained. To remind the reader this dataset only contains 94 images of COVID-19 Positive X-Rays and 94 images of Pneumonia X-Rays. When beginning the training of the GANs I merged both the train / test data for each class into two folders one marked Normal and the other marked Pneumonia each containing the 94 images of their respective class. I merged both the test and the training data into the two files previously mentioned in order to utilize all the data available for augmenting the respective class. Most researchers suggest a minimum of 50k to 100k images to train a high quality GAN as mentioned on NVIDIA's website[49]. I attained some success with this DCGAN model surprisingly and augmented both the normal and pneumonia classes with 1,000 new images.

The design of the DCGAN is as follows:

```

1
2  discriminator = keras.Sequential(
3      [

```

```

4     keras.Input(shape=(128, 128, 3)),
5     layers.Conv2D(64, kernel_size=4, strides=2, padding="same"),
6     layers.LeakyReLU(alpha=0.5),
7     layers.Conv2D(128, kernel_size=4, strides=2, padding="same"),
8     layers.LeakyReLU(alpha=0.5),
9     layers.Conv2D(128, kernel_size=4, strides=2, padding="same"),
10    layers.LeakyReLU(alpha=0.5),
11    layers.Flatten(),
12    layers.Dropout(0.4),
13    layers.Dense(1, activation="sigmoid"),
14  ],
15  name="discriminator",
16 )
17 discriminator.summary()
18
19 # Create the generator.
20 generator = keras.Sequential(
21 [
22     keras.Input(shape=(latent_dim,)),
23     layers.Dense(8 * 8 * 128),
24     layers.Reshape((8, 8, 128)),
25     layers.Conv2DTranspose(256, kernel_size=4, strides=2,
26                           padding="same"),
27     layers.LeakyReLU(alpha=0.2),
28     layers.Conv2DTranspose(512, kernel_size=4, strides=2,
29                           padding="same"),
30     layers.LeakyReLU(alpha=0.2),
31     layers.Conv2DTranspose(1024, kernel_size=4, strides=2,
32                           padding="same"),
33     layers.LeakyReLU(alpha=0.2),
34     layers.Conv2DTranspose(2048, kernel_size=4, strides=2,
35                           padding="same"),
36     layers.LeakyReLU(alpha=0.2),
37     layers.Conv2D(3, kernel_size=4, padding="same", activation="tanh"),
38  ],
39  name="generator",
40 )
41 generator.summary()

```

The following hyper parameters were used to train the DCGAN to produce images from the normal class of the dataset

| Latent Dimension | Generator Optimizer | Discriminator Optimizer | Generator Learning Rate | Discriminator Learning Rate | Generator Momentum | Discriminator Momentum | Steps per Epoch | Batch Size | Number of Epochs |
|------------------|---------------------|-------------------------|-------------------------|-----------------------------|--------------------|------------------------|-----------------|------------|------------------|
| 256              | RMSPROP             | RMSPROP                 | $1 \times 10^{-4}$      | $1 \times 10^{-4}$          | 0                  | 0                      | 47              | 2          | 100              |

Table 3.18: DCGAN for Producing Synthetic Normal Class Data for X-ray COVID19 dataset

The final model achieved a loss of 0.6890 for the discriminator and a loss of 0.7623 for the generator.

The augmentation of the pneumonia class had similar results as the normal class. Given the success of the DCGAN architecture for the normal class it made sense to reuse this architecture when designing the DCGAN for the pneumonia class, the model also shares the same hyper-parameters. The final model had a discriminator loss of 0.6895 and a generator loss of 0.7757 which is roughly around the same as the DCGAN for the normal class.

## 3.7 GANs for Chest X-ray COVID-19

Due to this model having 11 classes and limited data for each class a decision was made to exclude this dataset from the research. This decision was made to conserve computational units and due to the limited data for each class.

## 3.8 Extensive COVID-19 X-Ray / CT

### 3.8.1 DCGANs

#### X-ray DCGANs

The extensive COVID-19 X-ray models were broken up into two classes COVID and Non-COVID. The first model trained was trained to produce synthetic COVID images and ran for a total of 200 epochs and used the following architecture

```

1
2 discriminator = keras.Sequential(
3     [
4         keras.Input(shape=(128, 128, 3)),
5         layers.Conv2D(64, kernel_size=4, strides=2, padding="same"),
6         layers.LeakyReLU(alpha=0.5),
7         layers.Conv2D(128, kernel_size=4, strides=2, padding="same"),
8         layers.LeakyReLU(alpha=0.5),
9         layers.Conv2D(128, kernel_size=4, strides=2, padding="same"),

```

```

10     layers.LeakyReLU(alpha=0.5),
11     layers.Flatten(),
12     layers.Dropout(0.4),
13     layers.Dense(1, activation="sigmoid"),
14 ],
15 name="discriminator",
16 )
17 discriminator.summary()
18
19 # Create the generator.
20 generator = keras.Sequential(
21 [
22     keras.Input(shape=(latent_dim,)),
23     layers.Dense(8 * 8 * 128),
24     layers.Reshape((8, 8, 128)),
25     layers.Conv2DTranspose(128, kernel_size=4, strides=2,
26     ↪ padding="same"),
27     layers.LeakyReLU(alpha=0.3),
28     layers.Conv2DTranspose(256, kernel_size=4, strides=2,
29     ↪ padding="same"),
30     layers.LeakyReLU(alpha=0.3),
31     layers.Conv2DTranspose(512, kernel_size=4, strides=2,
32     ↪ padding="same"),
33     layers.LeakyReLU(alpha=0.3),
34     layers.Conv2DTranspose(1024, kernel_size=4, strides=2,
35     ↪ padding="same"),
36     layers.LeakyReLU(alpha=0.3),
37     layers.Conv2D(3, kernel_size=4, padding="same", activation="tanh"),
38 ],
39 name="generator",
40 )
41 generator.summary()

```

along with the following hyper parameters

| Latent Dimension | Generator Optimizer | Discriminator Optimizer | Generator Learning Rate | Discriminator Learning Rate | Generator Momentum | Discriminator Momentum | Steps per Epoch | Batch Size | Number of Epochs |
|------------------|---------------------|-------------------------|-------------------------|-----------------------------|--------------------|------------------------|-----------------|------------|------------------|
| 256              | RMSPROP             | RMSPROP                 | $1 \times 10^{-4}$      | $1 \times 10^{-4}$          | 0                  | 0                      | 253             | 16         | 100              |

Table 3.19: DCGAN for Producing Synthetic X-ray COVID Class Data for Extensive COVID 19 Dataset

Once training finished the model attained a discriminator loss of 0.6901 and a generator loss of 0.7557.

The next DCGAN architecture produced the Non-COVID class, this is the majority class but I wanted to compare and contrast the results from both DCGANs. The model uses the following architecture

```

1  discriminator = keras.Sequential(
2      [
3          keras.Input(shape=(128, 128, 3)),
4          layers.Conv2D(64, kernel_size=4, strides=2, padding="same"),
5          layers.LeakyReLU(alpha=0.5),
6          layers.Conv2D(128, kernel_size=4, strides=2, padding="same"),
7          layers.LeakyReLU(alpha=0.5),
8          layers.Conv2D(128, kernel_size=4, strides=2, padding="same"),
9          layers.LeakyReLU(alpha=0.5),
10         layers.Flatten(),
11         layers.Dropout(0.4),
12         layers.Dense(1, activation="sigmoid"),
13     ],
14     name="discriminator",
15 )
16 # Create the generator.
17 generator = keras.Sequential(
18     [
19         keras.Input(shape=(latent_dim,)),
20         layers.Dense(16 * 16 * 128),
21         layers.Reshape((16, 16, 128)),
22         layers.Conv2DTranspose(256, kernel_size=4, strides=2,
23             padding="same"),
24         layers.LeakyReLU(alpha=0.2),
25         layers.Conv2DTranspose(512, kernel_size=4, strides=2,
26             padding="same"),
27         layers.LeakyReLU(alpha=0.2),
28         layers.Conv2DTranspose(1024, kernel_size=4, strides=2,
29             padding="same"),
30         layers.LeakyReLU(alpha=0.2),
31         layers.Conv2D(3, kernel_size=4, padding="same", activation="tanh"),
32     ],
33     name="generator",
34 )

```

31 )

The model runs for 100 epochs and uses a learning rate of  $10^{-5}$  for the generator and discriminator instead of  $10^{-4}$ . The batch size was also increased to 64 to help the model train faster. The model achieved a final loss of 0.6912 for the discriminator and 0.7575 for the generator.

## CT DCGANs

For the DCGAN for CT Covid the batch size was chosen as 64 to increase the training speed. The following architecture was used for this DCGAN

```

1
2  discriminator = keras.Sequential(
3      [
4          keras.Input(shape=(128, 128, 3)),
5          layers.Conv2D(64, kernel_size=4, strides=2, padding="same"),
6          layers.LeakyReLU(alpha=0.5),
7          layers.Conv2D(128, kernel_size=4, strides=2, padding="same"),
8          layers.LeakyReLU(alpha=0.5),
9          layers.Conv2D(128, kernel_size=4, strides=2, padding="same"),
10         layers.LeakyReLU(alpha=0.5),
11         layers.Flatten(),
12         layers.Dropout(0.4),
13         layers.Dense(1, activation="sigmoid"),
14     ],
15     name="discriminator",
16 )
17 discriminator.summary()
18
19 # Create the generator.
20 generator = keras.Sequential(
21     [
22         keras.Input(shape=(latent_dim,)),
23         layers.Dense(8 * 8 * 128),
24         layers.Reshape((8, 8, 128)),
25         layers.Conv2DTranspose(128, kernel_size=4, strides=2,
26             ↵ padding="same"),
27         layers.LeakyReLU(alpha=0.2),
28         layers.Conv2DTranspose(256, kernel_size=4, strides=2,
29             ↵ padding="same"),
30
31     ]
32 )
33 generator.summary()
34
35 # Train the model, printing once per epoch
36 history = generator.fit(
37     train_dataloader,
38     epochs=100,
39     steps_per_epoch=100,
40     validation_data=val_dataloader,
41     validation_steps=10,
42     callbacks=[tensorboard_callback]
43 )
44
45 # Save the trained model
46 generator.save("ct_covid_gan.h5")
47
48 # Load the trained model
49 generator = keras.models.load_model("ct_covid_gan.h5")
50
51 # Generate images
52 generated_images = generator.predict(latent_dim)
53
54 # Save the generated images
55 save_images(generated_images, "generated_ct_covid.png")
56
57 # Print the final loss values
58 print(f"Discriminator Loss: {history.history['loss'][99]}")
59 print(f"Generator Loss: {history.history['generator_loss'][99]}")
```

```

28     layers.LeakyReLU(alpha=0.2),
29     layers.Conv2DTranspose(512, kernel_size=4, strides=2,
30         ↪ padding="same"),
31     layers.LeakyReLU(alpha=0.2),
32     layers.Conv2DTranspose(1024, kernel_size=4, strides=2,
33         ↪ padding="same"),
34     layers.LeakyReLU(alpha=0.2),
35     layers.Conv2D(3, kernel_size=4, padding="same", activation="tanh"),
36 ],
37 name="generator",
38 )
39 generator.summary()

```

and used the following hyper parameters

| Latent Dimension | Generator Optimizer | Discriminator Optimizer | Generator Learning Rate | Discriminator Learning Rate | Generator Momentum | Discriminator Momentum | Steps per Epoch | Batch Size | Number of Epochs |
|------------------|---------------------|-------------------------|-------------------------|-----------------------------|--------------------|------------------------|-----------------|------------|------------------|
| 128              | RMSPROP             | RMSPROP                 | $1 \times 10^{-4}$      | $1 \times 10^{-4}$          | 0                  | 0                      | 85              | 64         | 100              |

Table 3.20: DCGAN for Producing Synthetic CT COVID Class Data for Extensive COVID 19 Dataset

The model achieved a final loss score of 0.6443 for the discriminator and 0.9409 for the generator.

The next model for the non-covid class uses the following architecture

```

1
2 discriminator = keras.Sequential(
3 [
4     keras.Input(shape=(128, 128, 3)),
5     layers.Conv2D(64, kernel_size=4, strides=2, padding="same"),
6     layers.LeakyReLU(alpha=0.5),
7     layers.Conv2D(128, kernel_size=4, strides=2, padding="same"),
8     layers.LeakyReLU(alpha=0.5),
9     layers.Conv2D(128, kernel_size=4, strides=2, padding="same"),
10    layers.LeakyReLU(alpha=0.5),
11    layers.Flatten(),
12    layers.Dropout(0.2),
13    layers.Dense(1, activation="sigmoid"),
14 ],
15 name="discriminator",
16 )
17 discriminator.summary()

```

```

18
19 # Create the generator.
20 generator = keras.Sequential(
21 [
22     keras.Input(shape=(latent_dim,)),
23     layers.Dense(4 * 4 * 128),
24     layers.Reshape((4, 4, 128)),
25     layers.Conv2DTranspose(64, kernel_size=4, strides=2, padding="same"),
26     layers.LeakyReLU(alpha=0.2),
27     layers.Conv2DTranspose(128, kernel_size=4, strides=2,
28                           padding="same"),
28     layers.LeakyReLU(alpha=0.2),
29     layers.Conv2DTranspose(256, kernel_size=4, strides=2,
30                           padding="same"),
31     layers.LeakyReLU(alpha=0.2),
32     layers.Conv2DTranspose(512, kernel_size=4, strides=2,
33                           padding="same"),
34     layers.LeakyReLU(alpha=0.2),
35     layers.Conv2D(3, kernel_size=4, padding="same", activation="tanh"),
36 ],
37 name="generator",
38 )
39 generator.summary()

```

and the following hyper parameters

| Latent Dimension | Generator Optimizer | Discriminator Optimizer | Generator Learning Rate | Discriminator Learning Rate | Generator Momentum | Discriminator Momentum | Steps per Epoch | Batch Size | Number of Epochs |
|------------------|---------------------|-------------------------|-------------------------|-----------------------------|--------------------|------------------------|-----------------|------------|------------------|
| 256              | RMSPROP             | RMSPROP                 | $1 \times 10^{-4}$      | $1 \times 10^{-4}$          | 0                  | 0                      | 42              | 64         | 100              |

Table 3.21: DCGAN for Producing Synthetic CT Non COVID Class Data for Extensive COVID 19 Dataset

The model achieved a final loss score of 0.6522 for the discriminator and 1.0048 for the generator.

### **3.9 GANs in Conjunction**

### **3.10 Conclusion**

## Chapter 4

# Results of Research and Conclusions

### 4.1 Evaluation of Augmented CNN Models

In this section I will evaluate the augmented CNN models and compare and contrast with the original models. The section is broken into subsections for each datasets CNN models.

#### 4.1.1 Radiography CNN Models

When training the radiography CNN models I decided to use a higher batch size than the batch size of 8 which was previously used. I chose to use a batch size of 32 given the now much larger dataset to help the models train faster and to conserve compute units on colab. The non-augmented radiography dataset was imbalanced so a total of 6,570 images were generated for the COVID X-rays and masks and a total of 8,840 pneumonia X-ray and mask images were also generated to bring both classes in relative balance with the Normal class. The augmented dataset will be off by around 5 - 10 images for each class due to computational issues when trying to generate all files at once but the results still show a big improvement in some models.

#### Radiography Baseline Model

The radiography baseline model achieved a final training accuracy of 0.9320 and a final training loss of 0.1654 along with a final validation accuracy of 0.9310 and a validation loss of 0.1778 when the dataset was augmented. In comparison to the original model which had a training accuracy of 0.8882 and a training loss of 0.2721 and a validation accuracy of 0.8893 and a validation loss of 0.2749 when trained for twice as many epochs on a non-augmented set. The model trained on the augmented set shows a clear improvement in terms of accuracy and of loss. The training accuracy increased by 0.05 and the training loss decreased by 0.1067

along with the validation accuracy increasing by 0.014 and the loss decreased by 0.0971. The training / validation accuracy along with the training / validation loss of this model are shown below.

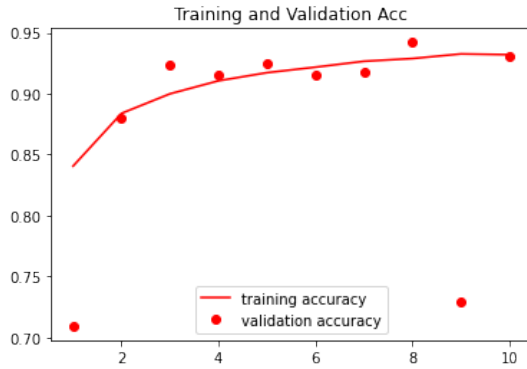


Figure 4.1: Radiography Augmented Baseline Model DCGAN Accuracy

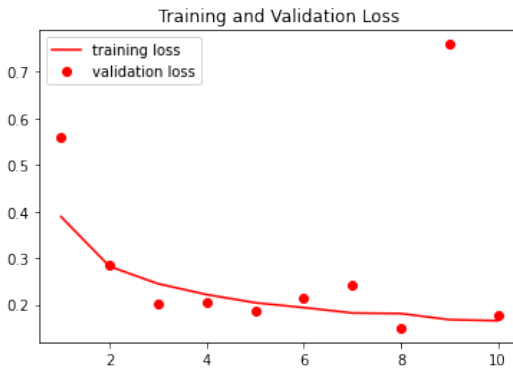


Figure 4.2: Radiography Augmented Baseline Model DCGAN Loss

### Radiography Xception Model

The augmented Radiography Xception model achieved a final training accuracy of 0.9723 and a final training loss of 0.0729 alongside a final validation accuracy of 0.8744 and a final validation loss of 0.3829 after 10 epochs. In comparison the original model achieved a training accuracy of 0.9328 and a training loss of 0.1679 alongside a validation accuracy of 0.9145 and a validation loss of 0.2138. The augmented model shows an increase of 0.0395 for the training accuracy and a decrease of 0.095 for the training loss. The validation accuracy had a decrease of 0.0401 and the validation loss had an increase of 0.1691. The model performed worse on the validation set but better on the training set when compared with the non-augmented model. The solution to this may be early stopping as on the last epoch the accuracy and loss for the validation set had a sudden change which can be seen in the model's validation accuracy and loss figures below. If early stopping were implemented and the model ran for 9 epochs instead

of 10 the final result of the training accuracy would be 0.9686 and the training loss would be 0.0794 alongside a validation accuracy of 0.9522 and a validation loss of 0.1168 which would be a clear improvement to the non-augmented model.

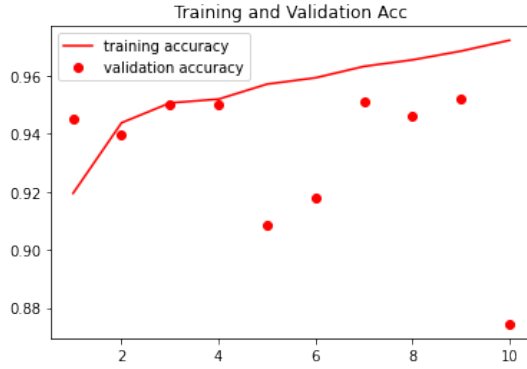


Figure 4.3: Radiography Augmented Xception Model DCGAN Accuracy

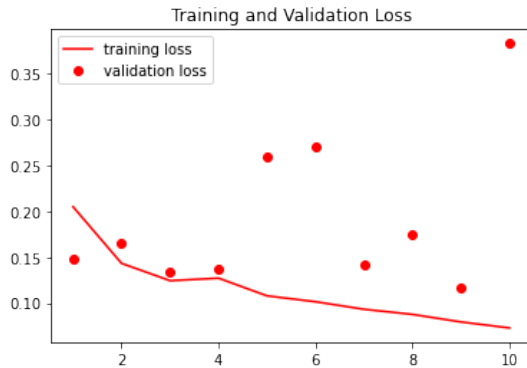


Figure 4.4: Radiography Augmented Xception Model DCGAN Loss

### Radiography ResNet50V2 Model

The augmented radiography ResNet50V2 Model attained a final training accuracy of 0.9608 and a training loss of 0.0986 alongside a validation accuracy of 0.8833 and a validation loss of 0.4177. To contrast this with the original model, the original model achieved a final training accuracy of 0.9031 and a training loss of 0.2395 along with a validation accuracy of 0.8898 and a validation loss of 0.2840. The augmented model performs better on the training set with an accuracy increase of 0.0577 and a loss decrease of 0.1409 but performed worse on the validation set with an accuracy decrease of 0.0065 and a loss increase of 0.1337. As shown in the figure below if early stopping where used on the 9th epoch the model would have finished with a training accuracy of 0.9571 and a training loss of 0.1055 alongside a validation accuracy of 0.9425 and a validation loss of 0.1477.

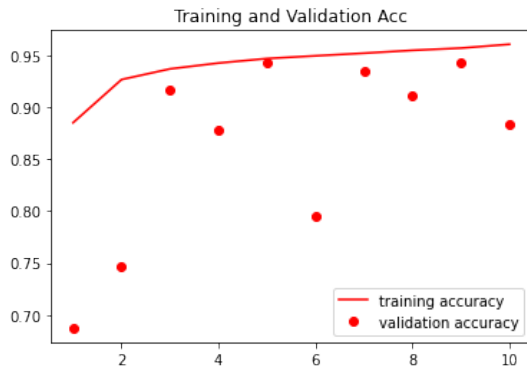


Figure 4.5: Radiography Augmented ResNet50V2 Model DCGAN Accuracy

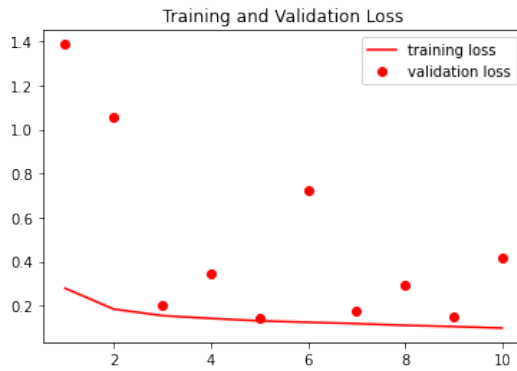


Figure 4.6: Radiography Augmented ResNet50V2 Model DCGAN Loss

### Radiography EfficientNetV2S Model

The augmented EfficientNetV2S Model completed training with a final training accuracy of 0.9642 with a training loss of 0.0922 alongside a validation accuracy of 0.9570 and a validation loss of 0.1105. In contrast the original model achieved a final training accuracy 0.9247 of and a training loss of 0.1896 alongside a validation accuracy of 0.9120 and a validation loss of 0.2348. This shows that the model's training accuracy increased by 0.0395 and its training loss decreased by 0.0974 and the validation accuracy increased by 0.045 and its validation loss decreased by 0.1243. The augmented model has shown clear improvements when compared with the base model however, as shown from the images below early stopping could have helped improve the accuracy for the validation set.

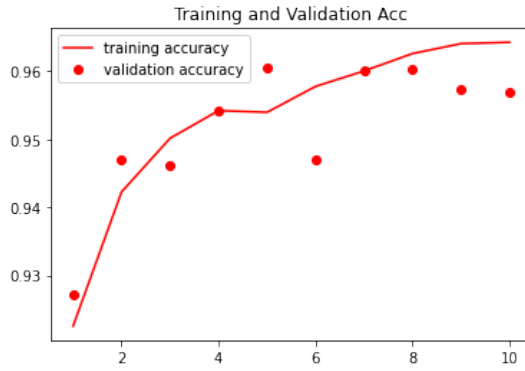


Figure 4.7: Radiography Augmented EfficientNetV2S Model DCGAN Accuracy

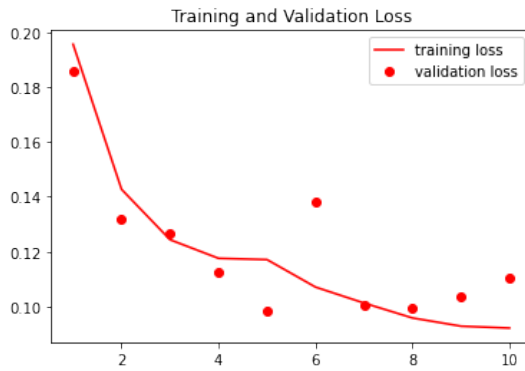


Figure 4.8: Radiography Augmented EfficientNetV2S Model DCGAN Loss

#### 4.1.2 Extensive CNN Models

##### Extensive CNN CT Baseline Model

The Extensive CNN CT baseline model achieved a final training accuracy of 0.9321 and a final training loss of 0.1599 along with a final validation accuracy of 0.9479 and a validation loss of 0.1372 when the dataset was augmented. In comparison to the original model which had a training accuracy of 0.9018 and a training loss of 0.2212 and a validation accuracy of 0.8012 and a validation loss of 0.5822 when trained for the same amount of epochs on a non-augmented set. The model trained on the augmented set shows a clear improvement in terms of accuracy and of loss. The training accuracy increased by 0.0303 and the training loss decreased by 0.0613 along with the validation accuracy increasing by 0.759 and the loss decreased by 0.445. The training / validation accuracy along with the training / validation loss of this model are shown below.

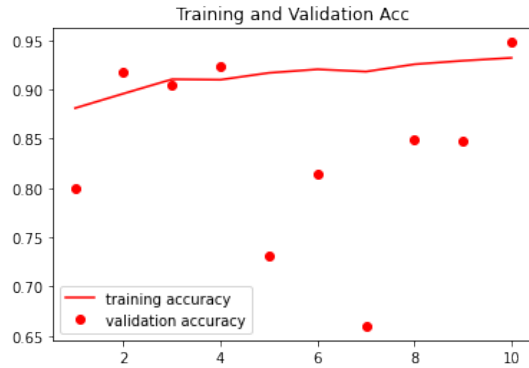


Figure 4.9: Extensive CT Augmented Baseline Model DCGAN Accuracy

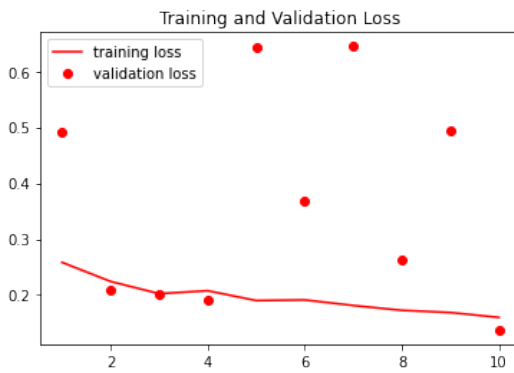


Figure 4.10: Extensive CT Augmented Baseline Model DCGAN Loss

### Extensive CNN CT Xception Model

The Extensive CNN CT Xception model achieved a final training accuracy of 0.9321 and a final training loss of 0.1599 along with a final validation accuracy of 0.9479 and a validation loss of 0.1372 when the dataset was augmented. In comparison to the original model which had a training accuracy of 0.9913 and a training loss of 0.0278 and a validation accuracy of 0.9317 and a validation loss of 0.2731 when trained for the same amount of epochs on a non-augmented set. The model trained on the augmented set shows an improvement in accuracy and loss of the validation set to the detriment of the performance on the training set. The training accuracy decreased by 0.0592 and the training loss increased by 0.1321 along with the validation accuracy increasing by 0.0162 and the loss decreased by 0.1359. In comparison to the original model it appears that the augmented model is no longer overfitting when training. The training / validation accuracy along with the training / validation loss of this model are shown below.

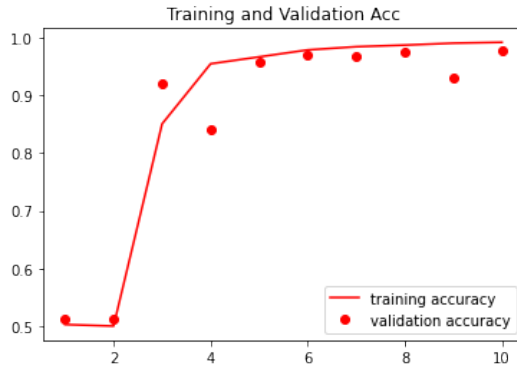


Figure 4.11: Extensive CT Augmented Xception Model DCGAN Accuracy

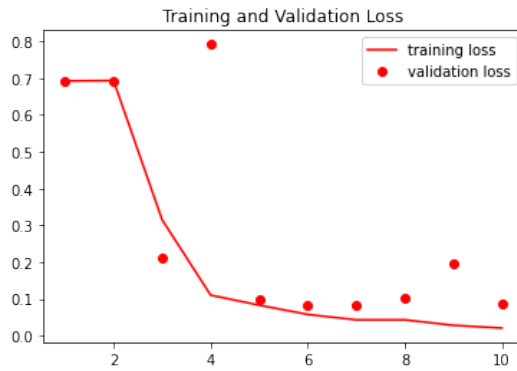


Figure 4.12: Extensive CT Augmented Xception Model DCGAN Loss

### Extensive CNN CT ResNet50V2 Model

The Extensive CNN CT ResNet50V2 model achieved a final training accuracy of 0.9587 and a final training loss of 0.1031 along with a final validation accuracy of 0.7735 and a validation loss of 0.6430 when the dataset was augmented. In comparison to the original model which had a training accuracy of 0.9362 and a training loss of 0.1631 and a validation accuracy of 0.8379 and a validation loss of 0.4626 when trained for the same amount of epochs on a non-augmented set. The model performed worse on the validation set and better on the training set when training on the augmented set. The training accuracy increased by 0.0225 and the training loss decreased by 0.06. The validation accuracy decreased by 0.0644 and the loss increased by 0.1804. Early stopping would have improved accuracy on the validation set as shown in the figures below.

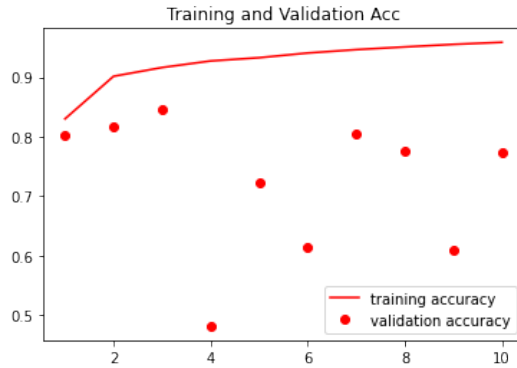


Figure 4.13: Extensive CT Augmented ResNet50V2 Model DCGAN Accuracy

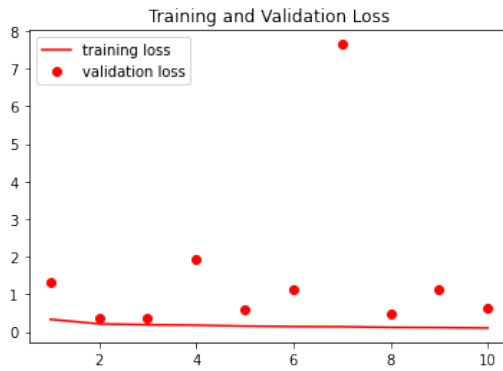


Figure 4.14: Extensive CT Augmented ResNet50V2 Model DCGAN Loss

### Extensive CNN CT EfficientNetV2S Model

The Extensive CNN CT EfficientNetV2S model achieved a final training accuracy of 0.9942 and a final training loss of 0.0185 along with a final validation accuracy of 0.9819 and a validation loss of 0.0639 when the dataset was augmented. In comparison to the original model which had a training accuracy of 0.9898 and a training loss of 0.0350 and a validation accuracy of 0.9689 and a validation loss of 0.1257 when trained for the same amount of epochs on a non-augmented set. The model performed better on both the validation set and on the training set when training on the augmented set. The training accuracy increased by 0.0044 and the training loss decreased by 0.0165. The validation accuracy increased by 0.013 and the loss decreased by 0.0618.

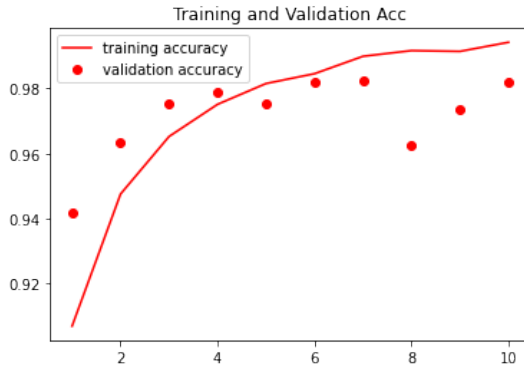


Figure 4.15: Extensive CT Augmented EfficientNetV2S Model DCGAN Accuracy



Figure 4.16: Extensive CT Augmented EfficientNetV2S Model DCGAN Loss

### Extensive CNN X-ray Baseline Model

The Extensive CNN X-ray baseline model achieved a final training accuracy of 0.9267 and a final training loss of 0.1952 along with a final validation accuracy of 0.5434 and a validation loss of 1.8485 when the dataset was augmented. In comparison to the original model which had a training accuracy of 0.9280 and a training loss of 0.1948 in addition to a validation accuracy of 0.7420 and a validation loss of 0.5361 when trained for the same amount of epochs on a non-augmented set. The model performed worse on both the validation set and on the training set when training on the augmented set. The training accuracy decreased by 0.0013 and the training loss increased by 0.0004. The validation accuracy decrease by 0.1986 and the loss increased by 1.3124. If the model was stopped one epoch earlier the model would have ended with a training accuracy of 0.9221 and a training loss of 0.2065 along with a validation loss of 0.3591 and a validation accuracy of 0.8728, which would be an improvement over the original model.

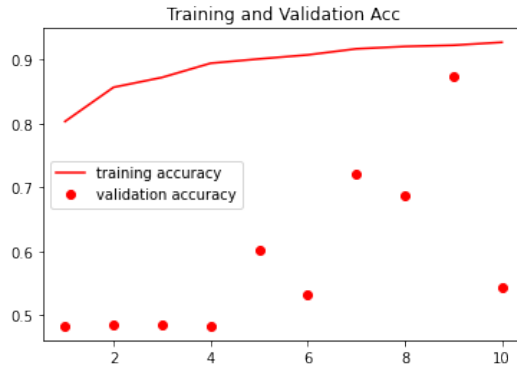


Figure 4.17: Extensive X-ray Augmented Baseline Model DCGAN Accuracy

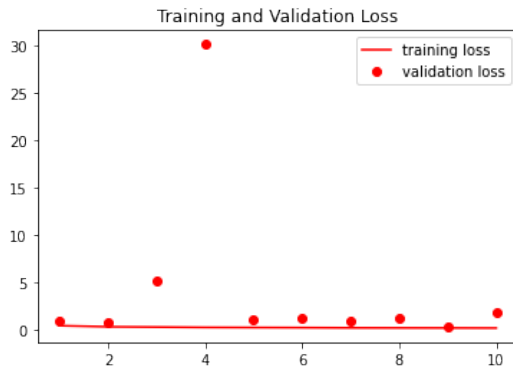


Figure 4.18: Extensive X-ray Augmented Baseline Model DCGAN Loss

### Extensive CNN X-ray Xception Model

The Extensive CNN X-ray Xception model achieved a final training accuracy of 0.9894 and a final training loss of 0.0237 along with a final validation accuracy of 0.9473 and a validation loss of 0.2634 when the dataset was augmented. In comparison to the original model which had a training accuracy of 0.9847 and a training loss of 0.0412 in addition to a validation accuracy of 0.9418 and a validation loss of 0.3183 when trained for the same amount of epochs on a non-augmented set. The model performed better on both the validation set and on the training set when training on the augmented set. The training accuracy increased by 0.0047 and the training loss decreased by 0.0175. The validation accuracy increased by 0.0055 and the loss decreased by 0.0549. If the model was stopped one epoch earlier the model would have ended with a training accuracy of 0.9864 and a training loss of 0.0320 along with a validation loss of 0.2255 and a validation accuracy of 0.9630, which would be a slightly larger improvement over the original model. The model trained for ten epochs performs slightly worse than if the model were trained for nine epochs.

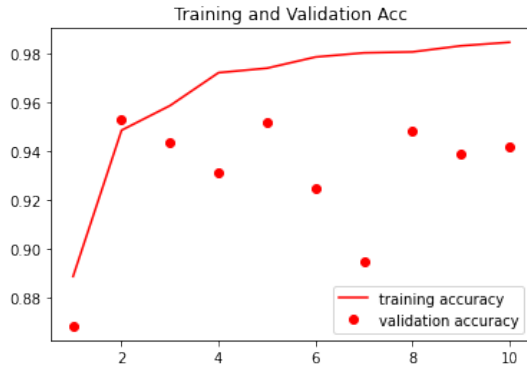


Figure 4.19: Extensive X-ray Augmented Xception Model DCGAN Accuracy

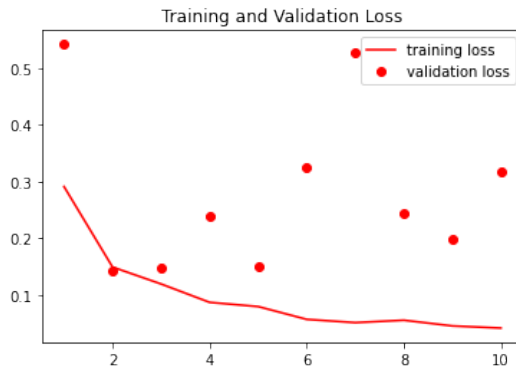


Figure 4.20: Extensive X-ray Augmented Xception Model DCGAN Loss

### Extensive CNN X-ray ResNet50V2 Model

The Extensive CNN X-ray ResNet50V2 model achieved a final training accuracy of 0.9624 and a final training loss of 0.0983 along with a final validation accuracy of 0.7584 and a validation loss of 0.9866 when the dataset was augmented. In comparison to the original model which had a training accuracy of 0.9368 and a training loss of 0.1786 in addition to a validation accuracy of 0.6890 and a validation loss of 0.9138 when trained for the same amount of epochs on a non-augmented set. The model performed better on both the validation set and on the training set when training on the augmented set. The training accuracy increased by 0.0256 and the training loss decreased by 0.0803. The validation accuracy increased by 0.0694 and the loss increased by 0.0728 If the model was stopped one epoch earlier the model would have ended with a training accuracy of 0.9623 and a training loss of 0.1077 along with a validation loss of 0.3643 and a validation accuracy of 0.8942, which would be a significant improvement over the original model. The model trained for ten epochs performs slightly worse than if the model were trained for nine epochs.

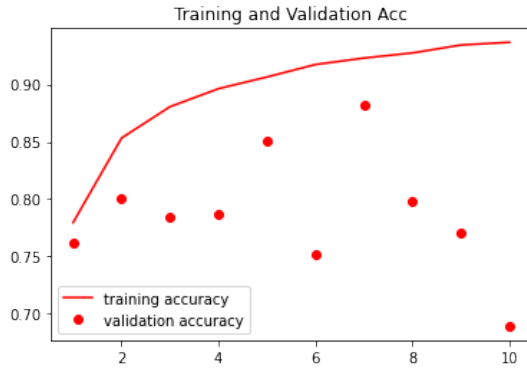


Figure 4.21: Extensive X-ray Augmented ResNet50V2 Model DCGAN Accuracy

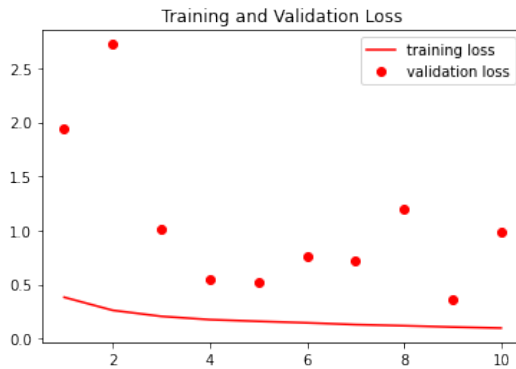


Figure 4.22: Extensive X-ray Augmented ResNet50V2 Model DCGAN Loss

### Extensive CNN X-ray EfficientNetV2S Model

The Extensive CNN X-ray EfficientNetV2S model achieved a final training accuracy of 0.9868 and a final training loss of 0.0351 along with a final validation accuracy of 0.9630 and a validation loss of 0.1661 when the dataset was augmented. In comparison to the original model which had a training accuracy of 0.9827 and a training loss of 0.0452 in addition to a validation accuracy of 0.9560 and a validation loss of 0.2095 when trained for the same amount of epochs on a non-augmented set. The model performed better on both the validation set and on the training set when training on the augmented set. The training accuracy increased by 0.0041 and the training loss decreased by 0.0101. The validation accuracy increased by 0.007 and the loss decreased by 0.0434 If the model was stopped one epoch earlier the model would have ended with a training accuracy of 0.9862 and a training loss of 0.0338 along with a validation loss of 0.1608 and a validation accuracy of 0.9696. If the model were trained for one less epoch it would have a slightly higher validation accuracy but at the expense of a slightly lower training accuracy.

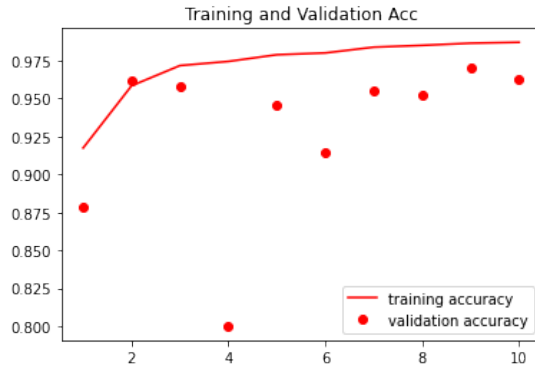


Figure 4.23: Extensive X-ray Augmented EfficientNetV2S Model DCGAN Accuracy

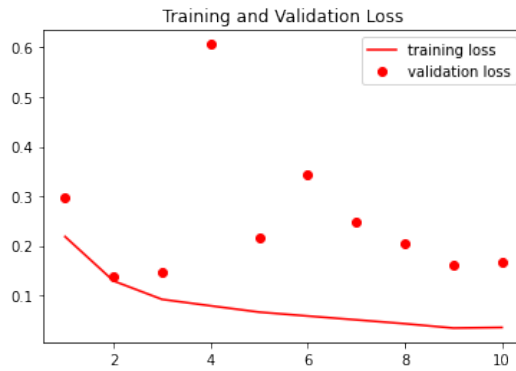


Figure 4.24: Extensive X-ray Augmented EfficientNetV2S Model DCGAN Loss

#### 4.1.3 X-ray COVID-19 dataset CNN Models

This dataset was augmented with 2000 artificially generated images, 1000 belonging to the pneumonia class and the other 1000 belonging to the normal class. The results from these models are also open to scrutiny given that a portion of the 2000 new images used to train the model are also in the validation set.

##### X-ray COVID-19 Baseline Model

The X-ray COVID-19 Baseline Model model achieved a final training accuracy of 0.9791 and a final training loss of 0.0396 along with a final validation accuracy of 0.9832 and a validation loss of 0.0299 when the dataset was augmented. In comparison to the original model which had a training accuracy of 0.8106 and a training loss of 0.4352 in addition to a validation accuracy of 0.8393 and a validation loss of 0.6788 when trained for the same amount of epochs on a non-augmented set. The model performed better on both the validation set and on the training set when training on the augmented set. The training accuracy increased by 0.1685 and the training loss decreased by 0.3956. The validation accuracy increased by 0.1439 and

the loss decreased by 0.6489. The model has frequent drops in accuracy during training which may possibly be due to the limited data available when training the GANs and indicates some images may be malformed.

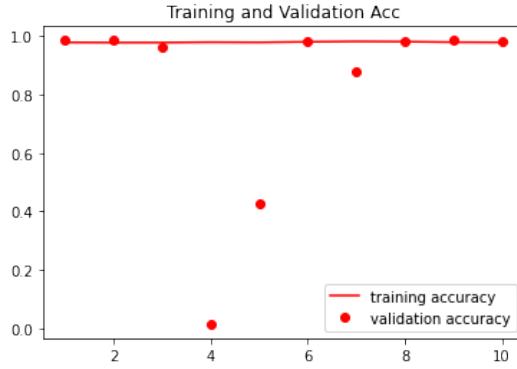


Figure 4.25: X-ray COVID-19 Augmented Baseline Model Model DCGAN Accuracy

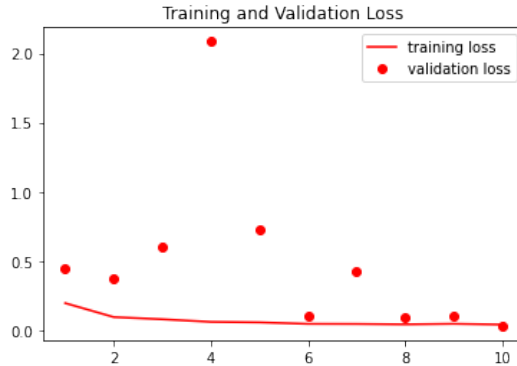


Figure 4.26: X-ray COVID-19 Augmented Baseline Model Model DCGAN Loss

### X-ray COVID-19 Xception Model

### X-ray COVID-19 ResNet50V2 Model

### X-ray COVID-19 EfficientNetV2S Model

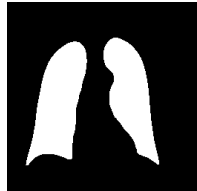
## 4.2 Evaluation of GAN Models

### 4.2.1 Radiography GAN Models

#### Radiography DCGAN for COVID-19 Class Augmentation

The radiography DCGAN for synthetically generated COVID-19 samples had mixed results. Some of the images generated by the DCGAN came out looking very similar to the masks of

patients lungs which were in the database. I have included a side by side comparison in figure 4.27a and 4.27b below



(a) Real COVID-19 Radiography Mask Example



(b) Generated COVID-19 Radiography Mask Example DCGAN

As shown in the above figures 4.27a and 4.27b, the synthetically generated COVID-19 mask looks very similar to the example taken from the dataset. However not every single generated image came out as well as those that I have shown for demonstration purposes. From reviewing the generated images it appears that a number of images have some issues. A common issue faced was images which were generated with artefacts and some images which were not up to standard with the images in the dataset.



(a) Synthetically generated COVID 19 mask with Artefacts(DCGAN)



(b) Malformed Image of synthetically generated COVID 19 Mask(DCGAN)

From training a number of models there appears to be a need for pruning out bad images generated by the GAN and determining which images resemble X-Rays and Masks and which are "garbage" images which don't resemble data in our dataset. This will require a lot of manual effort in determining which generated images are worth including in the augmented dataset and which are worth throwing away.

Similarly the augmentation of the X-ray images produced good results although, much like the synthetically generated masks, there were a number with artefacts and some images that were malformed. I have included two images below to compare the synthetically generated example 4.29b with a real example 4.29a below



(a) Real COVID-19 Radiography X-ray Example



(b) Generated COVID-19 Radiography X-ray Example DCGAN

As shown in the above figures 4.29a and 4.29b the two images look very similar to each other and there are clear similarities contained in the images. Malformed images are also present in the generated data and two such examples have been shown in the figures below.



(a) Malformed COVID-19 Radiography X-ray Example Number 1 Radiography DCGAN



(b) Malformed COVID-19 Radiography X-ray Example Number 2 Radiography DCGAN

### Radiography DCGAN for Pneumonia Class Augmentation

Much like in the previous section there was some success when augmenting the Pneumonia class despite it being a little less than half the size of the covid class(for reference the covid class contains 3,616 images in both the mask and X-ray folders where as the Pneumonia class contains 1,345 images in both the mask and X-ray folders). Most of the masks generated resembled those in the dataset an example of a synthetically generated pneumonia mask4.31b alongside a real example mask4.31a is visible in the figures below



(a) Real Pneumonia Radiography Mask Example

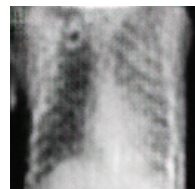


(b) Generated Pneumonia Radiography Mask Example DCGAN

The X-ray DCGAN also produced convincing results which are shown below



(a) Real Pneumonia Radiography X-ray Example



(b) Generated Pneumonia Radiography X-ray Example DCGAN

As shown in the above images 4.32a and 4.32b there appears to be a number of similarities between the two images but the synthetically generated X-ray does appear to lack the quality of the original.

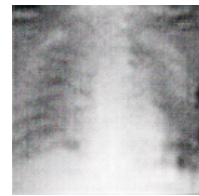
In conclusion the malformed images may have a detrimental effect on the training and it would require a lot of manual effort and computational power to both prune the augmented dataset and retrain the GANs. The examples above show that the DCGAN is a powerful method of generated synthetic data although it is not without its faults.

#### 4.2.2 Extensive X-Ray GAN Models

The X-ray DCGAN models achieved some success when synthetically generating both the X-rays for COVID and X-rays of non-COVID patients. The following images show a real example and a synthetic example side by side for comparison.



(a) Real COVID X-ray Example Extensive



(b) Synthetically Generated COVID X-ray Example Extensive DCGAN

As shown in the images above there are some similarities between the two X-rays although the synthetically generated example looks blurry and appears to be of low quality when compared with the real example. Unlike the Radiography dataset where images appeared to share characteristics there seems to be a lot more variance in this dataset as some X-rays are taken from the side where as others are taken straight forward. This is the reason that the synthetically generated images don't appear to match the quality of the synthetically generated radiography dataset images.

When using the model to produce non-COVID X-rays there seemed to be slightly better results as is shown with the images below



(a) Real Non COVID X-ray Example Ex-



(b) Synthetically Generated Non COVID X-ray Example Extensive DCGAN

The reason for the synthetically generated non-COVID examples having more quality is that there seems to be less variance in X-ray images in the non-COVID class and also the non-COVID class is the majority in this dataset.

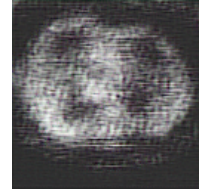
There were also the issues of malformed images and artefacts when training these DCGANs like the previous examples shown in figures 4.28b and 4.28a

#### 4.2.3 Extensive CT GAN Models

The CT GAN models had some issues reproducing the CT images this was due to their being a lot of variety in the CT dataset. Included in the figures below is an example of a real COVID CT scan along with the synthetically generated COVID CT scan.



(a) Real COVID CT Example Extensive



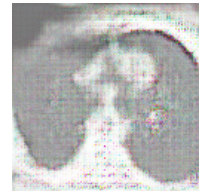
(b) Synthetically Generated COVID CT Example Extensive DCGAN

As shown in the figures above the synthetic example 4.35b appears to be grainy and lacking in quality despite sharing some similar features with the real example 4.35a. The poor quality may be caused by the variety of images in the dataset, as there are many differing features between the images in the dataset.

As with the COVID CT scans the non COVID CT scans had similar results which can be seen below



(a) Real non COVID CT Example Extensive



(b) Synthetically Generated non COVID CT Example Extensive DCGAN

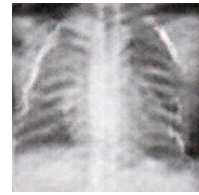
The above figures show the lack of quality in the synthetically generated image 4.36b when compared with the example taken from the dataset 4.36a. From trying a number of GAN architectures the same issue was seen with lack of quality augmented images being produced. However the synthetic images do share some features with the real example.

#### 4.2.4 X-ray COVID-19 dataset GAN Models

Surprisingly given the very small dataset the X-ray COVID-19 DCGANs produced relatively convincing images for both classes. Below are two X-ray examples for the normal class one image is generated by the DCGAN and the other is taken from the dataset



(a) Real Normal X-ray X-ray Dataset  
COVID-19

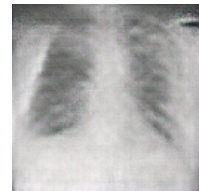


(b) Synthetically Generated Normal X-ray X-ray Dataset COVID-19 DCGAN

As shown in the figures above the synthetically generated example 4.37b lacks the quality of the original 4.37a but appears to have similar features. The next figures show an example of a synthetically generated pneumonia X-ray along with a sample taken from the dataset



(a) Real Pneumonia X-ray X-ray Dataset  
COVID-19



(b) Synthetically Generated Pneumonia X-ray X-ray Dataset COVID-19 DCGAN

The figure shown above 4.38b suffers from the same issue the synthetically generated images of the Normal class suffered from, in that the synthetic image appears grainy but does share some similar features with the original images 4.38a. Given the limited size of the dataset used to train the GANs there was no need to experiment further as this seems to be the best quality a DCGAN can produce.

### 4.3 Conclusion

# Chapter 5

## Future Work and Research

### 5.1 Limitations

In this section I will outline limitations faced when conducting this research and where possible include ways in which they may be mitigated when conducting future research into this problem domain.

#### 5.1.1 Computational Resources Offered by Google Colab Pro

Due to limitations with Google Colab Pro I wasn't able to surpass certain limits when training the Convolutional Neural Networks and Generative Adversarial Networks. This means that the number of units per layer of each model could not surpass a certain limit as the runtime would run out of memory and processing power. The model's performance may be improved in future experiments when more computational power is available.

Due to this limitation models with approximately 10 to 20 million unit parameters maxed out the resources available depending on a number of factors such as the hyper parameters of the model. The lack of computational resources also affected the GANs as I was not able to use high resolutions for the images and settled for a smaller resolution when training them on the images, as higher resolutions are more computationally expensive.

Larger models could be trained when the option was available to opt for premium GPU on Google Colab but Google has only allocated a certain amount of compute units per month to pro users, meaning that the access to premium GPUs were limited. This affected the training time and size of models I was able to create.

This limitation also meant that I was unable to train the GANs to produce higher resolution images. The images produced by the GANs mentioned in this paper have a resolution of  $128 \times 128$ , in future research the CNNs may possibly be improved by using a resolution consistent with that of the dataset.

### 5.1.2 Run time Limits in Google Colab Pro

Due to run time limits I was also frequently met with disconnects when training larger models, this meant that during the process of training the model the run time would disconnect and I would be forced to run the model again. This is due to Google conserving computational resources and limiting the amount of time a model can train while being idle. I was able to mitigate this somewhat by following advice from a stack overflow post and including the following code:

```
1 import IPython
2 js_code = '''
3 function ClickConnect(){
4 console.log("Working");
5 document.querySelector("colab-toolbar-button#connect").click()
6 }
7 setInterval(ClickConnect,60000)
8 '''
9 IPython.display.Javascript(js_code)
```

The above code was used to click the connect button after a certain amount of time to ensure the runtime was not disconnected. There was however an limit to the amount of time this code could be run without the notebook disconnecting which was estimated to be approximately 24 hours.

There was also an issue with Google taking away the use of a TPU and GPU backend, without a TPU or GPU to train the models they could take days to train. Due to this limitation the improvement of transfer learning models was greatly hindered as they require a lot of computational power to train.

### 5.1.3 Lack of Data

During the course of this study I was met with a desire for more data to use to train the GANs and CNNs, I found that the data in the classes which needed augmenting was not nearly enough to train a Generative Adversarial Model to produce perfect X-Rays nor to train a CNN to increase it's generalization ability. This greatly hindered progress when training the GANs as mode collapse frequently occurred and tended to produce black square images which looked just enough like X-Rays to fool the discriminator. If more data were available it may have mitigated a lot of the problems which occurred during the training of the GANs and possibly would have led to more realistic X-Rays being produced and a more various selection of X-Rays.

#### **5.1.4 Time**

Time was a major limitation during the writing of this thesis as Convolutional Neural Networks and Generative Adversarial Models can take a very long time to train and develop. Due to the time-consuming trial and error effort of adjusting the hyper parameters of models and rerunning the models to compare results of previous implementations I was spending a lot of my time waiting for models to train so that I could analyze the results. This became especially cumbersome as mode collapse occurred many times when training the GANs. The issue of time was also exacerbated by the computational limits of Google Colab which only allows a certain amount of memory and computational power to be allocated to the user.

#### **5.1.5 Financial Limitations**

The training of very large models was not limited due to financial limitations, as of today's date Google charges 11.38 euro for 100 compute units and 51.97 euro for 500 compute units. This meant I was only able to train the GAN models for a certain number of epochs which I limited to 100 epochs to conserve compute units.

## **5.2 Future Research**

This section will discuss future research into this problem domain and information which may be valuable to those wishing to explore and expand the use of GANs in the recreation of X-Ray / CT images.

### **5.2.1 Suggestions for Future Research**

#### **Advancements in The Field of Artificial Intelligence**

At the time this thesis was written, Tuesday 14<sup>th</sup> March, 2023, there has been much research and many advancements taking place in regards to Generative Adversarial Networks, Convolutional Neural Networks, synthetic data generation, and in the overall field of Artificial Intelligence. I advise researchers who wish to expand on this problem domain and this research to research new methodologies and advances in this field as technology moves at such a rapid pace and undoubtedly the implementation of the networks contained within this thesis will become archaic and under perform in comparison to the latest and greatest implementations of such networks.

The use of synthetic data appears to contain great promise for making data more ubiquitous and to encourage many people to enter the field of Machine Learning and Artificial Intelligence due to the abundance of data throughout various fields. Not only could the generation of synthetic data encourage new people to enter the fields of Machine Learning and Artificial Intelligence, but it would also yield more robust models of CNNs and machine learning models

in general which will perhaps be able to generalize better than our current models and assist experts in a variety of fields.

### **Conducting Experiments with More Data**

With more data around COVID-19 becoming public it may be possible at a future date to conduct these experiments with more data. More data would have greatly improved the training and performance of both the Convolutional Neural Networks and Generative Adversarial Networks. Advancements in medical imaging technology may also have a positive effect upon future research as would the use of standardised and high quality datasets.

I would therefore advise those looking to expand upon this research to seek out more datasets which will hopefully be more readily available in the future.

## **5.3 Conclusion of Work**

### **5.3.1 Issues Faced and How They Should be Mitigated in Future Research**

#### **Slow Training of Models Due to Lack of Computational Resources**

This issue could be mitigated by investing in faster hardware, due to the lack of an NVIDIA GPU the models were trained using Google Colab which can be slow(especially when using the free tier). To mitigate this issue I strongly suggest future researchers invest in a powerful NVIDIA GPU as NVIDIA has invested a lot of money into AI research and unlike AMD, NVIDIA has compatibility with most ML / AI frameworks.

#### **5.3.2 Summary of Results**

#### **Analysis of Results and Their Significance**

#### **5.3.3 Final Words**

# Bibliography

- [1] A. Binkheder *et al.*, “COVID-19 Data Explorer,” [Online]. Available: <https://www.ncbi.nlm.nih.gov/pmc/articles/PMC8701465/>.
- [2] S. Maior *et al.*, “Convolutional Neural Network Model Based on Radiological Images to Support COVID-19 Diagnosis: Evaluating Database Biases,” [Online]. Available: [https://journals.plos.org/plosone/article?id=10.1371/journal.pone.0247839#sec025/](https://journals.plos.org/plosone/article?id=10.1371/journal.pone.0247839#sec025).
- [3] A. Goodfellow *et al.*, “Generative Adversarial Nets,” 2014. [Online]. Available: <https://arxiv.org/pdf/1406.2661.pdf>.
- [4] P. Zhu *et al.*, “Unpaired Image-to-Image Translation using Cycle-Consistent Adversarial Networks,” 2020. [Online]. Available: <https://arxiv.org/pdf/1703.10593.pdf>.
- [5] A. Karras Laine, “A style-based generator architecture for generative adversarial networks,” 2019. [Online]. Available: <https://arxiv.org/pdf/1812.04948.pdf>.
- [6] K. Oord Kalchbrenner, “Pixel recurrent neural networks,” 2016. [Online]. Available: <https://arxiv.org/pdf/1601.06759.pdf>.
- [7] K. O’Shea and R. Nash, “An Introduction to Convolutional Neural Networks,” [Online]. Available: <https://arxiv.org/pdf/1511.08458.pdf>.
- [8] M. Hashemi, “Enlarging smaller images before inputting into convolutional neural network: zero-padding vs. interpolation,” [Online]. Available: <https://journalofbigdata.springeropen.com/articles/10.1186/s40537-019-0263-7>.
- [9] J. Delua, “Supervised vs. Unsupervised Learning: What’s the Difference?,” [Online]. Available: <https://www.ibm.com/cloud/blog/supervised-vs-unsupervised-learning>.
- [10] Multiple, “Tensorflow,” [Online]. Available: <https://www.tensorflow.org/>.
- [11] Multiple, “Tensorflow Case Studies,” [Online]. Available: <https://www.tensorflow.org/about/case-studies/>.
- [12] Multiple, “Keras,” [Online]. Available: <https://keras.io/>.
- [13] Multiple, “Keras Examples,” [Online]. Available: <https://keras.io/examples/>.

- [14] Multiple, “WHO Coronavirus (COVID-19) Dashboard,” [Online]. Available: <https://covid19.who.int/>.
- [15] Multiple, “WHO Coronavirus (COVID-19) Dashboard Ireland,” [Online]. Available: <https://covid19.who.int/region/euro/country/ie/>.
- [16] Multiple, “COVID-19 Deaths and Cases Statistics,” [Online]. Available: <https://www.cso.ie/en/releasesandpublications/ep/p-covid19/covid-19informationhub/health/covid-19deathsandcasesstatistics/>.
- [17] Our World In Data(multiple), “COVID-19 Data Explorer,” [Online]. Available: <https://ourworldindata.org/explorers/coronavirus-data-explorer?tab=map&facet=none&Metric=Confirmed+cases&Interval=Cumulative&Relative+to+Population=true&Color+by+test+positivity=false&country=USA~ITA~CAN~DEU~GBR~FRA~JPN>.
- [18] a. o. Ahmed Wang, “Automated Detection of COVID-19 Through Convolutional Neural Network Using Chest X-ray Images,” [Online]. Available: <https://journals.plos.org/plosone/article?id=10.1371/journal.pone.0262052/>.
- [19] C. E. Belman-López, “Detection of COVID-19 and Other Pneumonia Cases using Convolutional Neural Networks and X-ray Images,” [Online]. Available: [http://www.scielo.org.co/scielo.php?script=sci\\_arttext&pid=S0120-56092022000100108/](http://www.scielo.org.co/scielo.php?script=sci_arttext&pid=S0120-56092022000100108/).
- [20] J. P. Cohen, P. Morrison, and L. Dao, “COVID-19 image data collection,” *arXiv*, 2020. [Online]. Available: <https://github.com/ieee8023/covid-chestxray-dataset>.
- [21] C. Rahman *et al.*, “COVID-19 Radiography Database,” [Online]. Available: <https://www.kaggle.com/datasets/tawsifurrahman/covid19-radiography-database>.
- [22] Asraf, “COVID19 with Pneumonia and Normal Chest Xray(PA) Dataset,” [Online]. Available: <https://www.kaggle.com/datasets/amanullahasraf/covid19-pneumonia-normal-chest-xray-pa-dataset>.
- [23] F. E. A. E.-S. Walid El-Shafai, “Extensive COVID-19 X-Ray and CT Chest Images Dataset,” [Online]. Available: <https://data.mendeley.com/datasets/8h65ywd2jr/3>.
- [24] Multiple, “CDC Museum COVID-19 Timeline,” [Online]. Available: <https://www.cdc.gov/museum/timeline/covid19.html#Late-2019>.
- [25] A. Maxmen, “Wuhan market was epicentre of pandemic’s start, studies suggest,” [Online]. Available: <https://www.nature.com/articles/d41586-022-00584-8>.
- [26] S. M. Amy Maxmen, “The COVID lab-leak hypothesis: what scientists do and don’t know,” [Online]. Available: <https://www.nature.com/articles/d41586-021-01529-3>.

- [27] E. Gamillo, “Covid-19 Surpasses 1918 Flu to Become Deadliest Pandemic in American History,” [Online]. Available: <https://www.smithsonianmag.com/smart-news/the-covid-19-pandemic-is-considered-the-deadliest-in-american-history-as-death-toll-surpasses-1918-estimates-180978748/>.
- [28] A. Mckeever, “COVID-19 surpasses 1918 flu as Deadliest Pandemic in U.S. History,” [Online]. Available: <https://www.nationalgeographic.com/history/article/covid-19-is-now-the-deadliest-pandemic-in-us-history/>.
- [29] R. Roberts and Jarić, “Dating First Cases of COVID-19,” [Online]. Available: [https://journals.plos.org/plospathogens/article?id=10.1371/journal.ppat.1009620/](https://journals.plos.org/plospathogens/article?id=10.1371/journal.ppat.1009620).
- [30] W. D. Heaven, “Hundreds of AI tools have been built to catch covid. None of them helped.,” [Online]. Available: <https://www.technologyreview.com/2021/07/30/1030329/machine-learning-ai-failed-covid-hospital-diagnosis-pandemic/>.
- [31] A. Shrivastava, “Underfitting Vs Just right Vs Overfitting in Machine learning,” [Online]. Available: <https://www.kaggle.com/getting-started/166897>.
- [32] B. Mahmoudi *et al.*, “A Deep Learning-Based Diagnosis System for COVID-19 Detection and Pneumonia Screening Using CT Imaging,” [Online]. Available: <https://www.mdpi.com/2076-3417/12/10/4825/>.
- [33] I. Islam and Asraf, “A Combined Deep CNN-LSTM Network for the Detection of Novel Coronavirus (COVID-19) using X-ray Images,” [Online]. Available: <https://www.sciencedirect.com/science/article/pii/S2352914820305621>.
- [34] S. Hochreiter, “The Vanishing Gradient Problem During Learning Recurrent Neural Nets and Problem Solutions,” *International Journal of Uncertainty, Fuzziness and Knowledge-Based Systems*, pp. 107–116, [Online]. Available: <https://doi.org/10.1142/S0218488598000094>.
- [35] G. Chen, “A Gentle Tutorial of Recurrent Neural Network with Error Backpropagation,” pp. 1–10, [Online]. Available: <http://arxiv.org/abs/1610.02583>.
- [36] Tanaka and Aranha, “Data Augmentation Using GANs,” *Proceedings of Machine Learning Research*, pp. 1–16, 2019. [Online]. Available: <https://arxiv.org/pdf/1904.09135.pdf/>.
- [37] B. Chalwa *et al.*, “SMOTE: Synthetic Minority Over-sampling Technique,” *Journal of Artificial Intelligence Research* 16, pp. 321–357, 2002. [Online]. Available: <https://arxiv.org/pdf/1106.1813.pdf/>.
- [38] G. He Bai, “ADASYN: Adaptive Synthetic Sampling Approach for Imbalanced Learning,” *IEEE World Congress on Computational Intelligence*, pp. 1322–1328, 2008. [Online]. Available: [https://www.researchgate.net/publication/224330873\\_ADASYN\\_Adaptive\\_Synthetic\\_Sampling\\_Approach\\_for\\_Imbalanced\\_Learning](https://www.researchgate.net/publication/224330873_ADASYN_Adaptive_Synthetic_Sampling_Approach_for_Imbalanced_Learning).

- [39] Wang and Xiao, “Lychee Surface Defect Detection Based on Deep Convolutional Neural Networks with GAN-Based Data Augmentation,” *Agronomy*, vol. 11, 2021. [Online]. Available: <https://www.mdpi.com/2073-4395/11/8/1500>.
- [40] C. Jiang and Wang, “TransGAN: Two Pure Transformers Can Make One Strong GAN, and That Can Scale Up,” *Advances in Neural Information Processing Systems 34*, 2021. [Online]. Available: <https://arxiv.org/pdf/2102.07074.pdf>.
- [41] Girshick *et al.*, “Rich Feature Hierarchies for Accurate Object Detection and Semantic Segmentation,” *IEEE Conference on Computer Vision and Pattern Recognition*, 2014. [Online]. Available: <https://ieeexplore.ieee.org/document/6909475>.
- [42] Multiple, “Hardware and Software Support Reference Guide,” [Online]. Available: [https://docs.amd.com/en-US/bundle/Hardware\\_and\\_Software\\_Reference\\_Guide/page/Hardware\\_and\\_Software\\_Support.html](https://docs.amd.com/en-US/bundle/Hardware_and_Software_Reference_Guide/page/Hardware_and_Software_Support.html).
- [43] Multiple, “Image classification from scratch,” [Online]. Available: [https://keras.io/examples/vision/image\\_classification\\_from\\_scratch/](https://keras.io/examples/vision/image_classification_from_scratch/).
- [44] Z. Ramachandran and Le, “Searching for Activation Functions,” [Online]. Available: <https://arxiv.org/pdf/1710.05941.pdf/>.
- [45] N. Patwardhan, M. Ingalhalikar, and R. Walambe, “Aria: Utilizing richard’s curve for controlling the non-monotonicity of the activation function in deep neural nets,” Jul. 2018.
- [46] Multiple, “Keras Applications,” [Online]. Available: <https://keras.io/api/applications/>.
- [47] Multiple, “ImageNet,” [Online]. Available: <https://www.image-net.org/index.php/>.
- [48] F. Chollet, “DCGAN to Generate Face Images,” [Online]. Available: [https://keras.io/examples/generative/dcgan\\_overriding\\_train\\_step//](https://keras.io/examples/generative/dcgan_overriding_train_step//).
- [49] I. Salián, “NVIDIA Research Achieves AI Training Breakthrough Using Limited Datasets,” 2020. [Online]. Available: <https://blogs.nvidia.com/blog/2020/12/07/neurips-research-limited-data-gan/>.